U.PORTO

FEUP FACULDADE DE ENGENHARIA
UNIVERSIDADE DO PORTO

STRESS CONCENTRATION FACTOR EVALUATION IN OFFSHORE TUBULAR KT-JOINTS FOR FATIGUE DESIGN

PAULO JORGE SOEIMA CARMONA MENDES

Dissertação submetida para satisfação parcial dos requisitos do grau de

MESTRE EM ENGENHARIA CIVIL — ESPECIALIZAÇÃO EM ESTRUTURAS

Orientador: Professor Doutor José António Fonseca de Oliveira Correia

Coorientadores: Professor Doutor José Miguel de Freitas Castro

Professor Doutor Rui Artur Bártolo Calçada

JUNHO 2018

MESTRADO INTEGRADO EM ENGENHARIA CIVIL 2017/2018

DEPARTAMENTO DE ENGENHARIA CIVIL

Tel. +351-22-508 1901

Fax +351-22-508 1446

✉ miec@fe.up.pt

Editado por

FACULDADE DE ENGENHARIA DA UNIVERSIDADE DO PORTO

Rua Dr. Roberto Frias

4200-465 PORTO

Portugal

Tel. +351-22-508 1400

Fax +351-22-508 1440

✉ feup@fe.up.pt

http://www.fe.up.pt

Ao meu pai, à minha mãe e ao meu irmão…

Acknowledgement

I would like to express my sincere gratitude to everyone who, by their support, encouragement, help or remarks have contributed to the fulfilment of this work.

Thanks to my supervisors, Doctor José António Correia, Prof. José Miguel Castro and Prof. Rui Calçada, by the helpful discussions and useful comments.

A special acknowledgement to my thesis supervisor, Doctor José António Correia, for accepting me as his thesis student, for giving me the opportunity to explore this theme as much as possible, for all the valuable help provided thought-out this process and for taking me to the Delft University of Technology (TUDelft), Delft, Netherlands to see closely how my thesis would be worked on and to acquire fatigue knowledge on civil engineering.

Second but not last, I want to thank my family and friends for carrying me throughout this process and proving me all the support needed to conclude this work and succeed these years. Thanks for making "Casa do Joche" as one of best hosting places with so many good memories shared and where I was honored to be part of them.

I sincerely want to thank the Faculty of Engineering of the University of Porto (FEUP), the Institute of Science and Innovation in Mechanical and Industrial Engineering (INEGI) and the Engineering Structures Department of the Faculty of Civil Engineering and Geosciences at Delft University of Technology (Netherlands), by the support and facilities that were made available to me.

Author gratefully acknowledge the funding of SciTech - Science and Technology for Competitive and Sustainable Industries (NORTE-01-0145-FEDER-000022), and FADEST - Competence Development in R&D in the fatigue design of structures and Structural Details (NORTE-01-0247-FEDER-015670), R&D projects cofinanced by Programa Operacional Regional do Norte ("NORTE2020"), through Fundo Europeu de Desenvolvimento Regional (FEDER).

And I would like to thank to the rest of the people whom supported me in one or another way.

Paulo Mendes

June 25, 2018

NORTE2020 PROGRAMA OPERACIONAL REGIONAL DO NORTE

PORTUGAL 2020

UNIÃO EUROPEIA

Fundo Europeu de Desenvolvimento Regional

Agradecimentos

Gostaria de expressar a minha sincera gratidão a todos que com a sua ajuda, incentivo e marcas contribuiu para a conclusão deste trabalho.

Graças aos meus orientadores, Doutor José António Correia, Professor José Miguel Castro e Prof Rui Calçada por todos os comentários úteis e discussões construtivas que podemos partilhar.

Um especial obrigado ao meu orientador da tese, Doutor José António Correia, por me aceitar como seu aluno na realização da tese, por me ter dado a oportunidade de explorar este tema o máximo possível, por toda a ajuda valiosa neste processo e por me ter levado à universidade de Delft, Holanda to para ver de perto como é que a minha tese iria ser trabalhada e para adquirir conhecimentos de fadiga em Engenharia Civil.

Em segundo lugar, mas não em último, quero agradecer à minha família e aos meus amigos por me acompanharem ao longo deste processo e por me providenciarem toda a ajuda para concluir este trabalho e sucesso ao longo destes anos. Obrigado por fazerem da "Casa do Joche" um dos lugares mais acolhedores ao longo destes anos com tão boas memórias partilhadas e onde tive o prazer de fazer parte delas.

Os meus sinceros agradecimentos à Faculdade de Engenharia da Universidade do Porto (FEUP), ao Instituto da Ciência e Inovação em Engenharia Mecânica e Gestão Industrial (INEGI) e ao departamento de Engenharia Civil e das Geociências da Universidade de Delft pela ajuda e por facultar as instalações para a realização deste trabalho

O autor agradece o financiamento da SciTech - Science and Technology for Competitive and Sustainable Industries (NORTE-01-0145-FEDER-000022) e FADEST - Competence Development in R&D in the fatigue design of structures and Structural Details (NORTE-01-0247-FEDER-015670) cofinanciado pelo Programa Operacional Regional do Norte ("NORTE2020"), pelo Fundo Europeu de Desenvolvimento Regional (FEDER).

E gostaria de agradecer ao resto das pessoas que me ajudaram num ou noutro sentido

Paulo Mendes

25 de Junho de 2018

Abstract

The deployment of more renewable energy all around the world is resulting in a significant energy security, climate change mitigation and lots of economic benefits. Wind power, especially in offshore, is considered to be one of the most promising sources of 'clean' energy towards meeting the EU targets for 2020 and 2050. This interest is mainly motivated by the higher wind speed in the marine environment, unrestricted space, and lower social impact. Tubular structures are widely used in offshore installations, trusses, high rise buildings, towers for wind turbines, ski-lift installations, lightning, road pole signals etc., owing to their excellent structural performance and attractive appearance. Stress concentration, especially in the welded joints of these structures, is an important design consideration particularly for fatigue design. This study was developed with the objective of studying the parametric equations proposed by Lloyd and Efthymiou and applied on the mainly used design codes for offshore structures. To study the accuracy of the parametric equations suggested by several researchers, it was made an exhaustive review of the background and state of the art of the stress concentration factors used in fatigue life assessment and it was developed a finite element model of a typical offshore KT-joint. Based on this numerical study, were applied interpolation and extrapolation approaches with aims to determine the stress concentration factors and a comparison with analytical Lloyd's and Efthymiou's solutions were made.

KEYWORDS: Offshore, Stress Concentration Factor, Fatigue, Tubular joints, Hot-Spot approach, Finite elements analysis, Meshing.

Resumo

A implementação de mais energia renovável à volta do mundo resulta numa maior energia segura, uma atenuação das mudanças climáticas e muitos benefícios económicos. A força do vento, especialmente em offshore, é considerado uma das maiores fontes promissoras de energia "limpa" para atingir as metas da União Europeia para 2020 e 2050. Este interesse deve-se à maior velocidade do vento em ambiente marinho, à inexistência de espaços restritos e provoca um menor impacto social na sua construção. As estruturas tubulares são vulgarmente utilizadas em instalações offshore, arranha-céus, "trusses", torres eólicas, teleféricos, eletricidade, sinais de trânsito, etc., devido à sua excelente capacidade estrutural e aparência atrativa. A fator de concentração de tensões, especialmente em ligações soldadas nestas estruturas, é um ponto a considerar importante particularmente no dimensionamento à fadiga. Este estudo foi desenvolvido com o objetivo de estudar as equações propostas por Lloyd e Efthymiou e aplicadas na maioria dos códigos próprios para dimensionamento de estruturas offshore. Para estudar a precisão das equações paramétricas sugeridas por vários investigadores, foi feita uma revisão exaustiva do fundo e do estado de arte dos fatores de concentração de tensões usados na avaliação à fadiga e foi desenvolvido um modelo de elementos finitos de uma ligação KT típica. Baseado neste estudo numérico, foram aplicados métodos de interpolação e extrapolação com o objetivo de determinar os fatores de concentração de tensões e uma comparação das soluções analíticas de Lloyd e Efhymiou.

PALAVRAS-CHAVE: Offshore, Fator de concentração de tensões, Fadiga, Ligações tubulares, Abordagem hot-spot, Análise de elementos finitos, Malha

GENERAL INDEX

List of Figures

List of Tables

LIST OF ABBREVIATIONS

SCF – Stress concentration factor

EU – Europe union

UK – United Kingdom

MODU – Mobile Offshore Drilling Unit

FPS - Floating production systems
FPSO - Floating production and storage systems

TLP - Tension Leg Platforms

TBT – Tethered buoyant towers
BLS - Buoyant Leg Structures

HSS – Hot-spot stress

kPa - Kilopascal
FE – Finite element
HSE – Health and safety executive

SCF_{AS} – Stress concentration factor at the saddle for axial load

SCF_{AC} - Stress concentration factor at the crown for axial load

SCF_{MIP} - Stress concentration factor for in plane moment

SCF_{MOP} - Stress concentration factor for out of plane moment

HSS – Hot-Spot stress

1
Introduction

1.1. GENERAL ASPECTS

Fatigue failure in offshore structures, such as oil and gas structures and structures for renewable energy applications can occur due to the magnitude of cyclic loadings which they experience in service. Fatigue cracks can develop from pre-existing defects which may be introduced into structures during manufacturing, transportation and installation. Fatigue cracks, if not controlled can grow into failure or collapse of the structures when an unstable stage of the crack grow this reached. Therefore, defects or cracks in offshore structures need to be reliably inspected and monitored to ensure that the structures are fit for design purpose. Offshore structures are vulnerable to corrosion attacks due to the harsh marine lace a reduction in service life. Crack growth behaviour of steels used for offshore oil and gas applications has been studied over the years in order to understand the behaviour of the structures in marine environments. [1]

1.2. OBJECTIVES

It is inferred from the literature that stress concentration is a complex problem in the context of hollow section tubular and non-tubular joints. Detailed studies are needed to evaluate SCF for different types of loading conditions in the brace and chord, and different combination of brace and chord sections. In case of non-tubular joints, research progress so far is minimal. Ultimately the goal for the profession is to ensure a longer fatigue life for the tubular and the non-tubular joints employed in offshore and other structures. The development of simplified parametric equations to predict the SCF for tubular/non-tubular joints are required, which can be easily used by design engineers, and reduce the stress concentration at the welded joints are some affordable and easily implementable techniques needed to be developed. Undoubtedly, the availability of such equations and techniques will help in enhancing the fatigue performance of the tubular/non- tubular joints. [2] That way, the main objective of this thesis is understood how the developed parametric equations are in conformity with the finite element models which simulate real life scenarios.

1.3. Thesis Organization

For the realization of this thesis, it was necessary to first make a brief review about offshore structures, its loads, its components and its specifications then after the review was done, it was essential to make a finite element model and compare it with the fatigue design code. In Chapter 2, it was necessary to study offshore structures and its behaviour in the sea so it’s possible to simulate the case of study in the computer program called ANSYS in Chapter 4 as much real as it’s possible. The model made on the ANSYS program is then compared with the analytical calculations made from the stress concentration factor parametric equations from the fatigue design code and OTH 354 report. These calculations were

made on Chapter 3. In chapter 5 are presented all the conclusions and future works related with the study of stress concentration factor in offshore KT-joints.

2

Review on Structural Integrity of Renewable Energy and Oceanic Structures

2.1. INTRODUCTION AND DEFINITION OF OFFSHORE STRUCTURES

The demand for exploration and production of oil and gas has grown ever since the early offshore activities began in the North Sea in the 1960's. The first steel structures to operate in the North Sea were transferred from the Gulf of Mexico, where exploration and production activities had been on-going since the 1930's. [3] Since 1947, more than 10,000 offshore platforms of various types and sizes have been constructed and installed worldwide. As of 1995, 30% of the world's production of crude came from offshore.

An offshore structure has no fixed access to dry land and may be required to stay in position in all weather conditions. Offshore structures may be fixed to the seabed or may be floating. Floating structures may be moored to the seabed, dynamically positioned by thrusters or may be allowed to drift freely. While the majority of offshore structures support the exploration and production of oil and gas, there are other major structures like structures for harnessing power from the sea, offshore bases and offshore airports. A production unit can have several functions as processing, drilling, workover, accommodation, oil storage and riser support. Reservoir and fluid characteristics, water depth and ocean environment are the variables that primarily determine the functional requirements for an offshore facility. Although the function of the structure. together with the water depth and the environment primarily influences its size and configuration, other factors that are just as important are the site infrastructure, management philosophy and financial strength of the operator as well as the rules, regulations and the national law. [4] The size and other principal features of offshore structures are primarily determined by their intended function and their environment. Platforms may be used for exploratory drilling to identify producible hydrocarbons. [5] Bottom supported structures are either "fixed" such as jackets and gravity base structures, or "compliant" such as the guyed tower and the compliant tower. Floating structures are compliant by nature. The most attractive mobile drilling platforms are drill ships, jack-ups and semisubmersibles. Drill ships are applicable in benign waters, jack-ups are limited to small water depths, while semisubmersibles are preferable in deep, harsh waters. [5] In small water depths the functional requirements are fulfilled at the lowest costs by using structures supported on the seafloor (Jacket, Guyed Tower, Gravity platform). Fixed structures became increasingly expensive and difficult to install as the water depths increased. [5] At present, deep water is typically defined to cover the water depth greater than 305 m. For water depths exceeding 1524 m, a general term "ultra deep water" is often used. Bottom-supported steel jackets and concrete platforms are impractical in deep water from a technical and economic point of view giving way to floating moored structures. In deep and especially ultra-deep water, risers and mooring systems provide considerable challenge. These water depths are demanding new materials and innovative concepts. [4]

The need for renewable energy source has significantly increased the volume of the planned wind structures that will be installed offshore, for example. Marine renewable energy could provide up to 50% of Europe's electricity needs by 2050; which would contribute to energy supply and security, reduce CO2 emissions, improve the overall state of the environment, create jobs and improve quality of life [6]. Wind power, especially offshore, is considered one of the most promising sources of 'clean' energy towards meeting the EU and UK targets for 2020 and 2050.

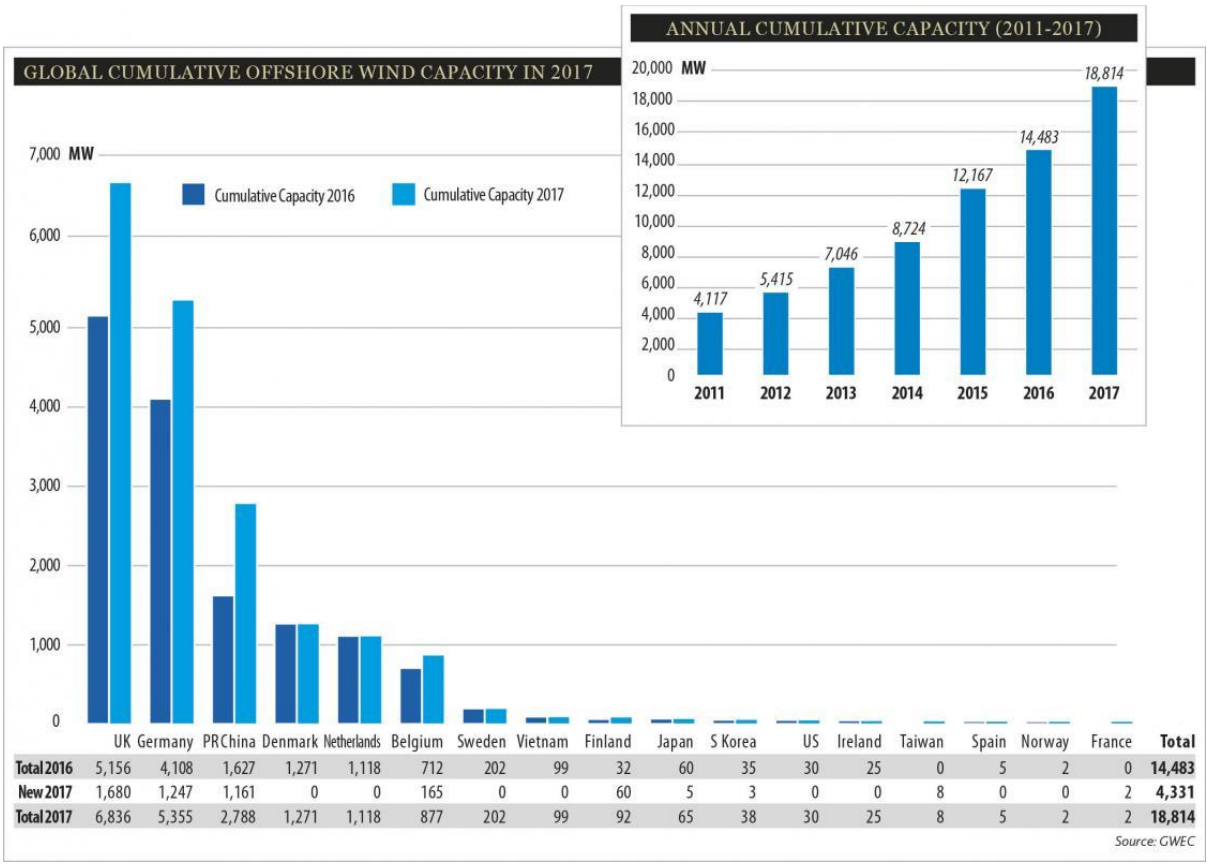

	UK	Germany	PR China	Denmark	Netherlands	Belgium	Sweden	Vietnam	Finland	Japan	S Korea	US	Ireland	Taiwan	Spain	Norway	France	Total
Total 2016	5,156	4,108	1,627	1,271	1,118	712	202	99	32	60	35	30	25	0	5	2	0	14,483
New 2017	1,680	1,247	1,161	0	0	165	0	0	60	5	3	0	0	8	0	0	2	4,331
Total 2017	6,836	5,355	2,788	1,271	1,118	877	202	99	92	65	38	30	25	8	5	2	2	18,814

Figure 1 - Global growth of wind sector in the world (Graphic from GWEC report)

The majority of the offshore wind farms in the UK are currently installed in shallow water depths of approximately 30 m with the wind turbines supported on monopile structures. Monopiles are the most commonly used wind turbine support structure due to their design simplicity and suitability for water depths of up to 30 m. One of the major design requirements of these types of structures is their ability to withstand load cycles of approximately 10^9 which is equivalent to a 20 year service life. However, a cost-effective design life can only be achieved if careful considerations are given to the volume of installations and the degree operational loads envelope, which the structures are subjected to in service compared to structures used for oil and gas applications. One of the most critical factors in the installation of wind structures is the suitability of the support structures for specific sites and this may depend primarily on water depths. [4] This implies that at increased water depth, the costs involved in the installation of the structures are likely to significantly increase. However, an advantage of the offshore wind structure over oil and gas structures, regardless of the initial capital cost, is the fact that the operating costs are lower when the structures are in operation. However, the major limitation of monopile supports is their flexibility in deeper waters. This is because monopiles experience some levels of deflection and vibration which are influenced by axial loads, lateral loads and bending moments. Therefore, the diameter and thickness of the monopile structures may have to be increased if they are intended for use in deeper water depth sand this will significantly increase the production and installation

costs. Research is ongoing on the use of other types of support structures such as jackets structures for larger wind turbines, with the possibility of harnessing more wind energy at increased water depths. Jacket structures are suitable for wind turbine installation in water depths of up to 50m and they have about 50% reduction in the quantity of steel used for their manufacture compared with the monopile structure. Another major challenge associated with the design of offshore wind turbine support structures is the effort involved to accurately predict the environmental and operational loads and the resulting structural dynamic responses of the wind turbine and support structures under the synergistic effects of wave and wind loading. [4]

2.2. TYPES OF MARINE STRUCTURES

2.2.1. FIXED OFFSHORE STRUCTURES

Fixed offshore structures are typically constructed from welded steel tubular members. These members act as a truss supporting the weight of the processing equipment, and the environmental forces from waves, wind and current. For a preliminary design, wind, wave and current forces can be applied quasi-statically to a structure along with the dead loads from the deck and structural self-weight. There are commonly known 3 types of fixed offshore structures: gravity base structures, guyed towers but the most common type of offshore platform is the fixed, pile-supported steel template platform, often called jacket. [4]

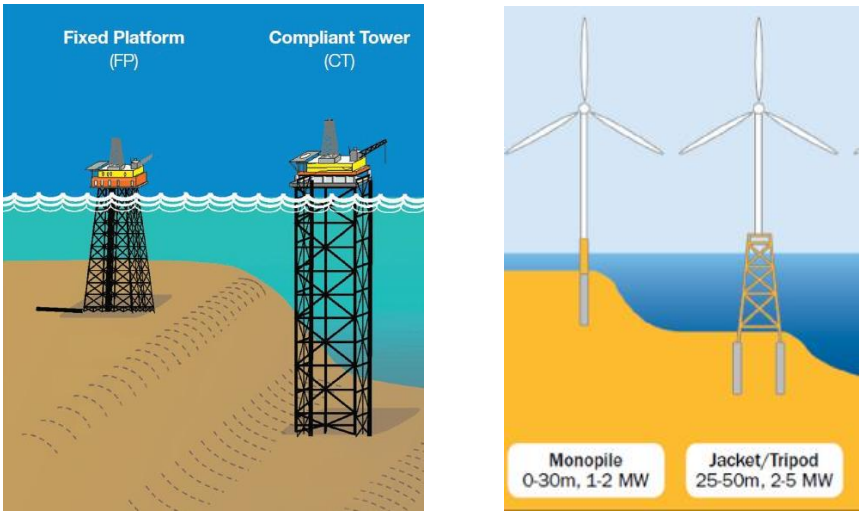

Figure 2 - Examples of fixed offshore structures (Illustration from the Bureau of Ocean Energy Management and European Wind Energy Association (EWEA), 2013)

For the marginal field development in shallow water, fixed production platforms with a small deck are often used. Jackets consist of a plate girder or truss deck structure, supported by a welded tubular steel space frame that is piled to the seafloor. The fixed platform deck loads are directly transmitted to the foundation material beneath the seabed. Thus, fixed platform jackets supporting the deck are typically long, slender steel structures extending from seabed to 20-25m above the sea surface. Fixed platform jackets are constructed on their side, loaded out on to a barge (except for jackets with flotation legs), transported to the installation site, launched and upended (or lifted and lowered) and secured to seabed with driven or drilled and grouted piles. Fixed platform jackets need to have adequate buoyancy to stay afloat during installation. These platforms generally support a superstructure having 2 or 3 decks with drilling and production equipment and workover rigs. Thus, they are typically constructed of small diameter tubulars that form a space frame. The design of jackets is primarily determined by requirements associated with the permanent operation conditions but may be influenced by temporary conditions

during transport, launching and offshore installation. The design of the joints between the circular tubular members in the truss is challenging because they exhibit complex shell behaviour and may suffer ultimate and fatigue failure. Newer types of structure, such as wind turbine structures, are being developed and installed offshore. Monopile structures have been the most commonly used support structures. [4]

2.2.2. FLOATING OFFSHORE STRUCTURES

The floating structures may be grouped as Neutrally Buoyant and Positively Buoyant (buoyant is the ability of something to float). The neutrally buoyant structures include Spars, Semi-submersible MODUs (Mobile Offshore Drilling Unit) and FPSs (Floating production systems), Ship-shaped FPSOs (Floating production and storage systems) and Drill ships. Positively buoyant structures. such as the Tension Leg Platforms (TLPs) and Tethered Buoyant Towers (TBTs) or Buoyant Leg Structures (BLS) are tethered to the seabed and are heave-restrained. [4]

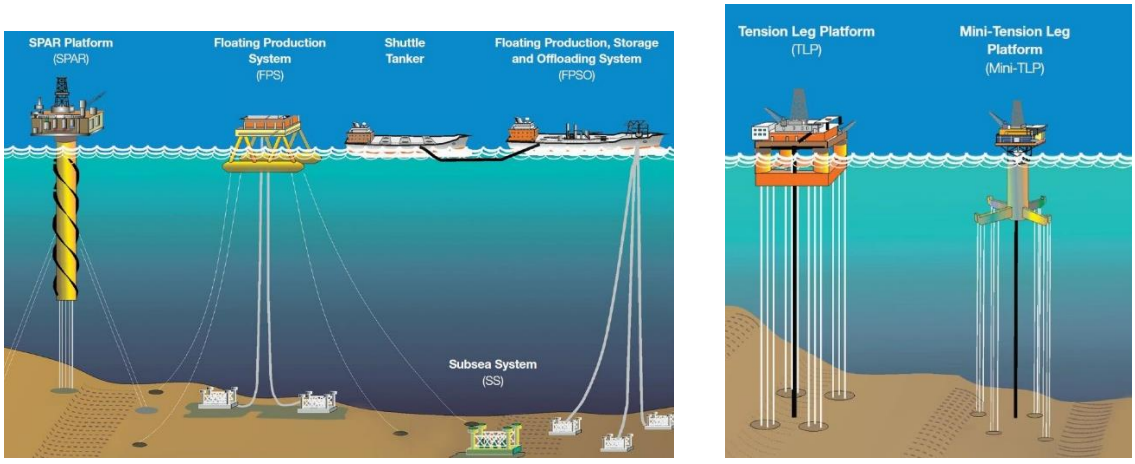

Figure 3 - Examples of floating offshore structures (Ilustration from the bureau of ocean energy management)

All these structures with global compliancy are structurally rigid. Compliancy is achieved with the mooring system. The sizing of floating structures is dominated by considerations of buoyancy and stability. Topside weight for these structures is more critical than it is for a bottom-founded structure. Semi-submersibles and ship-shaped hulls rely on waterplane area for stability. The centre of gravity is typically above the centre of buoyancy. Positively buoyant structures depend on a combination of waterplane area and tether stiffness to achieve stability. [4]

Floating structures are typically constructed from stiffened plate panels, which make up a displacement body. This method of construction involves different processes than those used in tubular construction for bottom-founded structures. Floating structures require dynamic risers to connect with wellheads on the seafloor. Drilling and production require a tieback at the mudline to the subsurface casing. Well control can require expensive subsea control systems (wet trees), or special low-motion vessels, which can support vertical risers in all weather conditions with well controls at the surface (dry trees). Floating platform functions may be grouped by their use as mobile drilling-type or production type. The most versatile MODUs are either ship-shaped or semi-submersibles. These units are also ideally suited not only to develop the field but also to produce from it. Most floating production units are neutrally buoyant structures (which allows six-degrees of freedom) which are intended to cost-effectively produce and export oil and gas. Since these structures have appreciable motions, the wells are typically subsea-completed and connected to the floating unit with flexible risers that are either a composite material or

a rigid steel with flexible configuration. While the production unit can be provided with a drilling unit, typically the wells are pre-drilled with a MODU and the production unit brought in to carry only a workover drilling system. Floating structures, except for Spars, TBTs and BLSs, are constructed upright, either dry or wet towed to installation site and connected to the mooring system or secured to the seabed with tethers. Floating structure hulls need to have adequate buoyancy to support the deck and various other systems. Thus, they are typically constructed of orthogonally stiffened large-diameter cylindrical shells or flat plates. Small diameter tubulars are susceptible to local instability and column buckling, while orthogonally stiffened systems are designed to meet hierarchical order of local, bay and general instability failure modes. [4] A unique aspect of floating structures is that, in addition to the applied functional deck gravity loads and environmental forces acting on the body, it is necessary to determine the inertial loads due to acceleration of the body in motion. A floating structure responds dynamically to wave, wind and current forces in a complicated way involving translation and rotation of the floater.

2.3. OFFSHORE LOADS AND STRUCTURES

2.3.1. INTRODUCTION

The static loads on the structure come from gravity loads, deck loads, hydrostatic loads and current loads. The dynamic loads originate from the variable wind and waves. [4] All offshore structures are subjected to this type of loads and in arctic or subarctic regions, ice loads may be important as well. Whilst the design of current buildings onshore is usually influenced mainly by the permanent and operating loads, the main challenge in the design of offshore structures is associated with environmental loads. Loads due to wind, waves and earthquake are discussed in more detail together with their idealizations for the various types of analyses. Fatigue cracks are therefore likely to evolve as a result of structures being subjected to environmental loads. Among these, waves and earthquakes are considered to be the most important sources of structural excitations. In spite of this, earthquake loads are only taken into consideration when assessing offshore structures close to or in tectonic fields. [7]

2.3.2. GRAVITY LOADS

Gravity loads include dead loads, operating and equipment weights, live loads and buoyancy loads. Live loads include the variable loads due to liquid and solid storage.

2.3.3. HYDROSTATIC LOADS

A floating structure when at rest in still water will experience hydrostatic pressures on its submerged part, which act normal to the surface of the structure. The forces generated from these pressures have a vertical component, which is equal to the gravitational force acting on the mass of the structure.

2.3.4. HYDRODYNAMIC AND DYNAMIC OF OFFSHORE STRUCTURES

The objective of studying the sea state is describing the forces acting on an offshore structure. It is of the essence that acceleration and velocity of a water particle is closely studied as these properties determine the force acting on the structure. DNV-GL provides recommended practice for assessing the sea state and converting of the ocean characteristics to hydrodynamic loads affecting offshore structures. The hydrodynamic and dynamic forces acting on a slender structure in general fluid are estimated by summing up all the sectional forces acting on each section of the structure. The force acting on a section is decomposed in a normal force f_N, a tangential force f_T, and in some cases a lift force f_L. [2] [8]

$$F_v = F_D + F_l = 0.5C_D\left(\frac{w}{g}\right)A|U| + \left(\frac{w}{g}\right)VC_m\left(\frac{dU}{dt}\right) \quad (1)$$

Where:

F_v - Hydrodynamic load vector per unit length acting normal to the axis of the member;

F_D - Drag force vector per unit length acting normal to the axis of the member in the member;

F_I - Inertia force per unit length acting normal to the axis of the member in the member;

C_d - Drag coefficient;

W - Weight density of the water;

g - Gravitational acceleration;

A - Projected area normal to the cylinder axis, per unit length (=D for circular members);

U - Component of the water velocity vector caused by wave plus current, normal to the axis of the member;

$|U|$ - Absolute value of U;

C_m - Inertia coefficient;

V‘- Displaced volume of the cylinder (= $\pi D^2/4$ for tubular members).

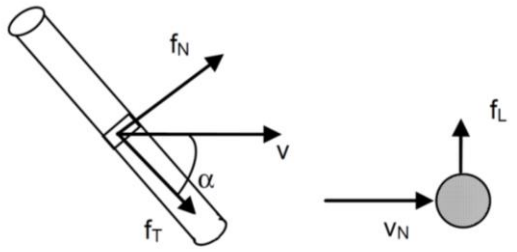

Figure 4 - Definition of normal force f_N, tangential force f_T and lift force f_L on an inclined slender structural member exposed to a water particle velocity V. [9]

Calculations of the hydrodynamic loads are based on linear wave theory and the application of the Morrison’s equation (see Equation (1)). Definition of the sea state is based on a scatter diagram valid for the Northern North Sea. When calculating the hydrodynamic loads on a structure based on Morison’s load formula, one should take account for the variation of the drag and mass coefficient. These coefficients are depending on the Reynolds number (R_e), the Keulegan-Carpenter number (K_c) and the surface roughness of the structure (Δ). [9]

The hydrodynamic coefficients are based on experimental data and the relation between these coefficients and the governing parameters are as follows:

$$C_D = C_D(R_e, K_C, \Delta)$$
$$C_M = C_M(R_e, K_C, \Delta) \quad (2)$$

Where:

C_D represents the drag coefficient and C_M the added mass coefficient.

The parameters in which the coefficients depend have lots of singularities and are defined as:

REYNOLDS NUMBER (RE)

The Reynolds number is a dimensionless parameter depending on the flow velocity, the cross-sectional diameter of the structure, and on the viscosity of the water.

$$R_e = \frac{u(D + 2t_m)}{v} \tag{3}$$

Where:

t_m - Thickness of marine growth;

D – Diameter;

v – Fluid kinematic viscosity.

The effect of marine growth must be considered when determining the effective diameter for the member under consideration. [9]

Table 1 - Marine thickness estimation

	56-69º N	59 – 72ºN	Marine growth density (kg/m3)
Water depth (m)	Thickness (mm)	Thickness (mm)	1325
+2-40	100	60	
Below 40	50	30	

For high Reynolds number ($R_e > 10^6$) and large K_C number, the dependence of the drag coefficient on roughness $\Delta = k/D$ may be taken as:

$$C_{DS}(\Delta) = \begin{cases} 0.65\ ;\ \Delta < 10^{-4}\ (smooth) \\ (29 + 4 * \log_{10}(\Delta))/20\ \ ;\ 10^{-4} < \Delta < 10^{-2} \\ 1.05\ ;\ \Delta > 10^{-2}\ (rough) \end{cases} \tag{4}$$

The variation of the drag coefficient as a function of Keulegan-Carpenter number K_C for smooth and marine growth covered (rough) circular cylinders for supercritical Reynolds numbers can be approximated by:

$$C_D = C_{DS}(\Delta) * \psi(K_C) \tag{5}$$

Where:

Ψ - Wake amplification factor.

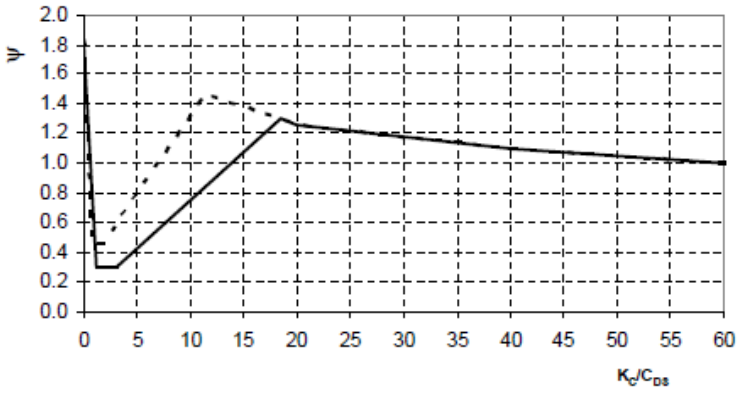

Figure 5 - Wake amplification factor ψ as function of K_C-number for smooth (C_{DS} = 0.65 - solid line) and rough (C_{DS} = 1.05 - dotted line) [9]

KEULEGAN-CARPENTER (K_c)

Depends on the wave height (*H*) and the cross-sectional diameter of the structure (*D*). For sinusoidal flow, the K_C is obtained by the following equation:

$$K_C = \frac{2\pi}{D + 2t_m} \tag{6}$$

For $K_C < 3$, C_M can be assumed to be independent of K_C number and equal to the theoretical value $C_M = 2$ for both smooth and rough cylinders. [9]

For $K_C > 3$, the mass coefficient can be found from the formula:

$$C_M = \begin{cases} 2 - 0.044(K_C - 3) \\ 1.6 - (C_{DS} - 0.65) \end{cases} \tag{7}$$

For low Keulegan-Carpenter numbers ($K_C < 12$), the wake amplification factor can be taken as:

$$\psi\,(K_C) = \begin{cases} C_\pi + 0.10(K_C - 12) & ; 2 \le K_C < 12 \\ C_\pi - 1 & ; 0.75 \le K_C < 2 \\ C_\pi - 1 - 2(K_C - 0.75) & ; K_C \le 0.75 \end{cases} \tag{8}$$

Where:

$$C_\pi = 1.50 - 0.024 * (\frac{12}{C_{DS}(\Delta)} - 10) \tag{9}$$

The Keulegan Carpenter number and the roughness of the material will have an impact on the mass coefficient for the case under consideration as well. The added mass coefficients for smooth and rough structures, for large values of K_C, is 1.6 for Smooth cylinders and 1.2 for rough cylinders

Further, for small values of K_C ($K_C < 3$), the added mass coefficient can be taken as C_A=1 for both rough and smooth cylinders. [9]

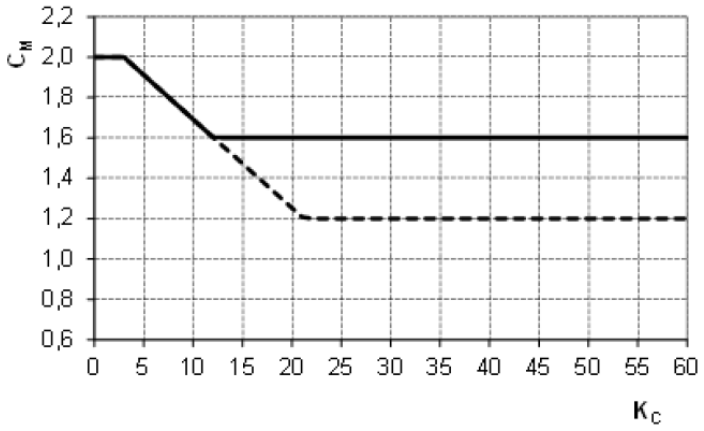

Figure 6 - Relation between the added mass and the Keulegan-Carpenter number for both rough and smooth cylinders [9]

2.3.4.1 CURRENT AND WAVE LOADS

Since the wave flow is not steady and since the linear wave flow follows a simple harmonic motion, the flow around the cylinder will be more complex than the steady flow. As the flow changes direction, the low-pressure region will move from the downstream to the upstream side. Thus, the force on the cylinder will change direction every half a wave cycle. Combining the effects of water particle velocity and acceleration on the structure, the loading on the structure due to a regular wave is computed from the empirical formula commonly known as the Morison equation. Offshore fixed structures are considered to be drag dominated, therefore the Morison's equation is employed by most researchers. The Morison's equation assumes that the total wave forces acting on a structure can be calculated by linear superimposition of the drag and inertia forces [9], mathematically formulated as:

$$F_W = F_D + F_I = \frac{1}{2} * C_D * \rho * D * |\vec{u}| * \vec{u} + \frac{1}{4} * C_M * \pi * \rho * D^2 * \frac{\partial \vec{u}}{\partial t} \quad (10)$$

Where:

F_w – Wave and Current force;

F_D – Drag force;

F_I - Inertia force;

C_D – Drag coefficient;

C_M – Coefficient of virtual mass;

ρ – Mass density of water;

D – Diameter;

$\vec{u}$ – Velocity of wave particles;

$\frac{\partial \vec{u}}{\partial t}$ – Local water particle acceleration.

Wind-generated gravity waves will be modelled in order to obtain $\vec{u}$ and $\frac{\partial \vec{u}}{\partial t}$, since they are responsible for a significant proportion of the environmental forces acting on offshore structures. To fatigue life analysis linear wave theory is relevant. Also, to evaluate the sea state, the wave conditions can be divided into two classes:

- Wind sea; and,
- Swell sea.

Wind sea is described as waves generated from local fetching winds, while swell sea is long period waves generated by distant storms. [10] The case of study is located on the Northern North Sea. Stokes Wave theory is the most commonly used in the analysis of offshore structures because of its accuracy in predicting the kinematic properties of the wave. The Stokes wave expansion is an expansion of the surface elevation in powers of the linear wave height, H. A first-order Stokes wave is identical to a linear wave. Linear waves and Stokes waves are based on perturbation theory and provide directly wave kinematics below z = 0. [9]

Therefore, three different waves will be chosen in reference with a scatter diagram valid for locations in the case of study sea (see Figure 7). The waves are simulated and assumed to be consecutively generated during the course of one day. The wave height is labelled as significant wave height while the period is labelled as peak period. The significant wave height H_S is defined as the average height of the highest one third waves in a short term record length. The peak period, T_p, is the wave period at which the wave

energy spectrum has its maximum value. In a short-term storm duration, or short term wave conditions, the sea state is assumed to be stationary for an interval of 20 minutes up to 3 or 6 hours. [4] [10]

Furthermore, for a storm duration of 3 hours, the wave loads acting on the jacket platform leg are to be calculated from the maximum wave height $H_{máx.}$

Experimental data show that for a 3-hour storm duration, the maximum wave height is to be taken from Equation (11): [11]

$$H_{max} = 1.86 * H_s \tag{11}$$

h_s (m)	t_p (s)																		
	3	4	5	6	7	8	9	10	11	12	13	14	15	16	17	18	19	20	>20
0.5	18	15	123	113	110	390	260	91	38	42	32	3	19	13	9	1	3	2	7
1.0	16	49	675	433	589	1442	1802	959	273	344	125	33	64	29	13	1	7	1	6
1.5	5	32	417	893	1107	1486	2757	1786	636	731	299	121	92	43	18	10	5	2	13
2.0	1	0	102	741	1290	1496	2575	1968	780	868	492	200	116	51	31	8	4	4	8
2.5	0	0	9	256	969	1303	2045	1892	803	941	484	181	157	58	23	19	5	1	8
3.0	0	0	1	45	438	1029	1702	1898	705	957	560	218	196	92	40	11	4	2	5
3.5	0	0	1	4	124	650	1169	1701	647	865	456	237	162	100	36	12	6	1	5
4.0	0	0	2	0	33	270	780	1369	573	868	427	193	157	91	51	13	3	0	1
4.5	0	0	0	0	3	90	459	1017	466	761	380	127	137	86	31	23	6	5	0
5.0	0	0	0	0	0	15	228	647	408	737	354	119	96	50	32	18	2	4	1
5.5	0	0	0	0	0	2	68	337	363	580	283	94	92	31	24	10	6	2	0
6.0	0	0	0	0	0	1	20	166	221	418	307	63	76	24	13	9	4	0	0
6.5	0	0	0	0	0	0	5	50	140	260	257	59	49	20	12	4	2	2	2

Figure 7 - Scatter diagram for the Northern North Sea [24]

Morrison's formula is applied when evaluating the hydrodynamic forces acting on slender tubular members. The waves are assumed to be unidirectional and linear wave theory is used to obtain the water particle motions at any given elevation. When linearizing the drag force, one must assess whether one should take account for the vibration amplitude of the structural component or not. If the vibration amplitude of the structural component is small in relation to the wave induced water particle motions, it is sufficient that the drag force is calculated without taking account for the velocity of the structural member. [12]

2.3.4.2 WIND LOADS

The obstruction to the free flow of wind by a structure produces a differential pressure, which results in wind forces [9]. The static drag force due to wind on large-scale structures accounts for approximately 25% of the total overturning moment and about 15% of the total force on the structure. The general wind force on a rigidly held, horizontal, circular cylinder is calculated as [13]:

$$F(z) = \frac{1}{2} C_D \rho S U_G(z)^2 \tag{12}$$

Where:
C_D – Drag coefficient;

ρ – density of the air (1.2kg/m^3);

S – Frontal area (facing the wind);
U_G – Gust wind at z;

z – Depth location.

The gust wind speed is defined as the average wind speed over a time interval of 3 seconds measured at an elevation of 10 m above sea water line, and can be estimated as:

$$U_G = U_G(10) * \left(\frac{z}{10}\right)^{0.1} \quad (13)$$

Where:

U_G (10) – Gust wind speed at 10 m above sea water line

Wind loads represent a contribution of ~ 5% of the environmental loading, while currents are often of unimportance due to the nature of their frequency - which is not sufficient to excite the considerable 214bigger structures. [14] However, currents remain an important factor when assessing stability of subsea equipment. [15]

2.3.5 Ice and Snow Loads

2.3.5.1 Snow

The snow actions given in NS 3491-3 for the relevant coastal municipality may be used as extreme snow action close to the shore. For other areas where more accurate meteorological observations have not been performed, characteristic snow action may be set equal to 0.5 kPa for the entire Norwegian continental shelf. The shape factors given in NS 3491-3 may be used. [9]

2.3.5.2 Ice

When calculating wave, current and wind actions, increases in dimensions and changes in the shape and surface roughness of the structure as a result of accumulated:

a) ice from sea spray which covers the whole circumference of the element;

b) ice from rain covers all surfaces facing upwards or against the wind. For tubular structures it may be assumed that ice covers half the circumference.

2.3.6. Accidental Loads

These loads may occur due to human error, operational or equipment failures or uncertainties associated with the methods used to predict operational, environmental or construction loads:

a) Vessel impact loads from construction equipment (barges, work boats, etc.), supply and crew boats, shuttle tankers, merchant vessels, fishing or pleasure boats cruising in the area.

b) Dropped objects. These may be drilling supplies (drill pipe, casing, collars, BOP stack, etc.), supply packages, equipment on skids and modules that may be dropped by deck or construction vessel-mounted cranes. Drill pipe is lifted to the deck in large quantities and dropped drill pipes and collars are the major sources of injury and damage to the platform components and well systems.

c) Fires and explosions caused by process equipment, vessel or pipe failures/leaks, blowouts and riser wall failures, etc.

d) Environmental events beyond those considered in the design. Environmental parameters carry high level of uncertainty and there have been a number of instances where extreme environmental effects much higher than what is assumed for the design return period have been experienced in the past. [4]

2.3.8. OFFSHORE STRUCTURES DESIGN

The design of offshore structures is complex, and it is different for every type of offshore structure. Since most of the offshore structures are jackets then the design of it will be focused deeply. The jacket design can be resumed in three essential phases:

- Preliminary Sizing;

- Detailed Analysis;

- Installation aids design.

In the preliminary sizing, it should be specified a preliminary set of sketches with main dimensions and tubular sizes, based on the specification. All the details about the structural components must be defined particularly the architecture, the external and internal forces applied, the diameters of the structure and the thicknesses associated. After all the architecture and sizes of the jacket tubes have been estimated it should be carried a three-dimensional study of the structure to perform a Fatigue and Seismic analysis. [16]

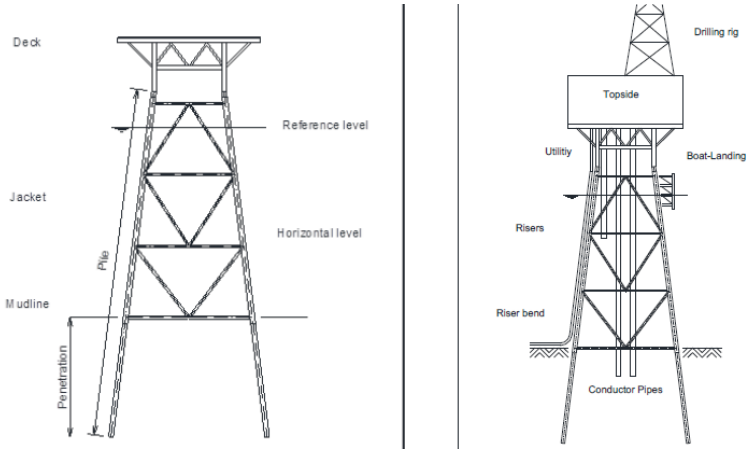

Figure 8 - Terminology for a Jacket type of structure [16]

2.4. OFFSHORE TUBULAR JOINTS

2.4.1. INTRODUCTION

Three dimensional structures fabricated from steel tubular sections are widely used these days in various structures such as trusses, high rise buildings, towers for offshore wind turbines, and offshore installations. On offshore structures its widely used circular tubular hollow sections. If connected two or more tubular sections, it's referred as tubular joint.

Many of these structures undergo several types of cyclic environmental/operational loading as wind, wave, ice and traffic loads during their service lives. [2]

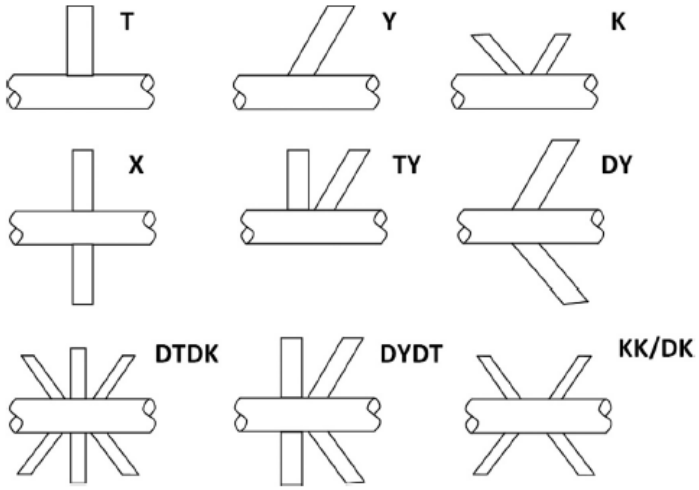

Figure 9 - Types of tubular joints along with their nomenclature [2]

For a brace to be considered as K-joint classification, the axial force in the brace should be balanced to within 10% by forces in other braces in the same plane and on the same side of the joint. [12]

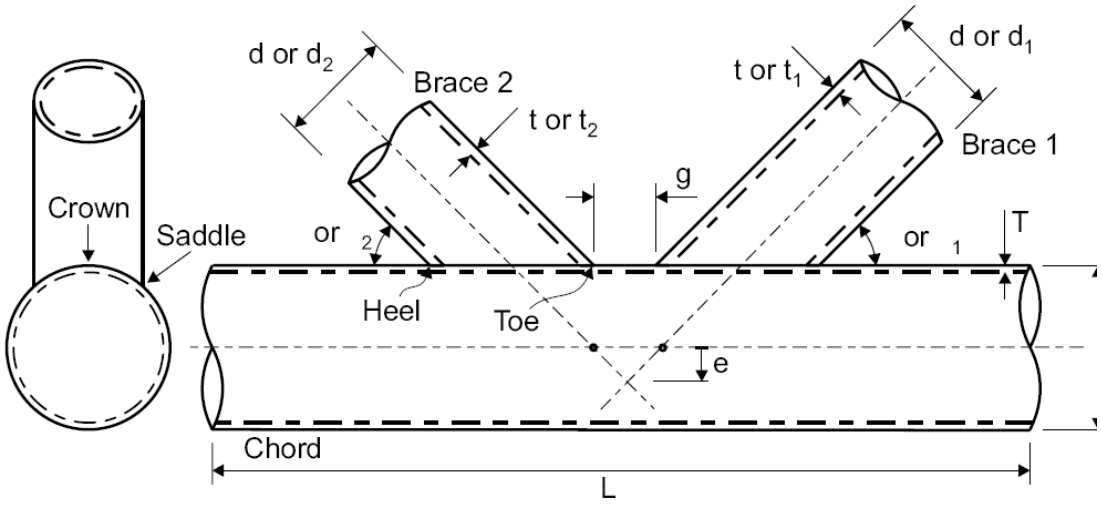

d = brace diameter
t = brace wall thickness
θ = angle of brace / chord intersection
L = chord length (distance between end restraints)
D = chord diameter
T = chord wall thickness
g = gap (distance between brace toes)
e = joint eccentricity

Figure 10 - Definition of the geometrical parameters of a K-Joint [7]

2.4.2. Definition of SCF or K_T

A stress concentration factor may be defined as the ratio of hot spot stress range over nominal stress range. Fabrication tolerances increase the stress range at butt welds and cruciform joints. For as welded butt welds and cruciform joints there are already included some tolerances in the S-N curves that are used. However, the value of fabrication tolerance to be included in design calculation depends also on what is the expected as-built tolerance as compared with that required in the fabrication standard. [9]

In hot-spot stress approach, the ratio of the hot-spot stress (σ_{ss}) and the nominal stress (σ_n) in an attached brace/chord is defined as the stress concentration factor (SCF) and is expressed as follow:

$$SCF = \frac{\sigma_{ss}}{\sigma_n} \tag{14}$$

Where:

σ_{ss} – Hot-spot stress;

σ_n – Nominal stress;

SCF – Stress concentration factor.

Generally, one member (brace/chord) is loaded at a time while evaluating SCF. If chord or other members are also loaded along with the brace member in a joint, additional hot-spot stresses are generated. If chord or other members are also loaded along with the brace member in a joint, additional hot-spot stresses are generated. [11] Assessing the magnitude of the stress concentration is a requirement to deal with the fatigue problem, because its presence has aggravated the fatigue of tubular joints in many existing offshore structures. [17]. For tubular welded joints, much research has been carried out towards the estimation of the HSS range through the SCF; SCFs may be obtained analytically from the elasticity theory, computationally from the FE method, and experimentally using methods such as photo elasticity or strain measurements. Although the analytical solutions assume that the material is isotropic and homogeneous, it is possible to achieve a good agreement with the experimental work if it is conducted with precision. [18]

2.4.3. Calculations on Stress Concentration Factor

Stress concentration factors for the different frame elements and the different loading conditions are calculated in reference with E. The stress concentration factors for the chord are calculated at two different locations in order to identify the location where the concentration is at its highest (check red line on K-Joint drawing). In order to calculate the stress concentration factors, first it is necessary to define the geometrical parameters of the tubular joints which are included in the calculation of the stress concentration factor. Furthermore, the hot spot stress is in reference with DNV to be evaluated at 8 spots around the circumference of the intersection, as shown in Figure 12.

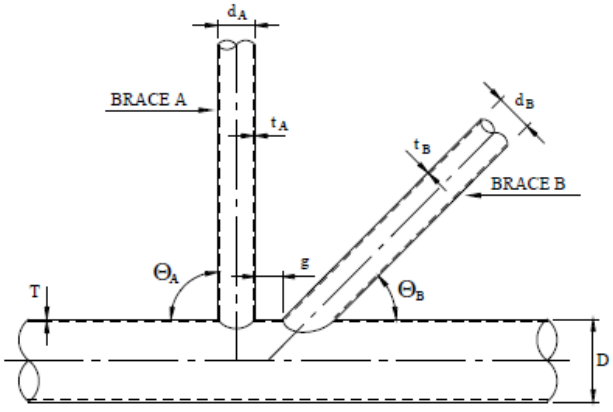

Figure 11 - Definition of geometrical parameters

The “d” means the diameter of the brace, “t” the thickness of the brace, “T” the thickness of the chord and “D” the diameter of the chord. There are three commonly named locations along the brace-chord intersection: saddle, crown toe and crown heel. To the estimation of the stress concentration factors, it

is necessary to also calculate the parameters associated with the thicknesses and the diameters of chord and braces, which are given by the following equations:

$$\beta = \frac{d}{D} \tag{15}$$

$$\tau = \frac{t}{T} \tag{16}$$

$$\gamma = \frac{D}{2T} \tag{17}$$

$$\zeta = \frac{g}{D} \tag{18}$$

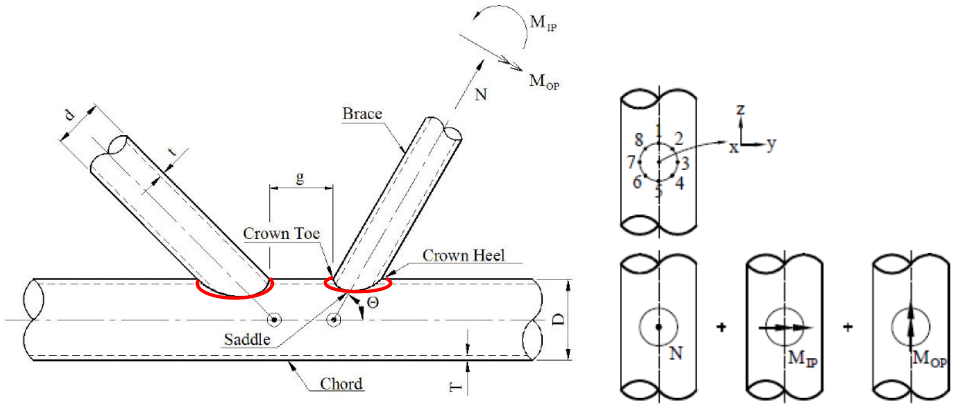

Figure 12 - Definition of the stress concentration zone and their superposition

The stresses in tubular joints due to brace loads are calculated at the crown and the saddle points. Then the hot spot stress at these points is derived by summation of the single stress components from axial, in-plane and out of plane action. [10]

$$\sigma_1 = SCF_{AC}\sigma_x + SCF_{MIP}\sigma_{my} \tag{19}$$

$$\sigma_2 = \frac{1}{2}(SCF_{AC} + SCF_{AS})\sigma_x + \frac{1}{2}\sqrt{2}\,SCF_{MIP}\sigma_{my} - \frac{1}{2}\sqrt{2}\,SCF_{MOP}\sigma_{mz} \tag{20}$$

$$\sigma_3 = SCF_{AS}\sigma_x + SCF_{MOP}\sigma_{mz} \tag{21}$$

$$\sigma_4 = \frac{1}{2}(SCF_{AC} + SCF_{AS})\sigma_x - \frac{1}{2}\sqrt{2}\,SCF_{MIP}\sigma_{my} - \frac{1}{2}\sqrt{2}\,SCF_{MOP}\sigma_{mz} \tag{22}$$

$$\sigma_5 = SCF_{AC}\sigma_x - SCF_{MIP}\sigma_{my} \tag{23}$$

$$\sigma_6 = \frac{1}{2}(SCF_{AC} + SCF_{AS})\sigma_x - \frac{1}{2}\sqrt{2}\,SCF_{MIP}\sigma_{my} + \frac{1}{2}\sqrt{2}\,SCF_{MOP}\sigma_{mz} \tag{24}$$

$$\sigma_7 = SCF_{AS}\sigma_x + SCF_{MOP}\sigma_{mz} \tag{25}$$

$$\sigma_8 = \frac{1}{2}(SCF_{AC} + SCF_{AS})\sigma_x + \frac{1}{2}\sqrt{2}\,SCF_{MIP}\sigma_{my} + \frac{1}{2}\sqrt{2}\,SCF_{MOP}\sigma_{mz} \tag{26}$$

Where:

- σ_x, σ_{my} and σ_{mz} are the maximum nominal stresses due to axial load and bending in-plane and out-plane, respectively;
- SCF_{AS} and SCF_{AC} is the stress concentration factor at the saddle for axial load and SCF_{AC} is the stress concentration factor at the crown; and,
- SCF_{MIP} is the stress concentration factor for in plane moment and SCF_{MOP} is the stress concentration factor for out of plane bending. More calculations are done to calculate the SCF values for the different type of loads further on chapter 3 when using DNVGL-RP-C203. [10]

2.4.4. Stress Concentration Factors for Different Tubular Joints

SCF parametric formulas have been determined based on a large number of finite element analyses and cross-checked with either full scale or model tests. They are based on many man years of work by numerous research and there are different researchers with their own parametric equations and its accuracy when compared with simulated models. In Figures 13 and 14 are presented different parametric formulas to calculate the SCF for different type of joints, the parametric equations shown are based on Efthymiou's research and are frequently used on the fatigue design code. [10]

Load type and fixity conditions	*SCF equations*	*Eqn. No.*	*Short chord correction*
Axial load- Chord ends fixed 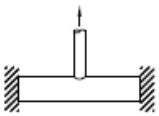	Chord saddle: $\gamma\tau^{1.1}\left(1.11-3(\beta-0.52)^2\right)(\sin\theta)^{1.6}$	(1)	F1
	Chord crown: $\gamma^{0.2}\tau\left(2.65+5(\beta-0.65)^2\right)+\tau\beta(0.25\alpha-3)\sin\theta$	(2)	None
	Brace saddle: $1.3+\gamma\tau^{0.52}\alpha^{0.1}\left(0.187-1.25\beta^{1.1}(\beta-0.96)\right)(\sin\theta)^{(2.7-0.01\alpha)}$	(3)	F1
	Brace crown: $3+\gamma^{1.2}\left(0.12\exp(-4\beta)+0.011\beta^2-0.045\right)+\beta\tau(0.1\alpha-1.2)$	(4)	None
Axial load- General fixity conditions 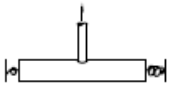	Chord saddle: $(\text{Eqn.}(1))+C_1(0.8\alpha-6)\tau\beta^2\left(1-\beta^2\right)^{0.5}(\sin2\theta)^2$	(5)	F2
	Chord crown: $\gamma^{0.2}\tau\left(2.65+5(\beta-0.65)^2\right)+\tau\beta(C_2\alpha-3)\sin\theta$	(6a)	None
	Alternatively $SCF_{Cc}=\gamma^{0.2}\tau(2.65+5(\beta-0.65)^2)-3\tau\beta\sin\theta+\frac{\sigma_{Bending\,Chord}}{\sigma_{Axial\,brace}}SCF_{att}$ where $\sigma_{Bending\,Chord}$ = nominal bending stress in the chord $\sigma_{Axial\,brace}$ = nominal axial stress in the brace. SCF_{att} = stress concentration factor for an attachment = 1.27	(6b)	
	Brace saddle: (Eqn. (3))		F2
	Brace crown: $3+\gamma^{1.2}\left(0.12\exp(-4\beta)+0.011\beta^2-0.045\right)+\beta\tau\left(C_3\alpha-1.2\right)$	(7a)	None
	Alternatively $SCF_{Bc}=3+\gamma^{1.2}(0.12\exp(-4\beta)+0.011\beta^2-0.045)-1.2\beta\tau+\frac{0.4\sigma_{Bending\,Chord}}{\sigma_{Axial\,brace}}SCF_{att}$	(7b)	

Load type and fixity conditions	*SCF equations*	*Eqn. No.*	*Short chord correction*
In-plane bending 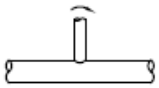	Chord crown: $1.45\beta\,\tau^{0.85}\gamma^{(1-0.68\beta)}(\sin\theta)^{0.7}$ Brace crown: $1+0.65\beta\,\tau^{0.4}\gamma^{(1.09-0.77\beta)}(\sin\theta)^{(0.06\gamma-1.16)}$	(8) (9)	None None
Out-of-plane bending 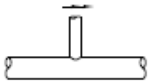	Chord saddle: $\gamma\,\tau\,\beta\left(1.7-1.05\beta^3\right)(\sin\theta)^{1.6}$ Brace saddle: $\tau^{-0.54}\gamma^{-0.05}\left(0.99-0.47\beta+0.08\beta^4\right)\cdot$ (Eqn.10))	(10) (11)	F3 F3
Short chord correction factors (α < 12) $F1=1-\left(0.83\beta-0.56\beta^2-0.02\right)\gamma^{0.23}\exp\left(-0.21\,\gamma^{-1.16}\alpha^{2.5}\right)$ $F2=1-\left(1.43\beta-0.97\beta^2-0.03\right)\gamma^{0.04}\exp\left(-0.71\,\gamma^{-1.38}\alpha^{2.5}\right)$ $F3=1-0.55\,\beta^{1.8}\gamma^{0.16}\exp\left(-0.49\,\gamma^{-0.89}\alpha^{1.8}\right)$ where $\exp(x)=e^x$		Chord-end fixity parameter C1 = 2(C-0.5) C2 = C/2 C3 = C/5 C = chord end fixity parameter 0.5 ≤ C ≤ 1.0, Typically C = 0.7	

Figure 13 - Stress concentration factors for simple tubular T/Y joints [10]

Load type and fixity conditions	*SCF equation*	*Eqn. no.*
Axial load (balanced) 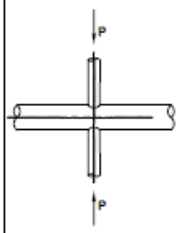	Chord saddle: $3.87\,\gamma\,\tau\,\beta\left(1.10-\beta^{1.8}\right)(\sin\theta)^{1.7}$ Chord crown: $\gamma^{0.2}\tau\left(2.65+5(\beta-0.65)^2\right)-3\,\tau\,\beta\sin\theta$ Brace saddle: $1+1.9\,\gamma\,\tau^{0.5}\beta^{0.9}\left(1.09-\beta^{1.7}\right)(\sin\theta)^{2.5}$ Brace crown: $3+\gamma^{1.2}\left(0.12\exp\left(-4\beta\right)+0.011\,\beta^2-0.045\right)$ In joints with short cords (α < 12) the saddle SCF can be reduced by the factor F1 (fixed chord ends) or F2 (pinned chord ends) where $F1=1-\left(0.83\beta-0.56\beta^2-0.02\right)\gamma^{0.23}\exp\left(-0.21\,\gamma^{-1.16}\alpha^{2.5}\right)$ $F2=1-\left(1.43\beta-0.97\beta^2-0.03\right)\gamma^{0.04}\exp\left(-0.71\,\gamma^{-1.38}\alpha^{2.5}\right)$	(12) (13) (14) (15)
In plane bending 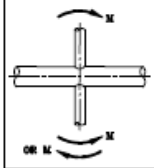	Chord crown: (Eqn. (8)) Brace crown: (Eqn. (9))	
Out of plane bending (balanced) 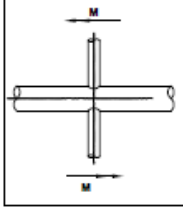	Chord saddle: $\gamma\,\tau\,\beta\left(1.56-1.34\beta^4\right)(\sin\theta)^{1.6}$ Brace saddle: $\tau^{-0.54}\gamma^{-0.05}\left(0.99-0.47\beta+0.08\beta^4\right)\cdot$ (Eqn.(16)) In joints with short chords (α < 12) eqns. (16) and (17) can be reduced by the factor F3 where: $F3=1-0.55\,\beta^{1.8}\gamma^{0.16}\exp\left(-0.49\,\gamma^{-0.89}\alpha^{1.8}\right)$	(16) (17)

Load type and fixity conditions	*SCF equation*	*Eqn. no.*
Axial load in one brace only 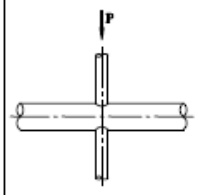	Chord saddle: $\left(1 - 0.26\beta^3\right) \cdot$ (Eqn.(5))	(18)
	Chord crown: (Eqn.6)) Brace saddle: $\left(1 - 0.26\beta^3\right) \cdot$ (Eqn.(3))	(19)
	Brace crown: (Eqn. (7)) In joints with short chords ($\alpha < 12$) the saddle SCFs can be reduced by the factor F1 (fixed chord ends) or F2 (pinned chord ends) where: $F1 = 1 - \left(0.83\beta - 0.56\beta^2 - 0.02\right)\gamma^{0.23}\exp\left(-0.21\gamma^{-1.16}\alpha^{2.5}\right)$ $F2 = 1 - \left(1.43\beta - 0.97\beta^2 - 0.03\right)\gamma^{0.04}\exp\left(-0.71\gamma^{-1.38}\alpha^{2.5}\right)$	
Out-of-plane bending on one brace only: 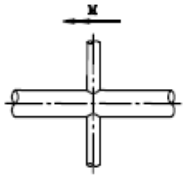	Chord saddle: (Eqn. (10)) Brace saddle: (Eqn. (11)) In joints with short chords ($\alpha < 12$) eqns. (10) and (11) can be reduced by the factor F3 where: $F3 = 1 - 0.55\beta^{1.8}\gamma^{0.16}\exp\left(-0.49\gamma^{-0.89}\alpha^{1.8}\right)$	

Figure 14 - Stress concentration factors for simple X tubular joints [10]

2.5. REVIEW ON FINITE ELEMENT ANALYSIS EVALUATION OF STRESS CONCENTRATION FACTOR

The high costs of testing scaled steel models have led most of the studies to use shell FE models for deriving the SCF parametric equations for all three load cases. There are several studies using finite element models to study the influence of different geometrical parameters on stress concentration factor evaluation. Many authors carried out lots of researches with simulated models in order to understand how the geometrical parameters and the loads associated influence the evaluation of the stress concentration factor on different tubular joints. Minguez developed a finite element analysis of a T-Joint where it was compared the main differences between a shell model and solid model in the evaluation of the stress concentration factor. Therefore, all degrees of freedom in the models were fixed at the chord ends. [19]

To the shell model, the stresses were measured at the mid-section, without considering the effect of a weld fillet. In order to reduce computational time, the mesh of all the models is characterised by fine elements near the intersection and coarser elements in regions where the stresses are more evenly distributed. T-joints with a brace length of about $0.4L$ were used in order to avoid the effect of short brace length. Chord lengths greater than $6D$ were used to ensure that stresses at the brace/chord intersection were not affected by the boundary conditions. The density, Young's modulus and Poisson's ratio were taken to be 7850 kg/m3, 207 GPa and 0.3, respectively. [19]

Solid models were characterised by eight-node hexahedral elements. Models were subjected to axial, IPB and OPB load cases, and both chord ends were rigidly fixed. The SCFs for the solid FE models without fillet weld were estimated directly from the values obtained at the brace/chord intersection in the same manner as for the Shell FE models, except that the maximum principal stresses were measured at the external surface. The mechanical properties and the restrictions of the brace and chord lengths were the same as the shell model. [19]

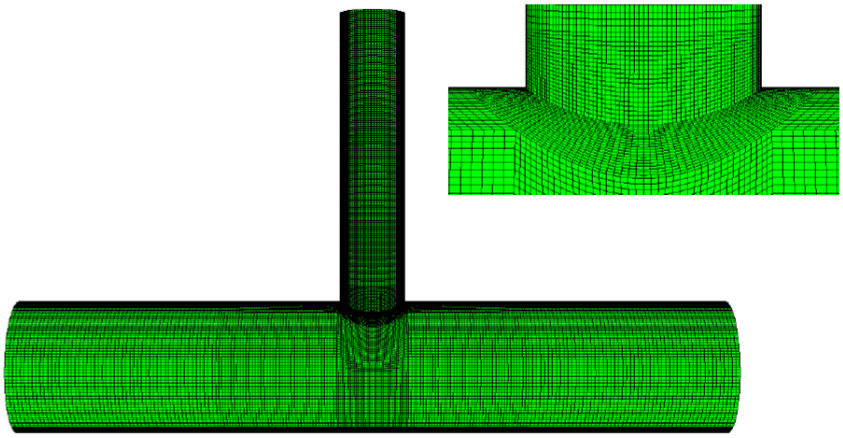

Figure 15 - Typical mesh used to model the T-joint [19]

In Table 2 are displayed all the results from the simulated model to comparison and discussion. To the analysis of the solid model, the stress concentration factors were estimated directly from the values obtained at the brace/chord intersection in the same manner as for the Shell FE models, except that the maximum principal stresses were measured at the external surface. That way it is not shown the results of the stress concentration factor for each brace and chord but the maximum values for the discussion. [19]

Table 2 - SCFs comparision [19]

	Approach	Chord		Brace	
		Crown	Saddle	Crown	Saddle
Axial	Efthymiou Equations	2.203	6.602	2.400	6.407
	Lloyd's Equations	2.596	5.960	1.883	4.707
	Shell FE results	1.788	5.805	2.681	8.218
		Crown		Saddle	
	Solid FE results	2.917		9.434	
In-plane bending	Efthymiou Equations	2.175	-	2.494	-
	Lloyd's Equations	1.895	-	1.067	-
	Shell FE results	2.020	0.064	2.865	0.247
		Crown		Saddle	
	Solid FE results	0.294		6.815	
Out-of-plane bending	Efthymiou Equations	-	5.060	-	5.391
	Lloyd's Equations	-	4.380	-	3.390
	Shell FE results	-	4.591	-	6.097
		Crown		Saddle	
	Solid FE results	0.294		6.815	

As observed for the shell FE models, the higher stress concentration is located at the saddle for axial and OPB cases, and close to the crown for the IPB case. If the shell FEA results are compared with these results, it can be observed that there is an increase of the SCF of 14.8% for axial loading. At the crown, there is an increase in the SCF of 11.7% for IPB loading. It is reasonable that the solid SCFs are slightly higher, since the shell results are measured at the mid-section, whereas the solid results are measured on the external surface. These studies measured the stresses at the mid-section of the brace-chord intersection without considering the effect of a weld fillet. A comparison between the fatigue life predictions obtained by the Efthymiou's SCFs and the hot-spot SCFs of 3D solid FE models considering the weldment was performed. The validation of the 3D solid FE models with the weldment was also carried out by analysing the results obtained by 3D solid and 3D shell FE models without the weldment. The hot-spot SCF values of the complete weld profile FE models were compared with the Efthymiou's SCFs and proven to be lower. It was proven clearly that even slight overestimations of the SCFs will represent a great reduction on service lives (even differences over 100 years), since the scale is logarithmic. [19]

2.5. Fatigue of Offshore Structures

2.5.1. Introduction

There are different approaches for fatigue life analysis of a welded joint. These methods are distinguished mainly by the parameters used for the description of fatigue life 'N' or fatigue strength. Welded joints are commonly assessed with respect to fatigue life by applying the S-N curve, also known as the Wöhler curve approach. S-N curves vary widely for different classes of material, and are affected by many factors such as temperature, mean stress, residual stress and chemical environment.

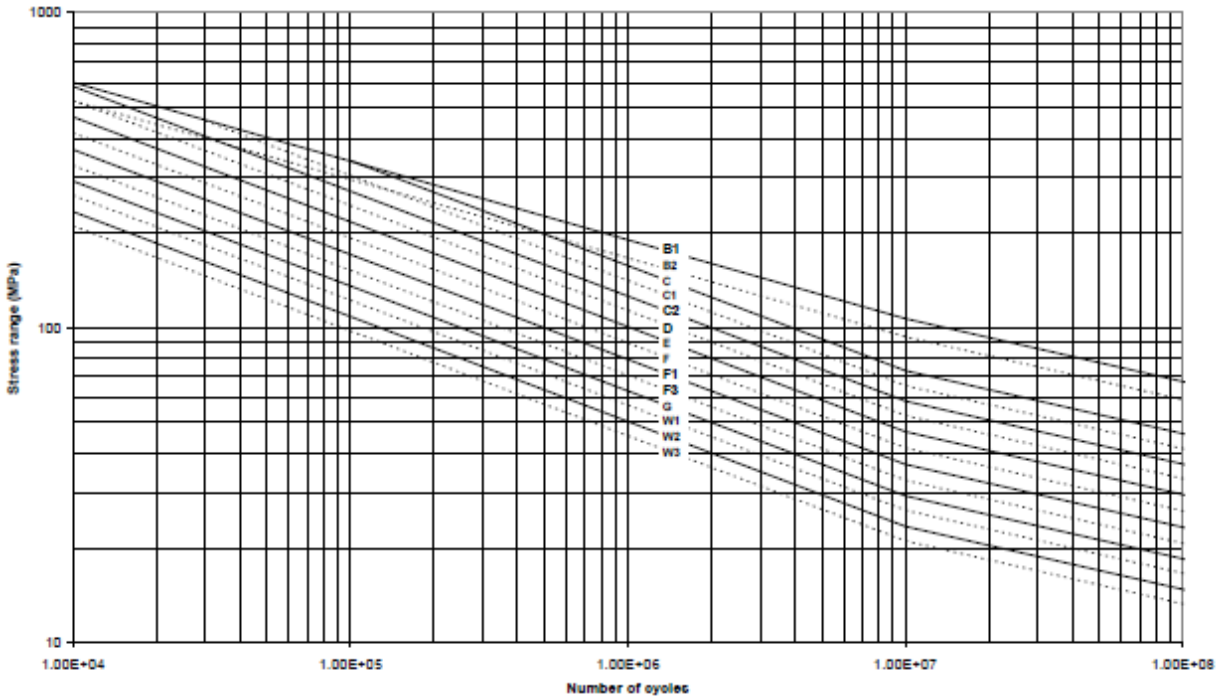

Figure 16 - Example of S-N curve [10]

These approaches include nominal stress approach, structural or hot-spot stress approach, notch stress or notch intensity approach, notch strain approach, crack propagation approach, etc. Among these, hot-spot stress is the most widely used and recommended by various fatigue design guidelines, especially

on a welded joint. [31] Engineers are continuously putting effort to improve monitoring techniques to raise structural health. The modern day technology allows us to measure the loading history on most of the existing civil structures, whether they are at sea or onshore.

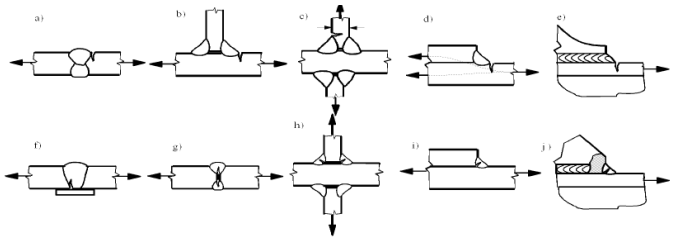

Figure 17 - Various locations of crack propagation in welded joints [21]

The fatigue life predictions of offshore welded joints are impaired by uncertainties in the loads, strengths and numerical models. These uncertainties may be classified into four groups:

- Physical or inherent uncertainty is related to natural variability. For example: marine growth, wind speed, current velocity, wave height and period, corrosion, scour, heat affected zone, or yield stress due to production variability.
- Measurement uncertainty is produced by imperfect measurements. For example: crack length, strain or stress measurements.
- Statistical uncertainty is caused by limited sample sizes of observed quantities. For example: drag and inertia coefficients, S-N curve coefficients, or soil properties.
- Model uncertainty is due to limited knowledge or idealizations of the mathematical models used or to the choice of probability distribution types for the stochastic variables. For example: joint thickness effect, wave theory selection, element type and mesh density of FE models, or the use of a linear damage accumulation concept instead of a nonlinear approach. [22]

The multiaxial fatigue life evaluations can be made using several criteria, such as, criteria based on stresses, strains and energy. There are several multiaxial damage parameters being proposed in the literature covering low-cycle fatigue, high-cycle fatigue, proportional and non-proportional loading conditions. The multiaxial fracture mechanics approaches are defined using the three cracks deformation modes. To procedure into the fatigue analysis of the offshore connections there are some steps to take account for:

- Definition of the global/local interface with the critical region identification and interpolation region specification;
- Local model definition of the connection in order to build the local model using linear-elastic analysis aiming at obtaining the stiffness of the joint;
- An elastoplastic analysis of the local model is also required to determine the maximum principal stresses and strains at the fatigue critical points;
- Local multiaxial fatigue damage analysis at the critical point using a multiaxial damage criterion. [6]

2.5.2. DAMAGE ACCUMULATION METHOD

The fatigue life may be calculated based on the S-N fatigue approach under the assumption of linear cumulative damage (Palmgren-Miner rule).

When the Fatigue Demand and Fatigue Strength are established, they are compared and the adequacy of the structural component with respect to fatigue is assessed using a damage accumulation rule and a fatigue safety check. Regarding the first of these, it is accepted practice that the fatigue damage experienced by the structure from each interval of applied stress range can be obtained as the ratio of the number of cycles (*n*) of that stress range applied to the structure to the number of cycles (N) that will cause a fatigue failure at that stress range, as determined from the S-N curve. The total or cumulative fatigue damage (*D*) is the linear summation of the individual damage from all the considered stress range intervals. [10]

$$D = \sum_{i=1}^{j} \frac{n_i}{N_i} \tag{27}$$

Where:

D – Cumulative fatigue damage;

n_i - Number of cycles the structural detail endures at stress range S_i;

N_i - Number of cycles to failure at stress range S_i;

j - Number of considered stress range intervals.

2.5.3. NOMINAL STRESS APPROACH

The fatigue resistance S-N curves of classified structural details are based on nominal stress, disregarding the stress concentrations due to the welded. When assessing other types of structural details (i.e. welding details), the nominal stress range should be modified in order to take account for the local conditions affecting the stresses at a specific location. The local stress at this location is expressed by a stress concentration factor multiplied with the nominal stress. It is most common that the stress concentration factor results into an amplification of the nominal stress. However, there are cases where a stress concentration factor less than 1 can validly exist. Fatigue life of the part in question is calculated based on the nominal stress in the proximity of the potential site of cracking. [23]

In simple components the nominal stress can be determined using elementary theories of structural mechanics based on linear-elastic behaviour. Nominal stress is the average stress in the weld throat or in the plate at the weld toe as indicated in the tables of structural details. [24]

$$\sigma_{nominal} = \frac{F}{A} \pm \frac{M}{I} y \tag{28}$$

Where:

$\sigma_{nominal}$ – Nominal stress;

F - Force action on cross section;
A - Cross section area;

M – Applied bending moment;

I – Section inertia; and,

y – Position of the extreme fiber.

2.5.4. HOT-SPOT STRESS APPROACH

The hot-spot stress method, also known as geometric stress method, considers the stress raising effect due to structural discontinuity except the stress concentration due to weld toe, this means without considering the localized weld notch stress [31] and has evolved since the 1970s for the analysis of tubular joints in fixed structures. [4] To determine the hot-spot stresses, the stress at the weld toe position should be extracted from the stress field outside the region influenced by the local weld toe geometry. The structural hot spot stress can be determined either by measurement or by calculation. The non-linear peak stress is eliminated by linearization of the stress through the plate thickness or by extrapolation of the stress at the surface to the weld toe. The following considerations focus on surface stress extrapolation procedures of the surface stress, which are essentially the same for both measurement and calculation.

Radaj [25] demonstrated, particularly for plate and shell structures, that the hot-spot stress corresponds to sum of the membrane and bending stress at the weld toe. The membrane stress is constant and bending stress varies linearly throughout the thickness. The stress distribution through the thickness on a welded plate can be distributed into three components: membrane stress, bending stress and non-linear stress part. Hence, in hot-spot stress method, the latter part (non-linear part, σ_{nlp}) is excluded from the structural stress. This is because, the exact and detailed weld profile cannot be certainly known during the design phase. A $S_{rhs} - N_f$ curve shows the relation between hot-spot stress range and the number of cycles to failure. This method gives an advantage over the other methods as a reduced number of $S_{rhs} - N_f$ curves are needed to evaluate the fatigue life of welded details by the stress concentration factors. [11] The notch stress is the peak stress, which is situated at the weld toe region. The notch stress concept is attractive since it is a real stress, in contrast to the extrapolated conceptual HSS which incorporates the effects of joint geometry but neglects the influence of the weld. However, the HSS approach has been adopted in the development of most design guidance for offshore structures, since notch stresses cannot be measured directly at the weld using strain gauge measurements. [28]

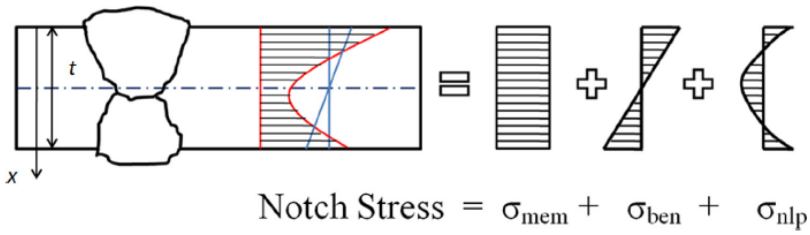

Figure 18 - Stress distribution through the thickness of the weld plate and its components [2]

Where:

σ_{mem} – Membrane stress;

σ_{ben} – Bending stress; and,

σ_{nlp} – Non-linear stress

The location from which the stresses must be extrapolated, extrapolation region, depends on the dimensions of the joint and on the position along the intersection. Two extrapolation methods and two types of hot-spots can be defined for determination of hot-spot stresses. The extrapolation methods can be linear or quadratic and the hot-spot stress can be divided into two types of hot-spot according to their location on the plate and their orientation: weld toe can be on plate surface or weld toe can be at the plate edge. [2]

Table 3 - Types of hot spots

Type	Description	Determination
a	Weld toe on plate surface	FEA or measurement and extrapolation
b	Weld toe at plate edge	FEA or measurement and extrapolation

If the structural hot-spot stress is determined by extrapolation, the element lengths are determined by the reference points selected for stress evaluation. In order to avoid an influence of the stress singularity, the stress closest to the hot spot is usually evaluated at the first nodal point. Therefore, the length of the element at the hot spot corresponds to its distance from the first reference point. If finer meshes are used, the refinement should be introduced in the thickness direction as well. Usually two types of stress are considered in determining the hot spot stress, the stress perpendicular to the weld (primary stresses) and the maximum principal stresses. In general, analysis of structural discontinuities and details to obtain the structural hot spot stress is not possible using analytical methods. Parametric formulae are rarely available. Thus, finite element analysis is generally applied. [21]

For the quadratic extrapolation that will be used, a minimum of three points are required. The first point of extrapolation is 0.4t from the weld toe but not less than 4 mm. The second and third points are respectively, 0.5t and 1.0t away from the first point. Also, if the weld is not modelled, extrapolation to the structural intersection point is recommended in order to avoid stress underestimation due to the missing stiffness of the weld. [29] The identification of the critical points (hot spots) can be made by:

a) Measuring several different points;

b) Analysing the results of a prior FEM analysis; and,

c) Experience of existing components, especially if they failed. [21]

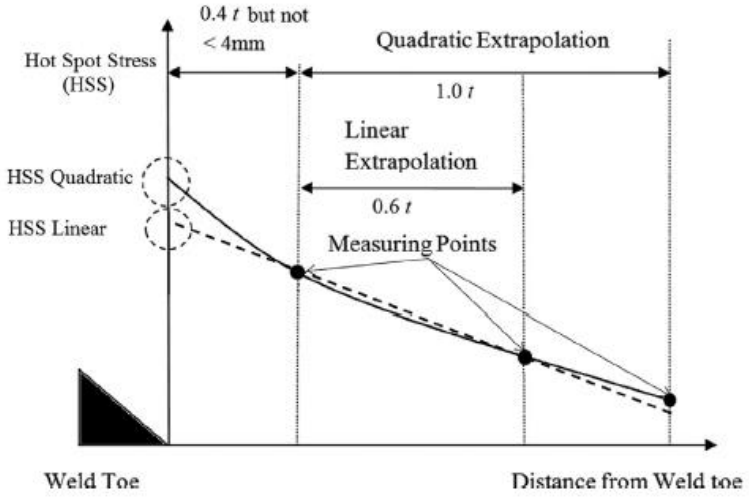

Figure 19 - Extrapolation region and extrapolation points [2]

2.5.4.1. TYPE "A" HOT SPOTS

The structural hot spot stress σ_{hs} is determined using the reference points and extrapolation equation as given below. Fine mesh as defined in 1) above: Evaluation of nodal stresses at three reference points 0.4 t, 0.9t and 1.4t, and quadratic extrapolation (see Equation (23)). This method is recommended for cases

of pronounced non-linear structural stress increase towards the hot spot, at sharp changes of direction of the applied force or for thick walled structures.

$$\sigma_{hs} = 2.52 * \sigma_{0.4t} - 0.67 * \sigma_{0.9t} + 0.72 * \sigma_{1.4t} \quad (29)$$

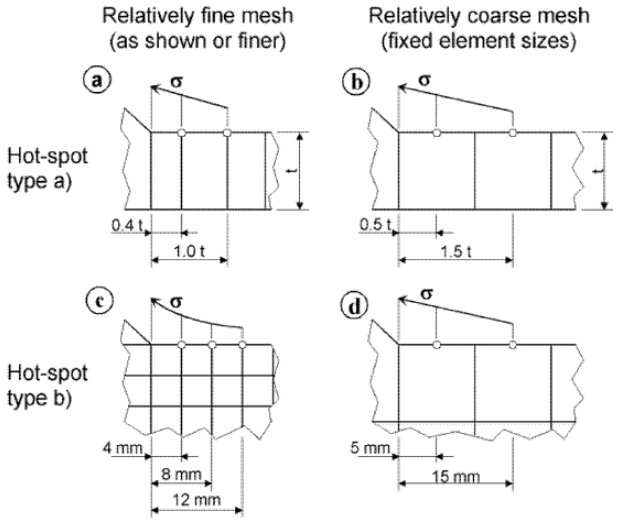

Figure 20 - Reference points at different types of meshing

Application of the usual wall thickness correction is required when the structural hot spot stress of type "a" is obtained by surface extrapolation. The influence of plate thickness on fatigue strength should be taken into account in cases where the site for potential fatigue cracking is the weld toe. The lower fatigue strength for thicker members is taken into consideration by multiplying the FAT class of the structural detail by the thickness reduction factor *f(t)*:

$$f(t) = \left(\frac{t_{ref}}{t_{eff}}\right)^n \quad (30)$$

Where:

t_{ref} – Reference thickness;

t_{eff} – Effective thickness;

n – Thickness correction exponent;

For circular tubular joints, the wall thickness correction exponent of n=0.4 is recommended. [21]

2.5.4.2. TYPE "B" HOT SPOTS

The stress distribution is not dependent on plate thickness. Therefore, the reference points are given at absolute distances from the weld toe, or from the weld end if the weld does not continue around the end of the attached plate. Fine mesh with element length of not more than 4 mm at the hot spot: Evaluation of nodal stresses at three reference points 4 mm, 8 mm and 12 mm and quadratic extrapolation (see Equation (31)). [21]

$$\sigma_{hs} = 3 * \sigma_{4mm} - 3 * \sigma_{8mm} + \sigma_{12mm} \quad (31)$$

2.5.5. DESIGN FATIGUE CURVES

The present fatigue endurance resistance data for welded joints are expressed as S-N curves. However, there are different definitions of failure in conventional fatigue endurance testing. In general, small welded specimens are tested to complete rupture, which is usually very close to through-thickness cracking. In large components or vessels, the observation of a larger or through-wall crack is usually taken as a failure. The fatigue failure according to the present S-N curves effectively corresponds to through-section cracking. The design S-N curves which follows are based on the mean-minus-two-standard-deviation curves for relevant experimental data. It should be noted that, in any welded joint, there are several locations at which fatigue cracks may develop, e. g. at the weld toe in each of the parts joined, at the weld ends, and in the weld itself. [25] Each location should be classified separately. The output from the experimental data represents the number of cycles and a constant stress range that will cause fatigue failure. The basic design S-N curve is given as: [16]

$$\log N = \log \bar{a} - m \log(\Delta\sigma) \tag{32}$$

Where:

$\Delta\sigma$ - Stress range in MPa;

N - Predicted number of cycles until failure for stress range $\Delta\sigma$;

m - Negative inverse slope of S-N curve;

$log\ \bar{a}$ - Intercept of log N-axis.

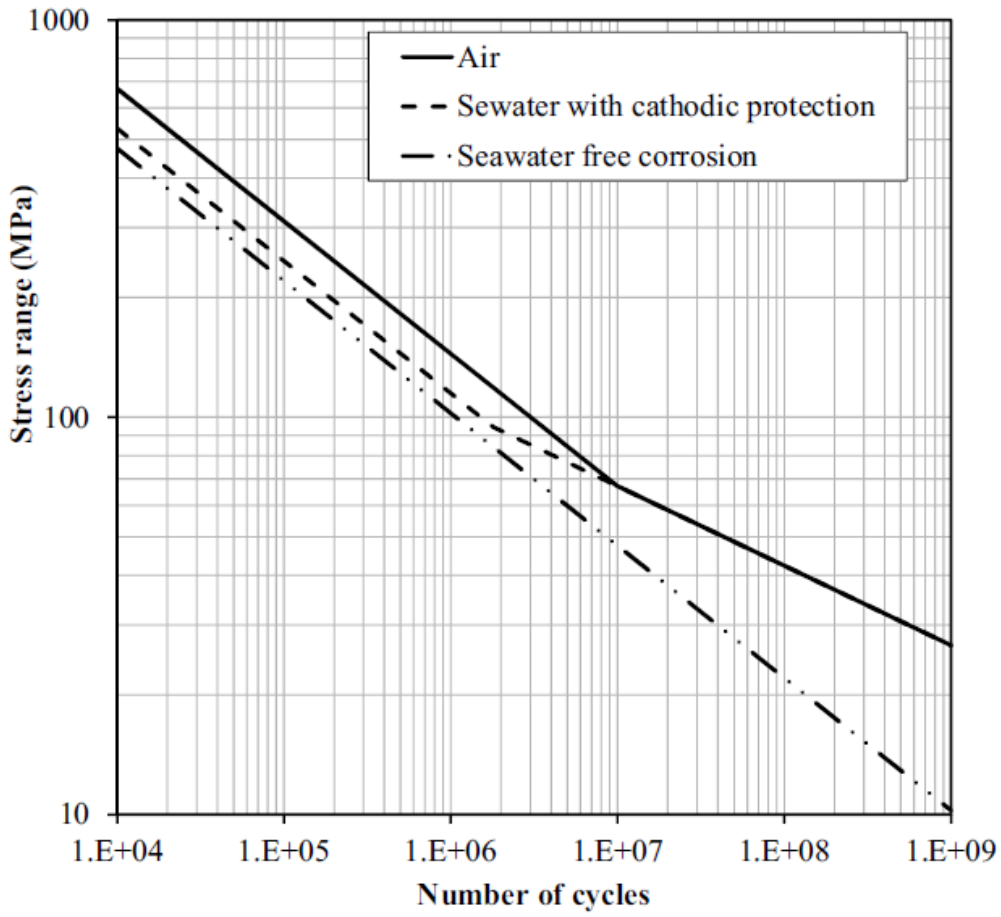

Figure 21 - S-N curves for tubular joints in air and in seawater with cathodic protection

Table 4 - S-N curves for tubular joints [10]

Environment	m_1	$log\,\overline{a_1}$	m	$log\,\overline{a_2}$	Fatigue limit at 10^7cycles (MPa)	Thickness exponent k
Air	N ≤ 10^7 cycles		N > 10^7 cycles			
	3	12.4	5	16.1	67.09	0.25
Seawater with cathodic protection	N ≤ 1.8*10^6 cycles		N > 1.8*10^6 cycles			
	3	12.1	5	16.1	67.09	0.25
Seawater free corrosion	3	12	3	12.0	0	0.25

3

SCF Evaluation of an Offshore Tubular KT-Joint based on Design Code

3.1. INTRODUCTION

The first parametric SCF equations covering simple tubular joints were derived by Toprac and Beale in 1967 using a limited steel joint database. [19] The prohibitive cost of testing scaled steel models led Reber, Visser and Kuang et al to use finite element (FE) analyses based on analytical models of cylindrical shells. Subsequent equations by Wordsworth and Smedley using acrylic model specimens and by Efthymiou and Durkin employing 3-D shell FE analyses, have made considerable advances both in the accuracy of parametric equations and in the range of joints covered. [27] The tubular KT-joint is a quite common joint type found in steel offshore structures. Therefore, it is important to know the stress concentration factors associated to the connection in order to proceed into the fatigue analysis or estimate the fatigue life of a the joint. In this chapter, it is used the DNVGL-RP-C203, most known code used on offshore fatigue design which is based on Efthymiou equations, and Lloyd's parametric equations to where they are both compared and used as reference to comparison with the finite element model.

3.2. GEOMETRY OF THE TUBULAR KT-JOINT

The tubular KT-Joint (see Figure 23) is located on a jacket type offshore structure (see Figure 22). The coordinates to estimate the length of the braces and chord of the joint are displayed in Table 5. The coordinates of the members and the dimensions are represented in Table 5. It was done an intensive review of the members and throughout the review, it was settled to study only one plane when estimating the stress concentration factors around. Also the diameters and thicknesses of the members are represented in Table 5.

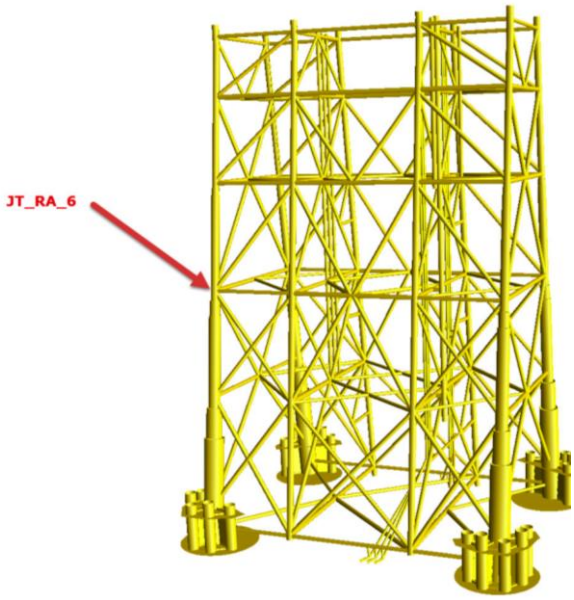

Figure 22 - Geometry of the structure and location of the joint

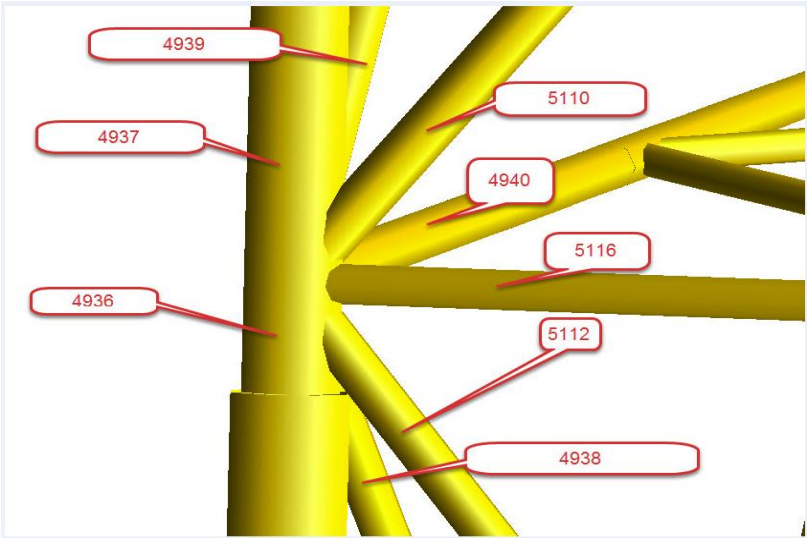

Figure 23 - Geometry of the KT-Joint

Table 5 - Coordinates of the members

	End 1			End 2		
Member	**X**	**Y**	**Z**	**X**	**Y**	**Z**
4936	-40.000	-22.087	-46.685	-40.000	-21.768	-44.000
4937	-40.000	-21.768	-44.000	-40.000	-21.154	-38.824
5116	-40.000	-21.768	-44.000	-37.600	-21.768	-44.000
4940	-40.000	-21.768	-44.000	-40.000	-18.768	-44.000
5110	-40.000	-21.768	-44.000	-37.788	-21.437	-41.211
5112	-37.747	-22.106	-46.841	-40.000	-21.768	-44.000
4938	-40.000	-19.711	-46.740	-40.000	-21.768	-44.000
4939	-40.000	-21.768	-44.000	-40.000	-19.001	-40.313

Table 6 - Diameters and thicknesses of the members

Member	Diameter [m]	Thickness [m]
4936	2.300	0.095
4937	2.300	0.095
5116	1.000	0.030
4940	1.320	0.055
5110	1.200	0.040
5112	1.100	0.025
4938	1.100	0.025
4939	1.200	0.035

3.3. SCF CALCULATION BASED ON DNVGL CODE

In 1988, Efthymiou [29] published a comprehensive set of simple joint parametric equations covering T/Y, X, K and KT simple joint configurations. These equations were designed using influence functions to describe K, KT and multi-planar joints in terms of simple T braces with carry-over effects from the additional loaded braces. To start with the calculations of the stress concentration factors, it is necessary to estimate the geometrical parameters associated. Equations 33 and 34 are used to determine the stress concentration factors for the balanced axial load case. For the balanced in-plane bending and out-of-plane bending load cases, the stress concentration factors can be determined using the Equations 35 and 36, and Equations 37 to 43, respectively.

For the balanced axial load case, the stress concentration factors on the crown and the on saddle for the chord (see Equation (33)) and braces (see Equation (34)) are given by the following equations, respectively:

$$SCF_{AC/AS} = \tau^{0.9}\gamma^{0.5}\,(0.67 - \beta^2 + 1.16\beta)\sin\theta\,\left(\frac{\sin\theta_{max}}{\sin\theta_{min}}\right)^{0.30}\left(\frac{\beta_{max}}{\beta_{min}}\right)^{0.30}(1.64 + 0.29\beta^{-0.38}\,ATAN(8\xi)) \tag{33}$$

$$SCF_{AC/AS} = 1 + (1.97 - 1.57\beta^{0.25})\tau^{-0.14}(\sin\theta)^{0.7}SCF_{AC/AS} + \sin^{1.8}(\theta_{max} + \theta_{min})\big(0.131 - 0.084\,ATAN(14\zeta + 4.2\beta)\big)C\beta^{1.5}\gamma^{0.5}\tau^{-1.22} \tag{34}$$

Where:

C = 0 for gap joints;

C = 1 for the through brace;

C = 0.5 for the overlapping brace.

For the balanced in-plane bending load case, the stress concentration factors on the crown and on the saddle for the chord (see Equation (35)) and braces (see Equation (36)) are given by the following equations, respectively:

$$SCF_{MIP} = 1.45\beta\tau^{0.85}\gamma^{(1-0.68\beta)}(\sin\theta)^{0.7} \tag{35}$$

$$SCF_{MIP} = 1 + 0.65\beta\tau^{0.4}\gamma^{(1.09-0.77\beta)}(\sin\theta)^{(0.06\gamma-1.16)} \tag{36}$$

For the out-of-plane bending load case, the stress concentration factors on the crown and on the saddle for the chord (see Equation (37)) and braces (see Equation 38 and 39) are given by the following equations, respectively:

$$SCF_{MOP,chord} = \gamma\tau\beta(1.7 - 1.05\beta^3)(\sin\theta)^{1.6} * F3 \tag{37}$$

$$SCF_{MOP,brace(A)} = \tau^{-0.54}\gamma^{-0.05}(0.99 - 0.47\beta + 0.08\beta^4)\,SCF_{MOP,chord(A)} * (1 - 0.08(\beta_B\gamma)^{0.5}\exp(-0.8 * x_{AB}))(1 - 0.08(\beta_C\gamma)^{0.5}\exp(-0.8 * x_{AC})) + SCF_{MOP,chord(B)} * (1 - 0.08(\beta_A\gamma)^{0.5}\exp(-0.8 * x_{AB}))(2.05{\beta_{máx}}^{0.5}\exp(-1.3x_{AB}) + SCF_{MOP,chord(C)} * (1 - 0.08(\beta_A\gamma)^{0.5}\exp(-0.8 * x_{AC}))(2.05{\beta_{máx}}^{0.5}\exp(-1.3x_{AC}) \tag{38}$$

$$SCF_{MOP,brace(B)} = \tau^{-0.54}\gamma^{-0.05}\big(0.99 - 0.47\beta_B + 0.08{\beta^4}_B\big)\,SCF_{MOP,chord(B)} * (1 - 0.08(\beta_A\gamma)^{0.5}\exp(-0.8 * x_{AB}))^{P1}(1 - 0.08(\beta_C\gamma)^{0.5}\exp(-0.8 * x_{AC}))^{P2} + SCF_{MOP,chord(A)} * (1 - 0.08(\beta_B\gamma)^{0.5}\exp(-0.8 * x_{AB}))(2.05{\beta_{máx}}^{0.5}\exp(-1.3x_{AB}) + SCF_{MOP,chord(C)} * (1 - 0.08(\beta_B\gamma)^{0.5}\exp(-0.8 * x_{BC}))(2.05{\beta_{máx}}^{0.5}\exp(-1.3x_{BC}) \tag{39}$$

Where:

$$x_{AB} = 1 + \frac{\zeta_{AB}\sin\theta_B}{\beta_B} \tag{40}$$

$$x_{BC} = 1 + \frac{\zeta_{BC}\sin\theta_B}{\beta_B} \tag{41}$$

$$P_1 = \left(\frac{\beta_A}{\beta_B}\right)^2 \tag{42}$$

$$P_s = \left(\frac{\beta_C}{\beta_B}\right)^2 \tag{43}$$

In order to calculate the geometrical parameters on the plane needed for the estimation of the stress concentration factors it is necessary to check Figure 10 (see Section 2.4.1, Chapter 2) for complemental details. The gap (ζ A-C) calculated between braces A-B is 0.15304 and the gap (ζ B-C) between braces B-C is 0.03156. Also, it is necessary to correct the gap value as recommended on the design code, so the gap A is 0.619391 exactly as gap C, and gap B is 0.153043. For the estimation of the stress concentration factors associated to the braces and chord, it's necessary to use Table 7 for the angles of the members and use the geometrical parameters presented in Table 8.

Table 7 - Angles between braces and chord (ZX Plane)

θ	4936	4937	5116
4936	-	-	-
4937	180	-	-
5116	90	90	-
4940	-	-	-
5110	-	38.41849	51.58151
5112	38.41549	-	51.58451

Table 8 - Geometrical parameters and stress concentration factors calculation (ZX Plane)

	Member	β	τ	γ	α	SCF_{AC} SCF_{AS}	SCF_{MIP}	SCF_{MOP}
A	**4936-4937**	1	1	12.10	6.83	1.600	1.299	1.836
B						2.949	1.370	2.591
C						1.368	0.859	1.082
A	**5110**	0.52	0.42	12.10	6.83	1.823	1.623	2.689
B	**5116**	0.43	0.31	12.10	6.83	3.408	2.171	3.785
C	**5112**	0.47	0.26	12.10	6.83	1.785	1.514	2.943

Where:

SCF_{AS} is the stress concentration factor at the saddle for axial load;

SCF_{AC} is the stress concentration factor at the crown for axial load;

SCF_{MIP} is the stress concentration factor for in plane moment;

SCF_{MOP} is the stress concentration factor for out of plane moment.

3.4. LLOYD'S REGISTER KT JOINT EQUATIONS

The Lloyd's Register (LR) equations were developed as part of the "SCFs for simple tubular joints" project which was largely funded by the HSE, in 1991. These equations generally give the SCF at the saddle and crown locations (except for IPB) and may underestimate a larger SCF if located. Overall, it was felt that SCF equations that are currently used in offshore tubular joint design have an appropriate level of safety that's why it's not included any safety factor multiplied in the equations. [27] There are some points about the Lloyd's Register (LR) equations that should be noted:

(i) The LR equations use the Efthymiou short chord correction factors, which have not been independently verified;

(ii) The LR equations are limited to c ratios greater than c = 12, while a significant number of tubular joints are designed with c values below this limitation;

(iii) Short chord length effects, chord bending effects and the weld influence have been considered in deriving these equations;

(iv) The form of the equations, while being more complex for 'hand calculations', gives a more logical influence function format, which largely removes the problem of joint classification between these locations.

It is important to know that when α < 12 the basic saddle SCF equation should be multiplied by the appropriate short chord correction factor *F1*, *F2* etc. Modified β value needs to be used in SCFs predictions at the saddle on β=1 joints under axial load or Out-of-plane bending load cases.

For the balanced axial load case, the stress concentration factors for the central brace B and outer brace A can be determined using the Equations 44 to 47 and Equations 48 to 51, respectively:

$$SCF_{CS} = MAX\,[(T1_B S1_{BA} S1_{BC} - T1_A S1_{AB} S1_{AC} IF1_{BA}), (T1_B S1_{BC} S1_{BA} - T1_C S1_{CB} S1_{CA} IF1_{BC})] * (F1_B\ or\ F2_B) \quad (44)$$

$$SCF_{CC} = MAX\,[(T2_B S2_B - T2_A S2_A IF2_{BA}) + B0_B * B1_B, (T2_B S2_B - T2_C S2_C IF2_{BC}) + B0_B * B1_B)] \quad (45)$$

$$SCF_{BS} = MAX\,[(T3_B S1_{BA} S1_{BC} - T3_A S1_{AB} S1_{AC} IF3_{BA}), T3_B S1_{BC} S1_{BA} - T3_C S1_{CB} S1_{CA} IF3_{BC})] * (F1_B\ or * F2_B) \quad (46)$$

$$SCF_{BC} = MAX\,[(T4_B S2_B - T4_A S2_A IF4_{BA}), (T4_B S2_B - T4_C S2_C IF4_{BC})] \quad (47)$$

$$SCF_{CS} = (T1_A S1_{AB} S1_{AC} - T1_C S1_{CB} S1_{CA} IF1_{AC}) * (F1_A\ or\ F2_A) \quad (48)$$

$$SCF_{CC} = (T2_A S2_{AB} - T2_C S2_{CB} IF2_{AC}) + B0_A * B1_A \quad (49)$$

$$SCF_{BS} = (T3_A S1_{AB} S1_{AC} - T3_C S1_{CB} S1_{CA} IF3_{AC}) * (F1_A\ or\ F2_A) \quad (50)$$

$$SCF_{BC} = (T4_A S2_{AB} - T4_C S2_{CB} IF4_{AC}) \quad (51)$$

Where:

$$S2_B = MAX\ (S2_{BA} S2_{BC}),\ S2_A = MAX\ (S2_{AB} S2_{AC})\ and\ S2_C = MAX\ (S2_{CB}, S2_{CA}) \quad (52)$$

For the parametric equations from 53 to 56 are for the central brace and the parametric equations from 57 to 60 are for the outer brace A.

$$SCF_{CS} = MAX\,[(T1_B S1_{BA} S1_{BC} - T1_A S1_{AB} S1_{AC} IF1_{BA}), (T1_B S1_{Bc} S1_{BA} - T1_C S1_{CB} S1_{CA} IF1_{BC})] * (F1_B\ or\ F2_B) \quad (53)$$

$$SCF_{CC} = MAX\left[(T2_B S2_B - T2_A S2_A IF2_{BA}) + B0_B * B1_B, (T2_B S2_{BC} - T2_C S2_C IF2_{BC}) + B0_B * B1_B)\right] \quad (54)$$

$$SCF_{BS} = MAX\left[(T3_B S1_{BA} S1_{BC} - T3_A S1_{AB} S1_{AC} IF3_{BA}), T3_B S1_{BC} S1_{BA} - T3_C S1_{CB} S1_{CA} IF3_{BC})\right] * (F1_B \; or * F2_B) \quad (55)$$

$$SCF_{BC} = MAX\left[(T4_B S2_B - T4_A S2_A IF4_{BA}), (T4_B S2_B - T4_C S2_C IF4_{BC})\right] \quad (56)$$

$$SCF_{CS} = (T1_A S1_{AB} S1_{AC} - T1_C S1_{CB} S1_{CA} IF1_{AC}) * (F1_A \; or \; F2_A) \quad (57)$$

$$SCF_{CC} = (T2_A S2_{AB} - T2_C S2_{CB} IF2_{AC}) + B0_A * B1_A \quad (58)$$

$$SCF_{BS} = (T3_A S1_{AB} S1_{AC} - T3_C S1_{CB} S1_{CA} IF3_{AC}) * (F1_A \; or \; F2_A) \quad (59)$$

$$SCF_{BC} = (T4_A S2_{AB} - T4_C S2_{CB} IF4_{AC}) \quad (60)$$

Where:

$$S2_B = MAX\,(S2_{BA} S2_{BC}),\; S2_A = MAX\,(S2_{AB} S2_{AC}) \; and \; S2_C = MAX\,(S2_{CB}, S2_{CA}) \quad (61)$$

With the objective to complete the application of the Lloyd's register equations for KT-joints it is essential to use complementar equations given by Eqs. 62 to 76

$$T1 = \tau\gamma^{1.2}\beta(2.12 - 2\beta)\,(\sin\theta)^2 \quad (62)$$

$$T2 = \tau\gamma^{0.2}(3.5 - 2.4\beta)\,(\sin\theta)^{0.3} \quad (63)$$

$$T3 = 1 + \tau^{0.6}\gamma^{1.3}\beta(0.76 - 0.7\beta)\,(\sin\theta)^{2.2} \quad (64)$$

$$T4 = 2.6\beta^{0.65}\gamma^{(0.3-0.5^{\beta})} \quad (65)$$

$$T5 = \tau\gamma\beta(1.4 - \beta^5)\,(\sin\theta)^{1.7} \quad (66)$$

$$T6 = 1 + \tau^{0.6}\gamma^{1.3}\beta(0.27 - 0.2\beta^5)\,(\sin\theta)^{1.7} \quad (67)$$

$$T7 = 1.22\tau^{0.8}\beta\gamma^{(1-0.68\beta)}\,(\sin\theta)^{(1-\beta^3)} \quad (68)$$

$$T8 = 1 + \tau^{0.2}\gamma\beta(0.26 - 0.21\beta)\,(\sin\theta)^{1.5} \quad (69)$$

$$S1_{ij} = \left[1 - 0.4 * \exp\left(-30{x^2}_{ij} * \left(\frac{\beta_i}{\beta_j}\right)^2 * \left(\frac{\sin\theta_i}{Y}\right)\right)\right] \quad (70)$$

$$S2_{ij} = \left[1 + \exp - \left(2{x^2}_{ij} * \sin(\theta_j * \gamma^{-0.5})^{-2}\right)\right] \quad (71)$$

Where:

$$X_{ij} = 1 + \frac{\zeta_{ij}\sin\theta_i}{\beta_i} \quad (72)$$

$$IF1_{ij} = \beta_i(2.13 - 2\beta_i)\gamma^{0.2}\,(\sin\theta_i)\left(\frac{\sin\theta_i}{\sin\theta_j}\right)^p \exp(-0.3x_{ij}) \; where \begin{matrix} P = 1 \; if \; \theta_i > \theta_j \\ P = 5 \; if \; \theta_i < \theta_j \end{matrix} \quad (73)$$

$$IF2_{ij} = [20 - 8(\beta_i + 1)^2]\exp(-3x_{ij}) \quad (74)$$

$$IF3_{ij} = \beta_i(2 - 1.8\beta_i)\,\gamma^{0.2}\left(\frac{\beta_{min}}{\beta_{máx}}\right)\left(\frac{\sin\theta_i}{\sin\theta_j}\right)^{p}\exp(-0.5x_{ij})\; where \begin{matrix} P = 2\; if\; \theta_i > \theta_j \\ P = 4\; if\; \theta_i < \theta_j \end{matrix} \quad (75)$$

$$IF4_{ij} = [20 - 8(\beta_i + 1)^2]\exp(-3x_{ij}) \quad (76)$$

In this analysis the $IF4_{ij}$ parameter was assumed equal to $IF2_{ij}$ parameter. The OTH 354 report does not present the equation for the $IF4_{ij}$ variable.

Table 9 - Lloyd's SCF calculation

Balanced Axial	
BRACE A	
SCF(CS)	1.733
SCF(CC)	1.772
SCF(BS)	1.596
SCF(BC)	1.861
BRACE B	
SCF(CS)	0.935
SCF(CC)	1.598
SCF(BS)	0.216
SCF(BC)	1.479
BRACE C	
SCF(CS)	1.047
SCF(CC)	1.117
SCF(BS)	1.249
SCF(BC)	1.861

Balanced In-plane bending	
BRACE A	
SCF(C)	1.487
SCF(B)	1.390
BRACE B	
SCF(C)	1.861
SCF(B)	1.790
BRACE C	
SCF(C)	1.345
SCF(B)	1.347

Where:

SCF(CS) – Stress concentration on chord saddle
SCF(CC) - Stress concentration on chord crown
SCF(BS) – Stress concentration on brace saddle
SCF(BC) – Stress concentration on brace chord

3.5. DISCUSSION

There is a range of values to the geometrical parameters that must be fulfilled, and these limits came from different experimental researches when trying to estimate the SCF equations for both Efthymiou and Lloyd's parametric equations.

Table 10 - Validity range of values for both parametric equations

	β		τ		γ		θ		ζ	
Relations	MIN	MAX	MIN	MAX	MIN	MAX	MIN	MAX	MIN	MAX
Efthymiou	0.2	1	0.2	1	8	32	20º	90º	$\frac{-0.6\beta}{\sin\theta}$	1
Lloyd	0.13	1	0.25	1	10	35	30º	90º	0	1

Table 11 - SCF comparision between DNV code and Lloyd

		Lloyd's		DNV		Axial	In-plane bending
		SCF (Axial)	SCF (In-plane bending)	SCF (Axial)	SCF (In-plane bending)	DNV vs Lloyd	DNV vs Lloyd
Chord	A (5110)	1.77	1.48	1.60	1.29	-9.70%	-12.66%
	B (5116)	1.59	1.86	2.94	1.37	88.05%	-16.95%
	C (5112)	1.11	1.34	1.36	0.85	22.53%	-36.12%
Brace	A (5110)	1.86	1.39	1.82	1.62	-2.02%	16.74%
	B (5116)	1.47	1.79	3.40	2.17	130.49%	21.48%
	C (5112)	1.86	1.34	1.78	1.51	-4.07%	12.45%

In Table 11, it can be seen the comparison between Efthymiou's and Lloyd's parametric equations for this case of study. For axial loading case the SCF were almost the same on chord and brace side for brace A and C but for brace B on chord side and brace side Efthymiou's equations suffered an increase of 88% and 130.49% respectively. That way it's is conclusive that Lloyd's parametric equations are less conservative compared to Efthymiou's equations for axial loading case.

For in-plane bending case the SCF suffered a percentage increase between 13% and 36% for Lloyd's equations on chord side in any location, so that way the SCF calculation through DNV code is less conservative. On the other hand, for in-plane bending case on brace side Lloyd's equations are less conservative when compared to Efthymiou's equations.

4

SCF Evaluation of an Offshore Tubular KT-Joint based on Numerical Analysis

4.1. INTRODUCTION

This chapter aims to show that offshore and marine renewable application practices need to be based on contemporary FE models if the objective is to achieve optimum design while avoiding unnecessary costs of over-conservatism. For this purpose, a comparison between the fatigue life predictions obtained by the SCFs of 3D solid FE models not considering the weld fillet and the existing SCF parametric equations for tubular KT-joints, was made. Due to the complex geometric nature of tubular joints, the analytical solutions determining stress distributions are complex and difficult to be estimated. The structural and hot-spot stresses distributions around of intersection between chords and principal brace are obtained using the numerical modelling. [21]

4.2. FINITE ELEMENT MODELLING

4.2.1 DEFINITION OF THE FE MODEL

4.2.1.1 GEOMETRY AND MATERIAL PROPERTIES

In the definition of the finite element model, it was used the program ANSYS R19.0 to simulate the conditions and boundaries around the tubular joint and in the tubular joint itself. The choice of elements type for the analysis depends on the geometry of the joint and the purpose for which the results of the analysis will be used. The 3D numerical model was built using solid finite elements and a linear-elastic stresses analysis was used. The mechanical properties used in the numerical analysis of the KT-joint under consideration are presented in Table 12. The S420 QLO 2 steel was used in the offshore structure.

Table 12 - Material Properties

Density (ρ_{steel})	7.850E-6 kg/mm^3
Modulus of Elasticity (E)	210000 N/mm^2
Shear Modulus (G)	80770 N/mm^2
Poisson's ratio (u)	0.3

The yield strength is probably the most significant property that the designer will need to use or specify. The achievement of a suitable strength whilst maintaining other properties has been the driving force behind the development of modern steel making and rolling processes. Designers should note that yield strength reduces with increasing plate or section thickness. In Table 12 is given the variation of yield strength for several ranges of thickness values. [29]

Table 13 - The variation of minimum yield strength (N/mm^2) with thickness for S420 [30]

Steel used	Nominal thickness (mm)					
	≤ 16	> 16 ≤ 40	> 40 ≤ 63	> 63 ≤ 83	> 80 ≤ 100	> 100 ≤ 150
S420	420	400	390	370	360	340

In Table 14 are presented the chemical properties of the steel presented in the offshore tubular joint (S420 QLO 2).

Table 14 - Chemical properties of S420 steel [30]

Chemical Elements	**S420**
C	0.14
Si	0.15-0.55
Mn	1.65 Máx
P	0.02
S	0.007
Al	0.15 – 0.055
Cr	0.25
Mo	0.25
Ni	0.7
Cu	0.3
N	0.01
Nb	0.04
Ti	0.025
V	0.08

After having all the information regarding the components and the constitution of the joints, it is possible to build the model provided in chapter 3. Figures 25 and 25 show the different view perspectives of the model of the solid model created to simulate the linear-elastic stresses distribution in KT-joint under consideration. Members 5110, 5116 and 5112 are displayed as brace A, B and C, respectively (see Figure 24). In Figure 25 are identified the crown and saddle points by 1 and 2, and 3 and 4, respectively. These points around the intersection of the brace-chord are the points with the highest stress in the model. Figure 27 represents the highlighted zone with its boundary conditions where it should be refined in order to extract accurate results. Further in this chapter, meshing is discussed and all the effects of associated to it are clarified. The type of mesh elements (8-nodes solid elements) used on the braces and on the green highlighted zone is way more refined than the other zones in order to extract more accurate results since it's the zone where the stress concentration factors will be extracted and necessary to study. Figures 26 and 27 show the size of the elements used in the meshing of the model represented by the green highlighted zone (8-nodes cube solid elements) and in exterior zone.

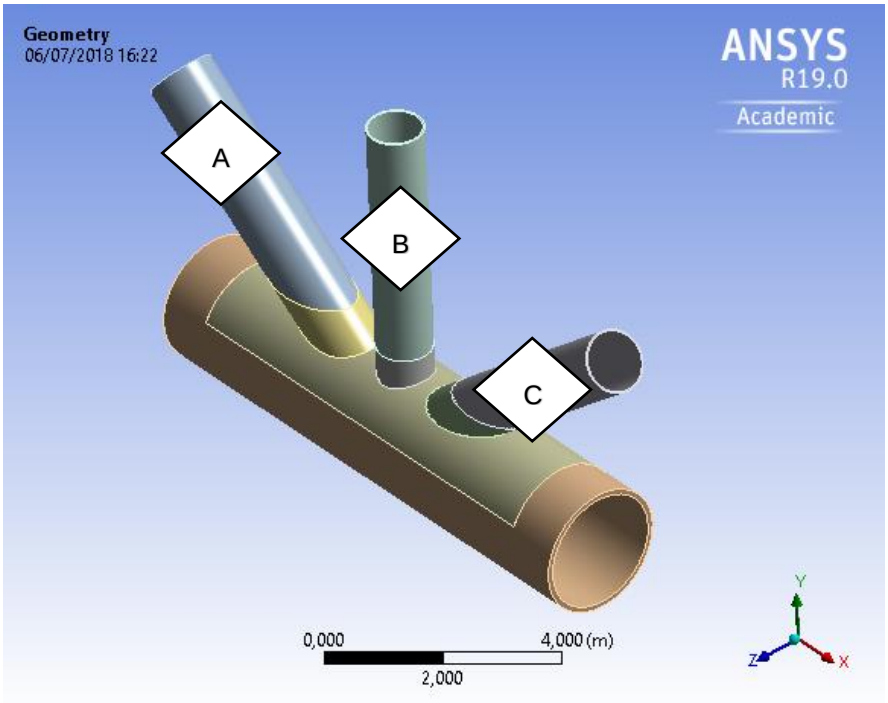

Figure 24 – Solid model with designation of the braces

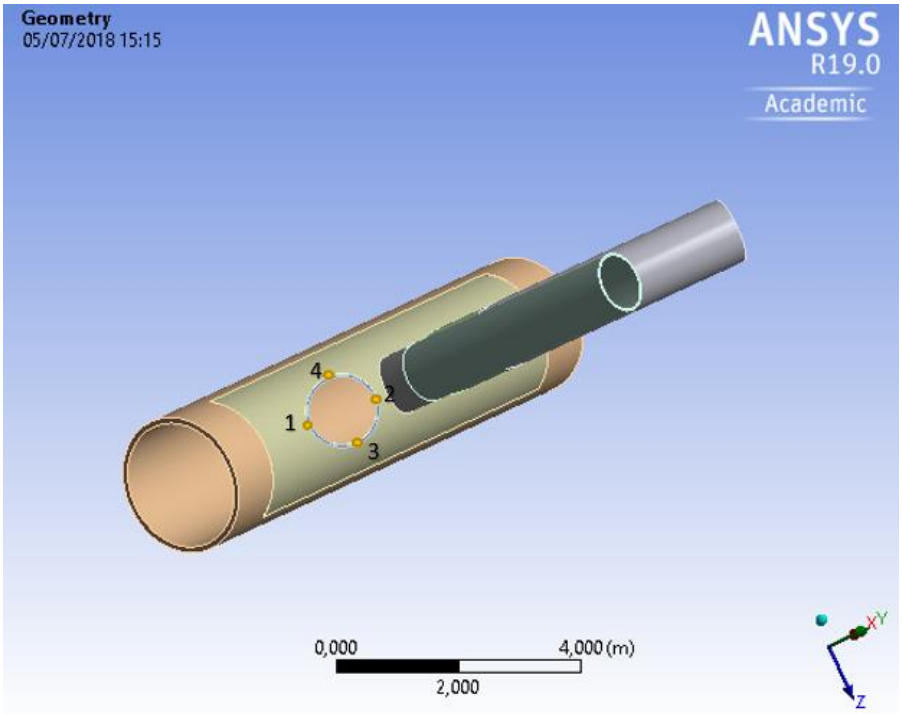

Figure 25 – Solid model with the principal stress points

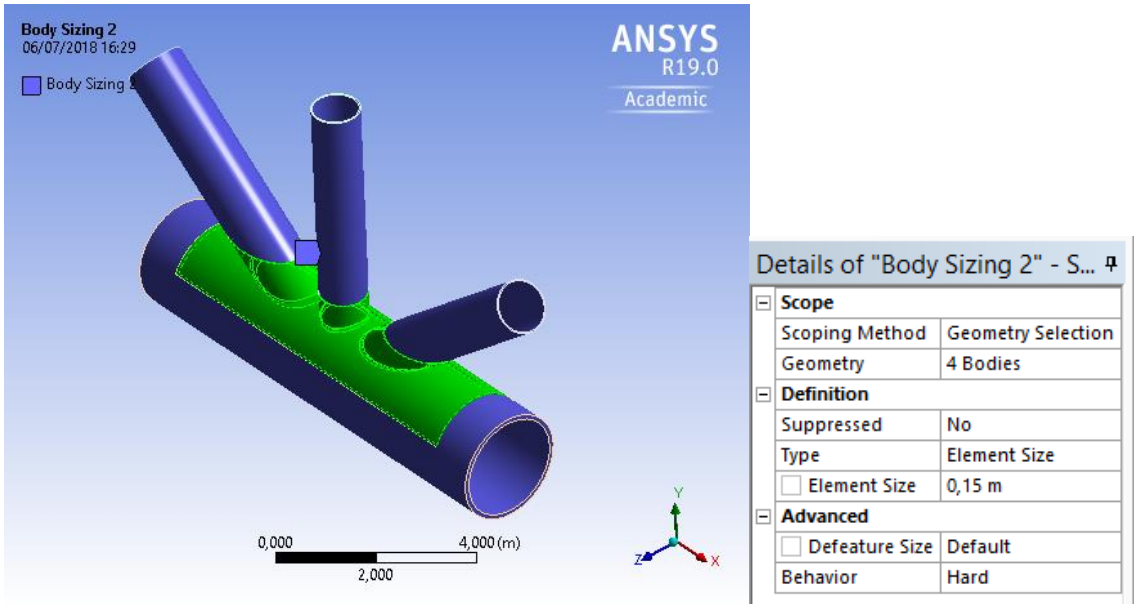

Figure 26 - Solid model with the details of the size of the 8-nodes cube solid elements and 6-nodes triangular solid elements in braces and chord, respectively in the blue zone (Exterior zone)

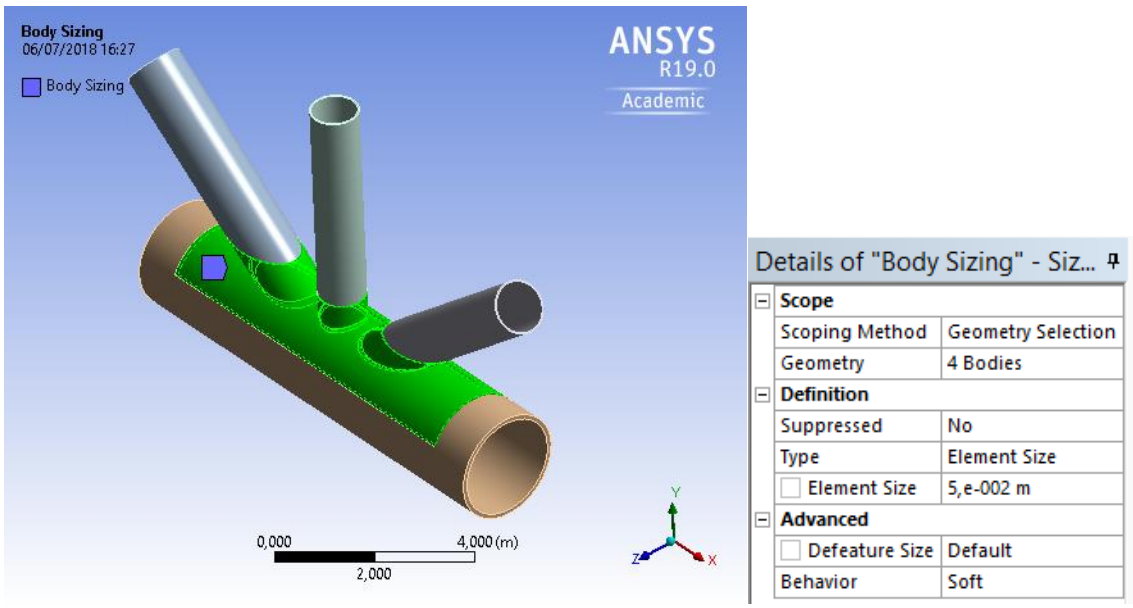

Figure 27 – Solid FE model with the details of the size of the 8-nodes solid elements in the green zone

The 3D finite element model of the KT-joint under consideration is presented in Figures 28 to 30, front view, side view and top view, respectively.

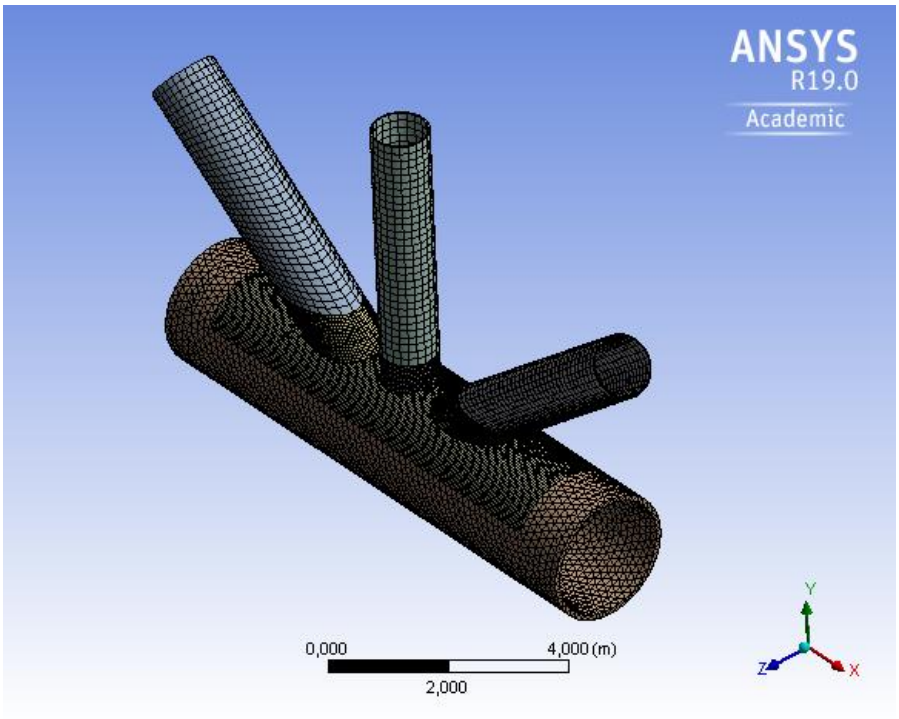

Figure 28 – Solid FE model with the designed meshing refinement (Front view)

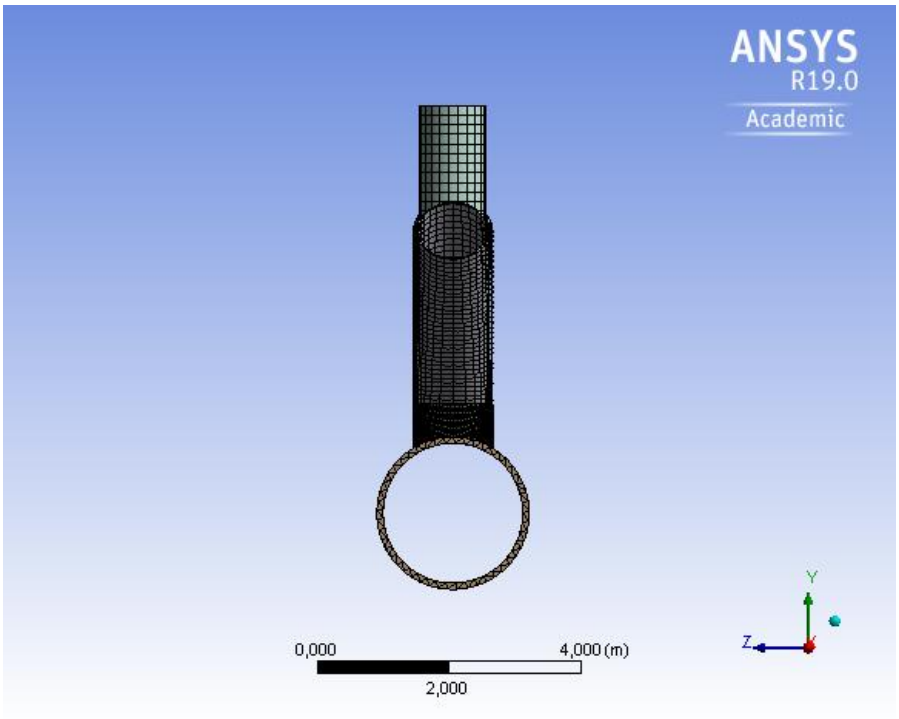

Figure 29 - Solid FE model with the designed meshing refinement (Side view)

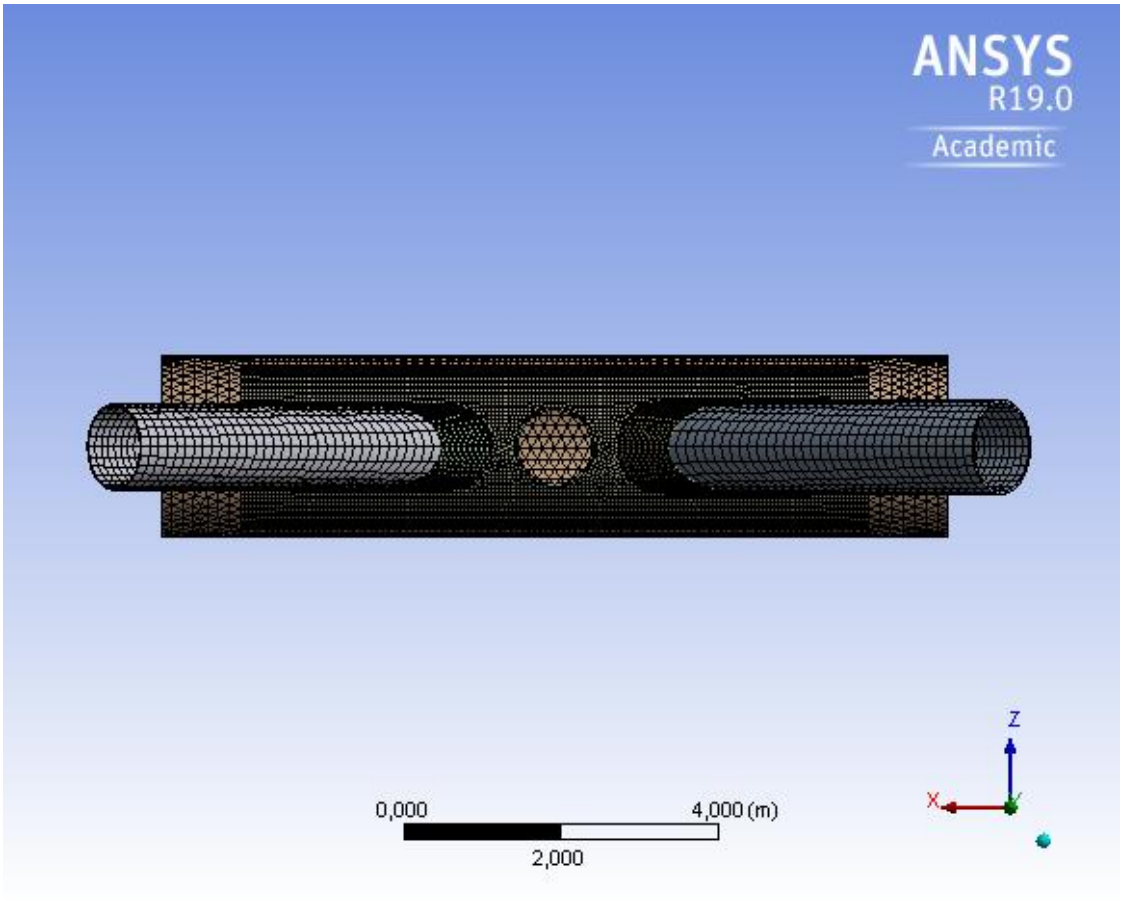

Figure 30 - Solid FE model with the designed meshing refinement (Top view)

In Figure 31 are displayed different perspectives with closed looks for both chord and brace elements meshing. The linear-elastic stresses distributions were obtained for the critical points identified in Figure 25.

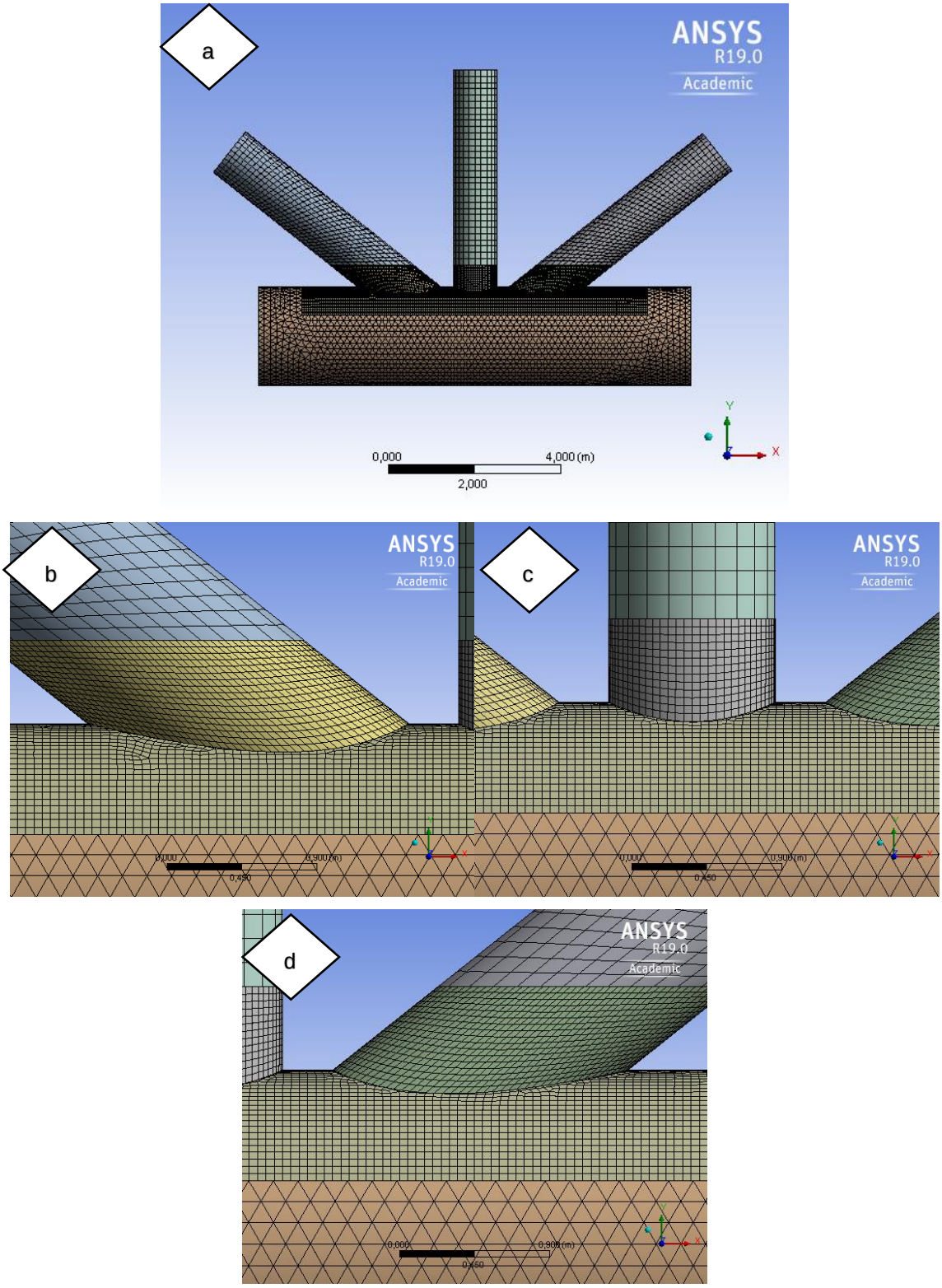

Figure 31 – 3D FE model of the KT-Joint under consideration

a) Front view | b) Brace A | c) Brace B | d) Brace C

4.2.1.2 INFLUENCE OF THE FE MESHING

A mesh convergence study is required to obtain the linear-elastic stresses distribution more suitable around of the intersection between chord and braces with aims to estimate the SCFs. However, it is important to clarify that the element size of green zone identified in Figure 27 is equal to 5E-2m (5cm). The element size is lower when compared to the IIW recommendations. The hot-spot stresses are obtained using the rules proposed by IIW recommendations and DNVGL code [19]. Otherwise, these stresses were obtained using the interpolation and extrapolation approaches.

4.2.2. LOADS

The loads to be considered in the finite element analysis of the KT-joint under consideration are presented in Table 15. These loads were available by Force Technology company from an example. The load cases, such as, axial force, in-plane bending and out-of-plane bending, are shown in Figures 32 to 34, respectively. In these figures are introduced the values of the loads.

Table 15 - Loads used in numerical model of the KT-joint.

Members	ΔF [MN]	ΔMy [MN.m]	ΔMz [MN.m]
4936	9.241	2.185	0.465
4937	1.659	0.867	0.521
4938	4.131	0.204	0.074
4939	4.018	0.582	0.102
4940	0.151	1.212	0.437
5110	1.001	0.422	0.662
5112	0.575	0.066	0.205
5116	0.269	0.128	0.073

In Table 16 are presented the nominal stresses applied in the KT-joint based on the loads considering in this study (see table 15). To calculate the nominal stresses, it's is essential to estimate section properties as well. Remember that to calculate the static moment is necessary to check Equations 77 to 79 for auxiliary information.

$$W_{el,y} = \frac{I_y}{y} \; and \; W_{el,z} = \frac{I_z}{y} \tag{77}$$

$$\Delta\sigma_y = \frac{\Delta My}{Wel_y} \; and \; \Delta\sigma_z = \frac{\Delta Mz}{Wel_z} \tag{78}$$

$$I_y = \frac{\pi r^4}{4} \; and \; I_z = \frac{\pi r^4}{4} \tag{79}$$

Where:

I_y- Moment of inertia in y-direction

I_z- Moment of inertia in z-direction

$W_{ed,y}$ – Elastic section modulus in strong axis y-y

$W_{ed,z}$ - Elastic section modulus in strong axis z-z

$\Delta\sigma_x$ – Nominal stress due to axial load;

$\Delta\sigma_{my}$ - Nominal stress due to in-plane bending load;

$\Delta\sigma_{mz}$ - Nominal stress due to out-plane bending load.

Table 16 - Nominal stresses and section properties

A	Wel,y	We,z	Δσx	Δσmy	Δσmz
0.336	0.185	0.185	27.495	11.786	2.507
0.336	0.185	0.185	4.937	4.677	2.813
0.042	0.011	0.011	96.745	17.847	6.491
0.065	0.018	0.018	61.815	30.766	5.421
0.1117	0.035	0.035	1.358	34.312	12.383
0.0741	0.021	0.021	13.515	19.634	30.813
0.0427	0.011	0.011	13.471	5.828	17.871
0.0464	0.011	0.011	5.819	11.404	6.496

4.2.2.1 AXIAL LOADING CASE

In the Figure 32, it is displayed the model with the axial forces for each associated brace. The loads associated to the joint are based in Table 15.

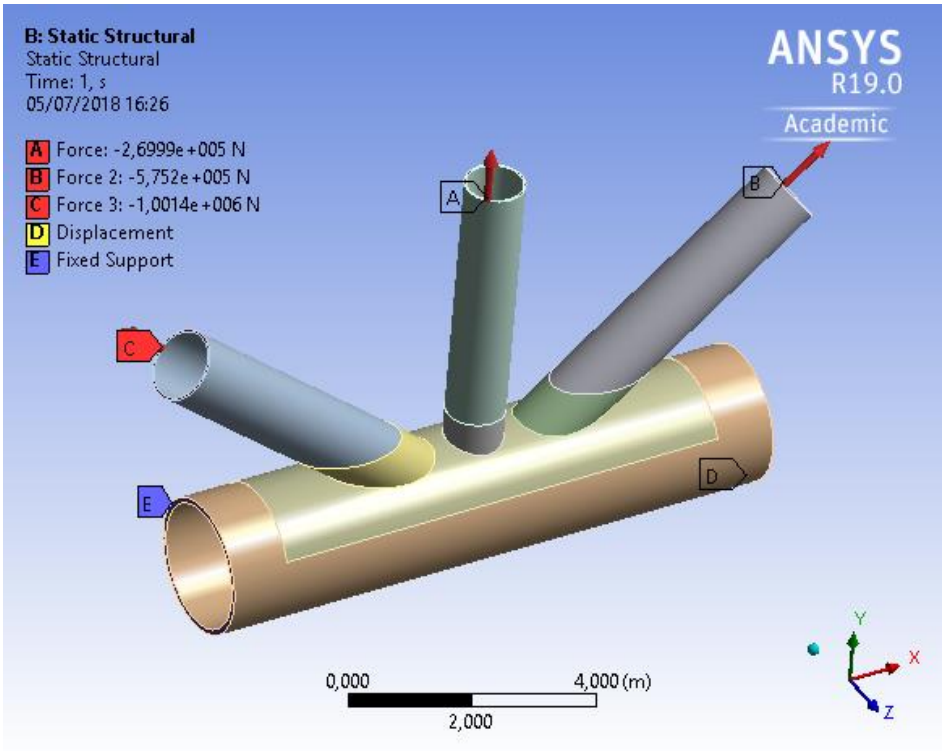

Figure 32 - Solid model with the representation of the axial forces

4.2.2.2. IN-PLANE BENDING CASE

In the Figure 33, it is displayed the model with the bending moments represented for the in-plane bending case represented. The loads associated to the joint are displayed in Table 15.

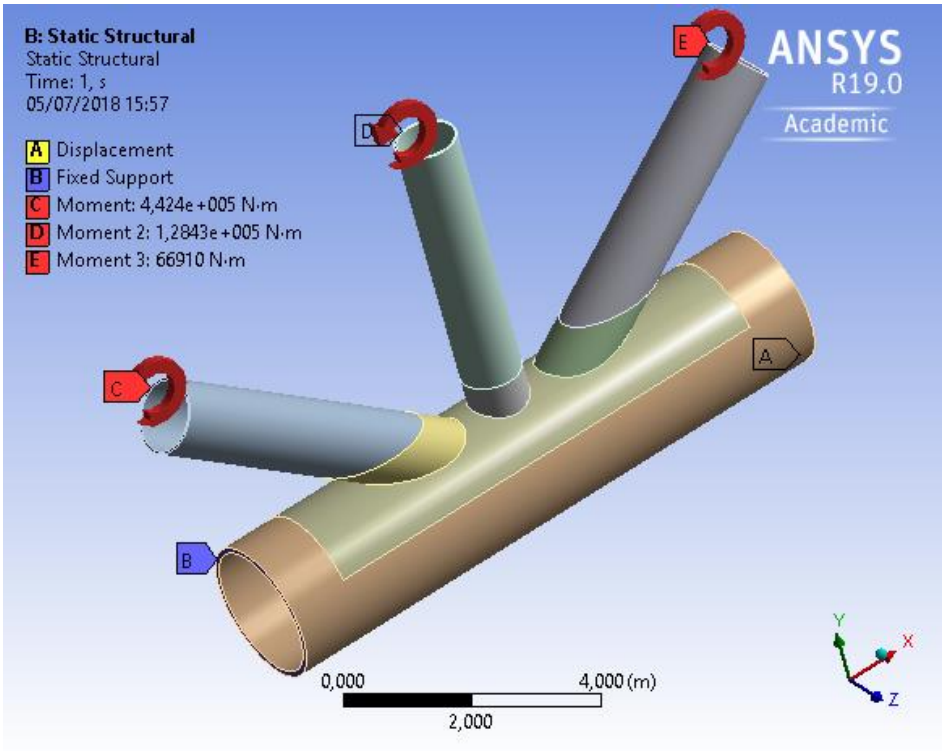

Figure 33 - Solid model with the representation of the in-plane bending moment

4.2.2.3 OUT-PLANE BENDING CASE

In the Figure 34, it's displayed the model with the moments for the unbalanced out-of-plane bending case represented. These loads are shown in Table 15.

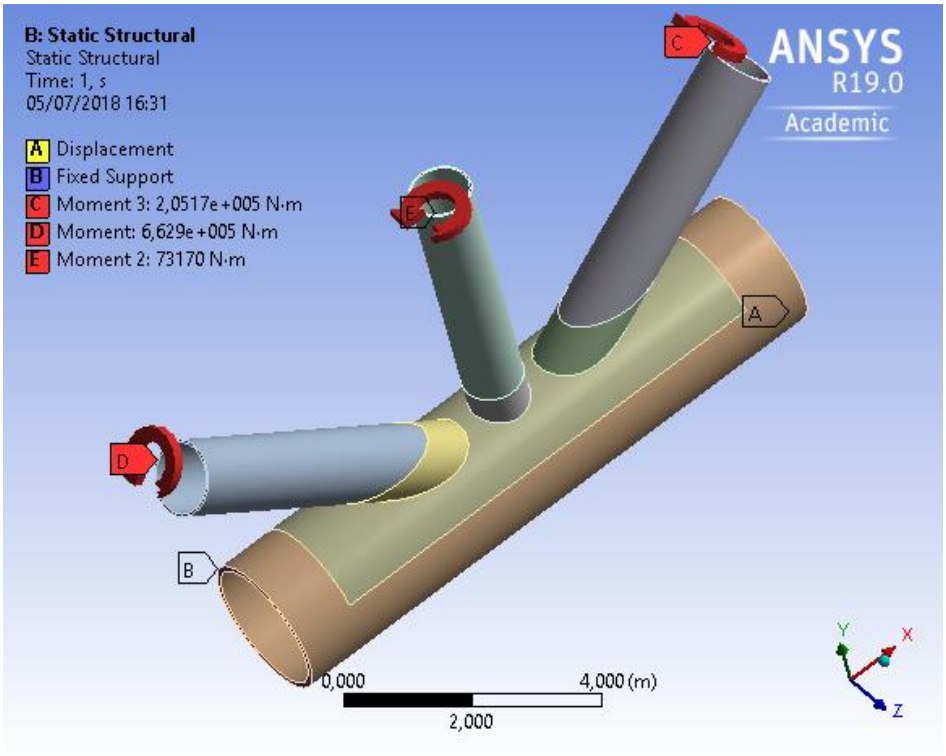

Figure 34 - Solid model with the representation of the in-plane bending moments

4.2.2.4 BOUNDARY CONDITIONS

The chord end fixity conditions of tubular joints in offshore structures may range from almost fixed to almost pinned, while generally being closer to almost fixed. On one side of the rope, all nodes were restricted in all directions, while on the opposite side, the Y and Z directions were restricted, and the X direction considered free from constraints. Figures 36 to 38 show all the information regarding the supports of the joint. [19]

Details of "Fixed Support"	
Scope	
Scoping Method	Geometry Selection
Geometry	1 Face
Definition	
Type	Fixed Support
Suppressed	No

a)

Details of "Displacement"	
Scope	
Scoping Method	Geometry Selecti...
Geometry	1 Face
Definition	
Type	Displacement
Define By	Components
Coordinate System	Global Coordinat...
X Component	Free
Y Component	0, m (ramped)
Z Component	0, m (ramped)
Suppressed	No

b)

Figure 35 - Details about the support conditions used in the FE model: a) Fixed support; b) Displacement.

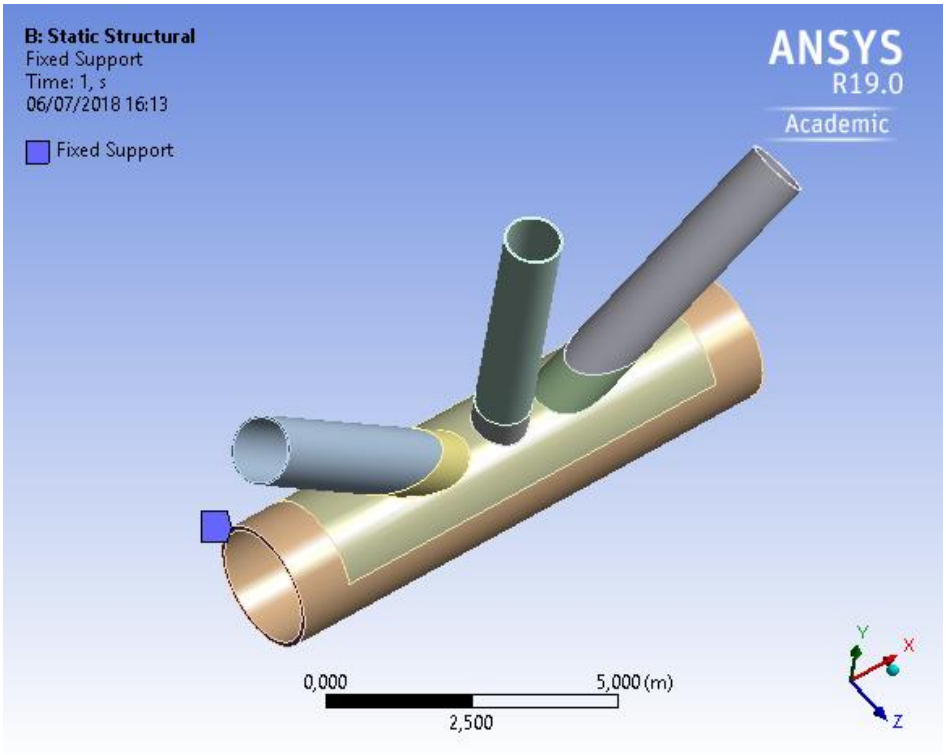

Figure 36 - Solid model with identification of fixed support

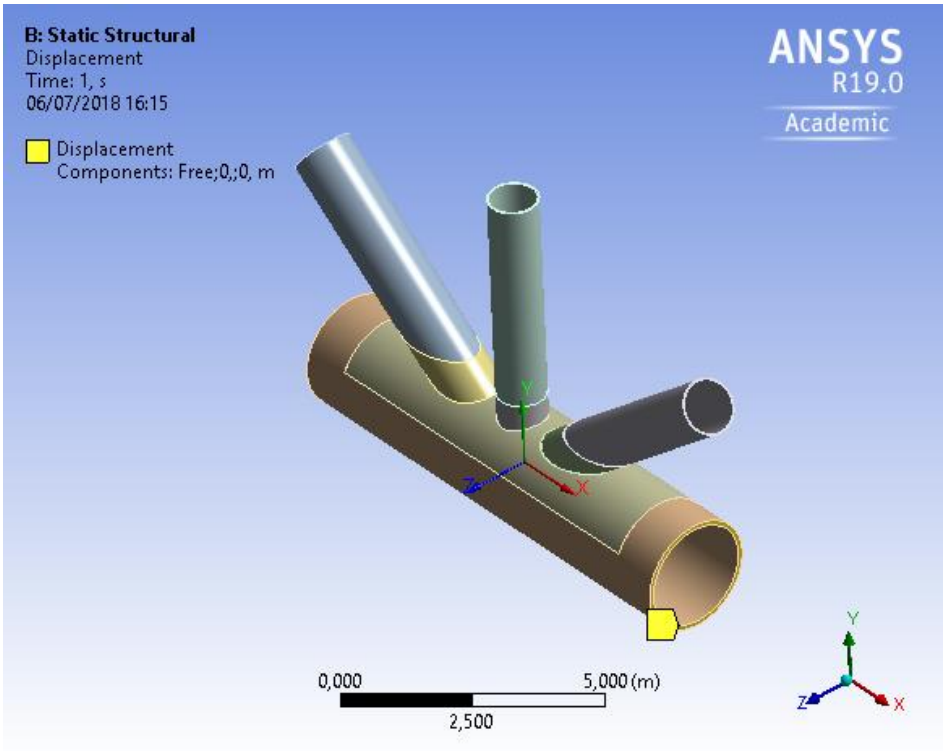

Figure 37 – Solid model with identification of restricted and free directions.

4.3. Estimation of the Structural and Hot-Spot Stresses Distribution

4.3.1 Axial loading case

In Figures 38 and 39 are shown the stress fields considering the axial loading case. It is possible identify that the highest stresses are found at the intersection between the chord and the braces at the so-called crown and saddle places. In more detail, the linear-stress distribution paths for each element of the KT-joint are shown in the following sections.

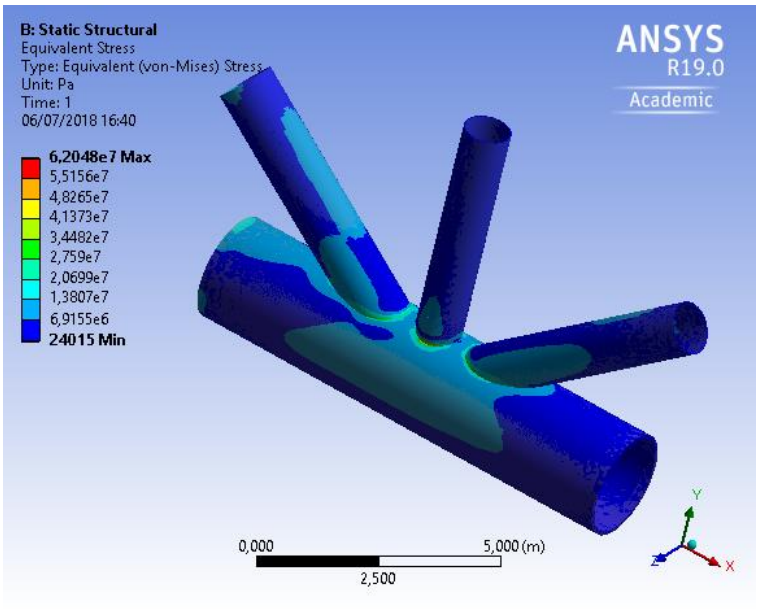

Figure 38 - Stress fields for axial loading case in the KT-joint under consideration

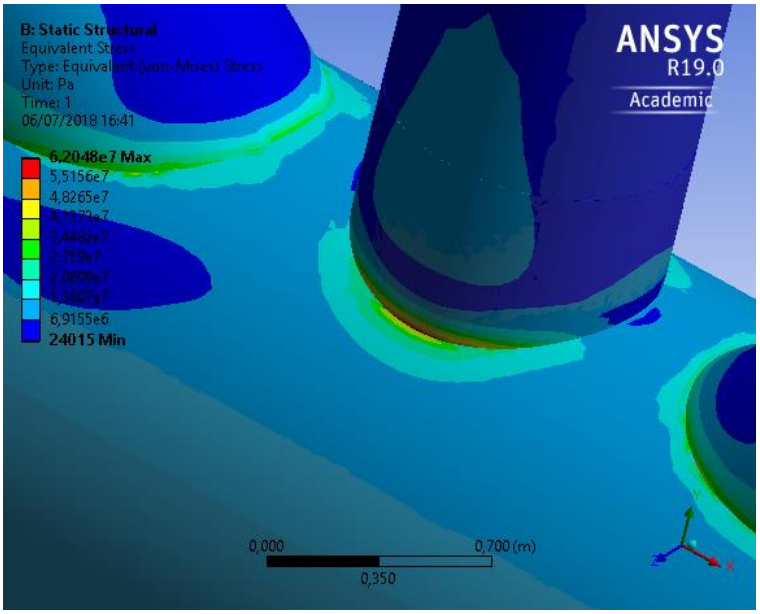

Figure 39 - Stress fields for axial loading case in the KT-joint under consideration (Closer look)

4.3.1.1 BRACE A (5110)

In Figures 40 to 43 are displayed the stress distribution paths for the axial loading case that are used in the study of the stress concentration factor evaluation of brace A. There are 4 paths for the brace to study and are displayed with the number 1 to number 2. (see Figure 25)

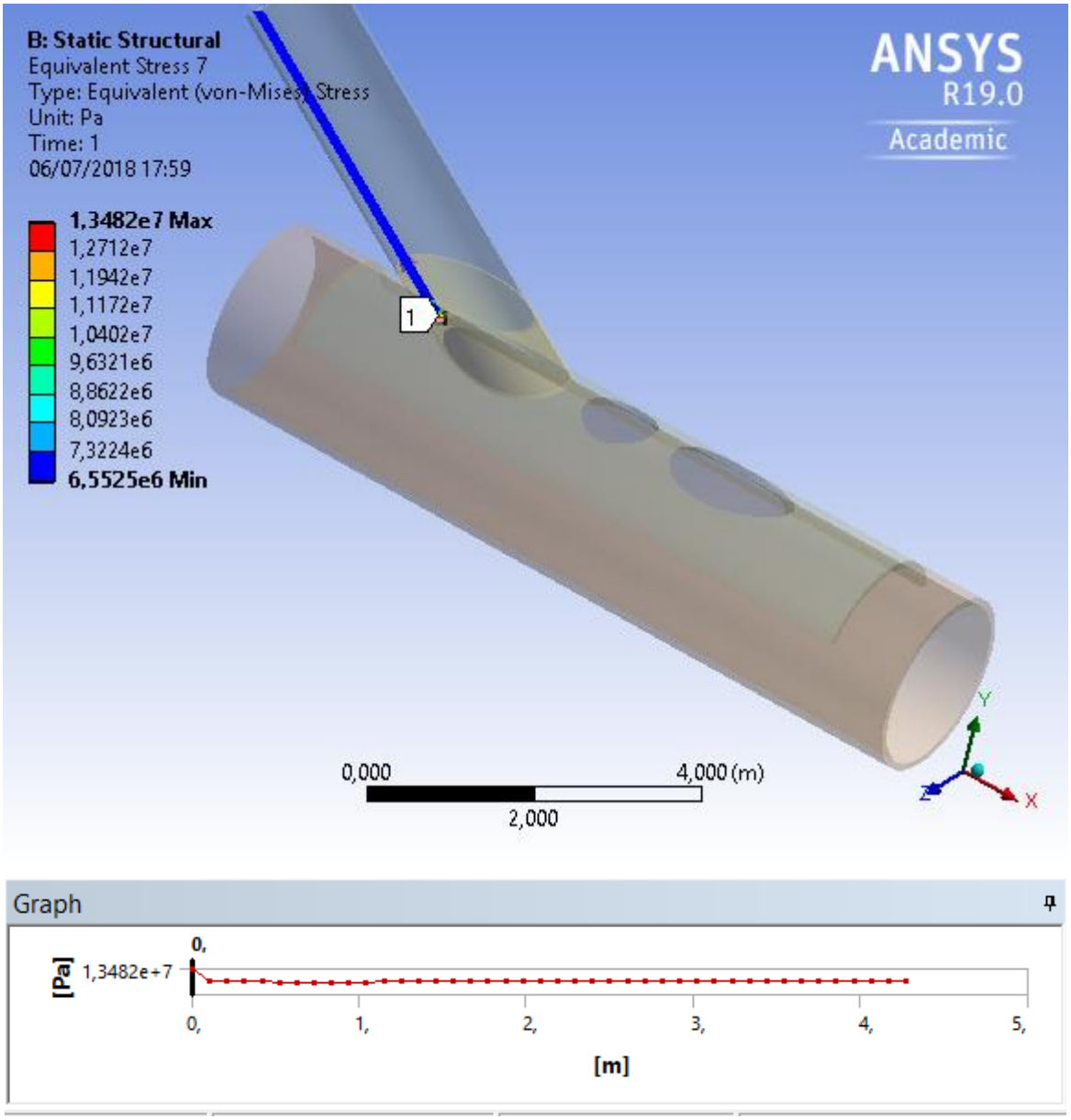

Figure 40 - Stress distribution in brace A for axial loading case: Side 1

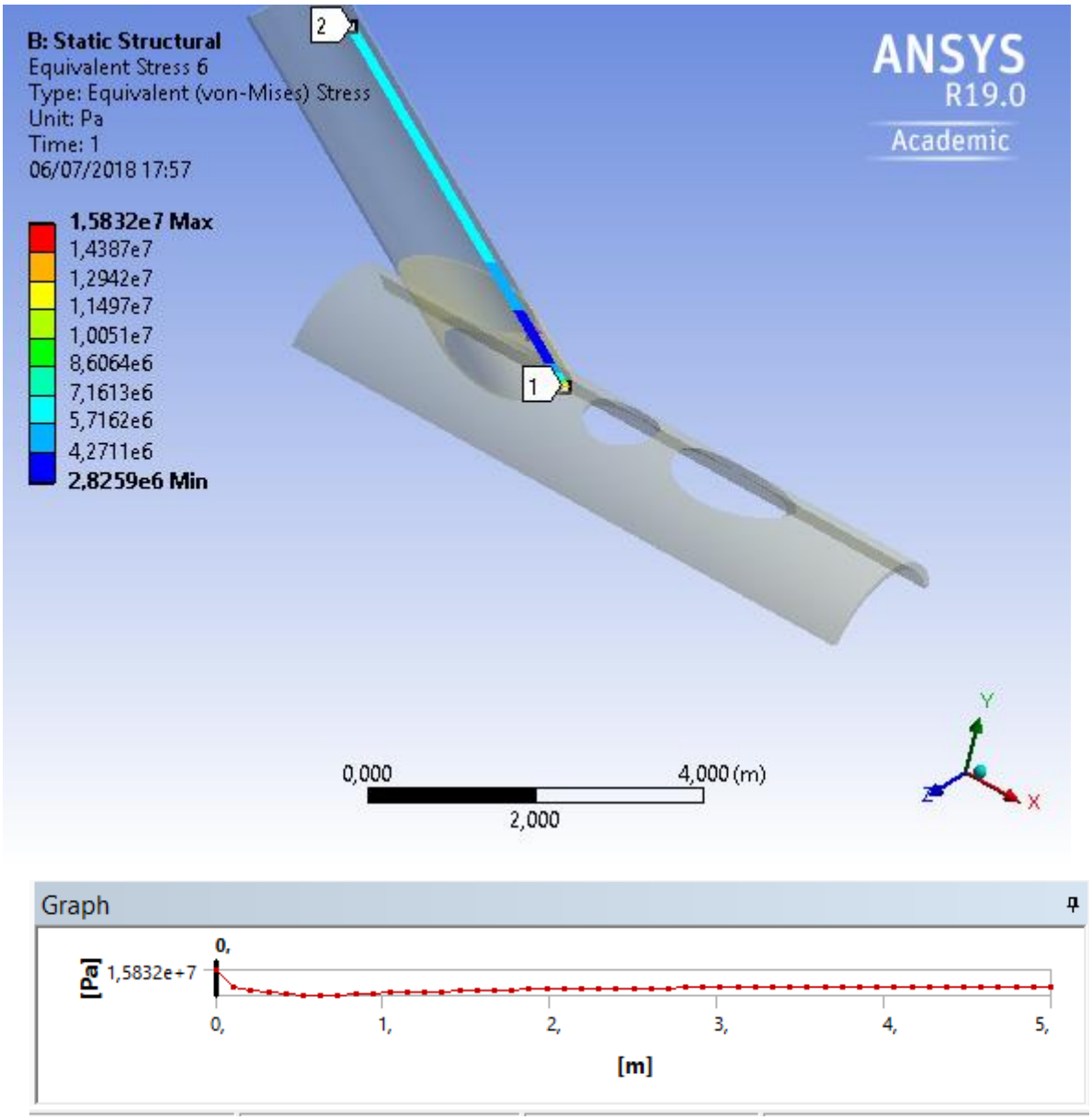

Figure 41 - Stress distribution in brace A for axial loading case: Side 2

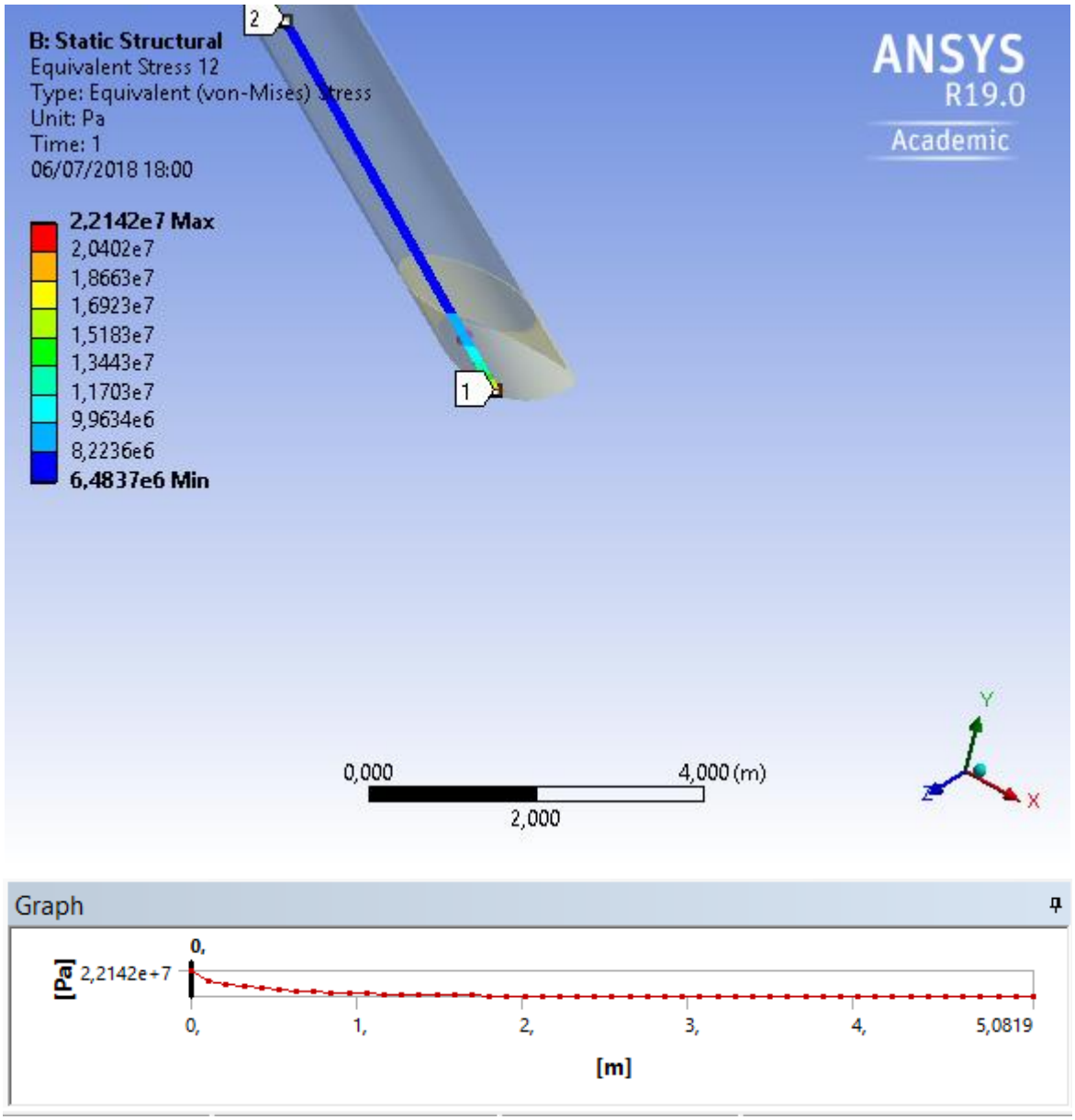

Figure 42 - Stress distribution in brace A for axial loading case: Side 3

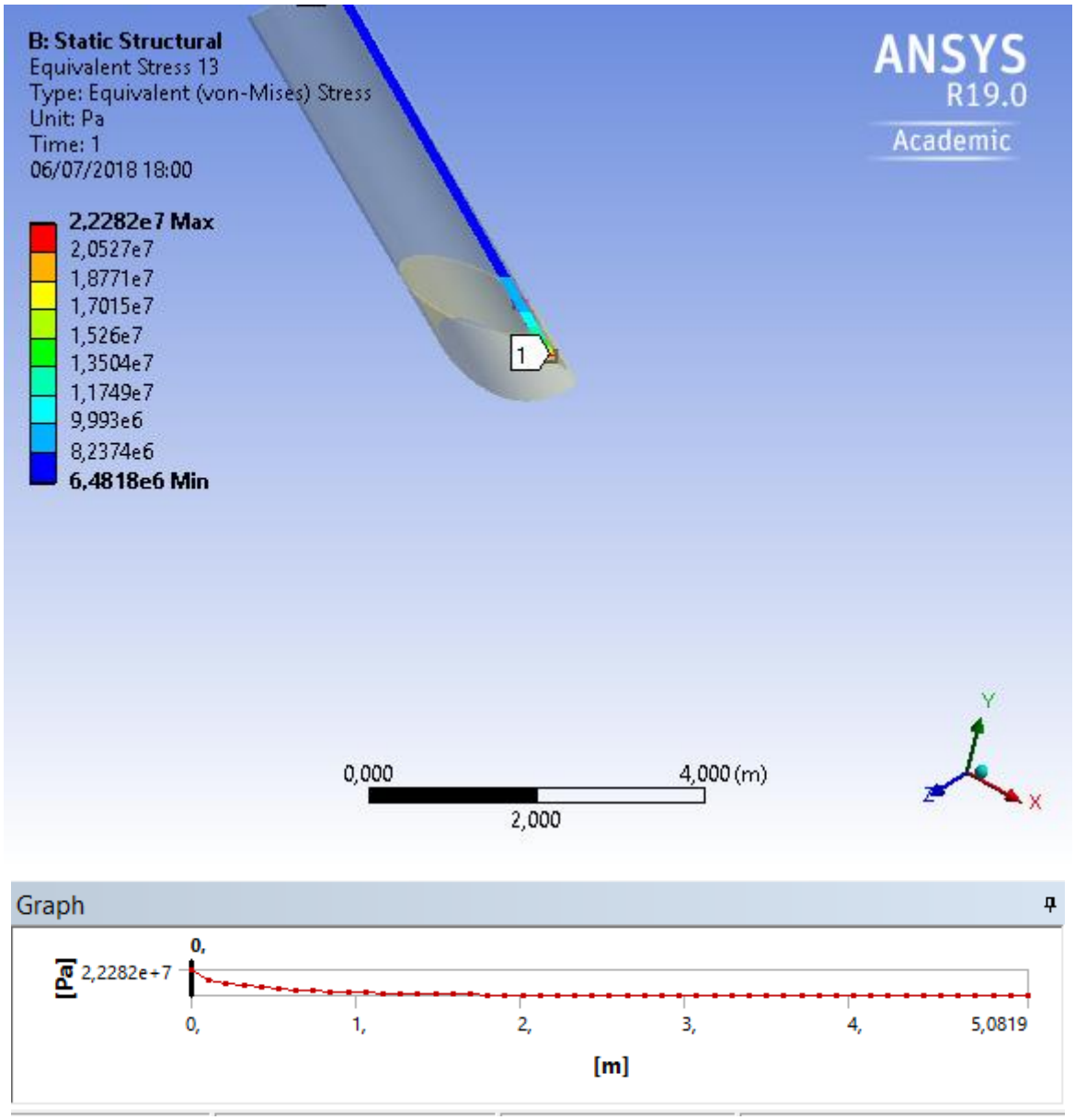

Figure 43 - Stress distribution in brace A for axial loading case: Side 4

4.3.1.2 BRACE B (5116)

In Figures 44 to 47 are displayed the stress distribution paths for the axial loading case that are used in the study of the stress concentration factor evaluation of brace B. There are 4 paths for the brace to study and are displayed with the number 1 to number 2. (see Figure 25)

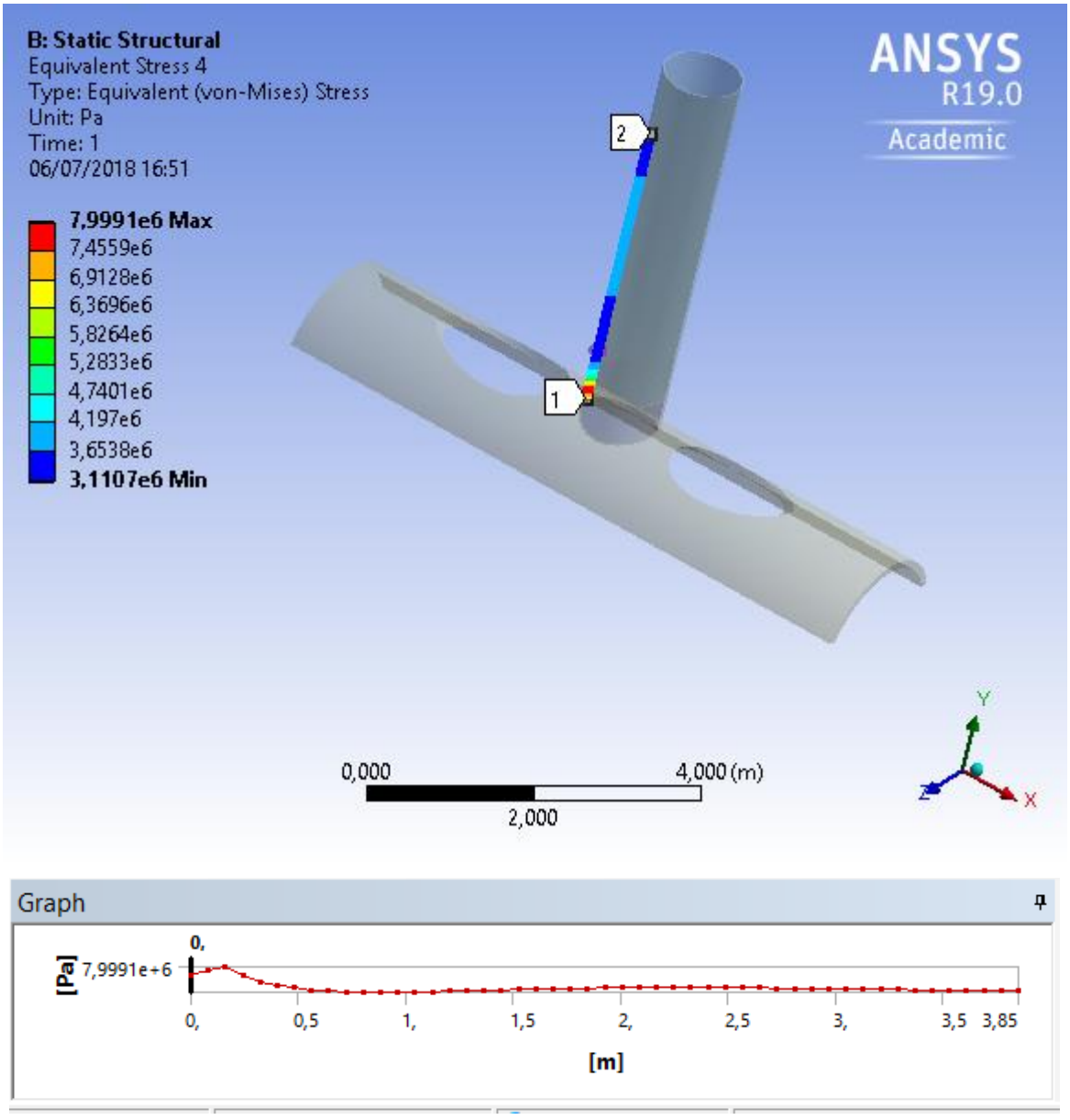

Figure 44 - Stress distribution in brace B for axial loading case: Side 1

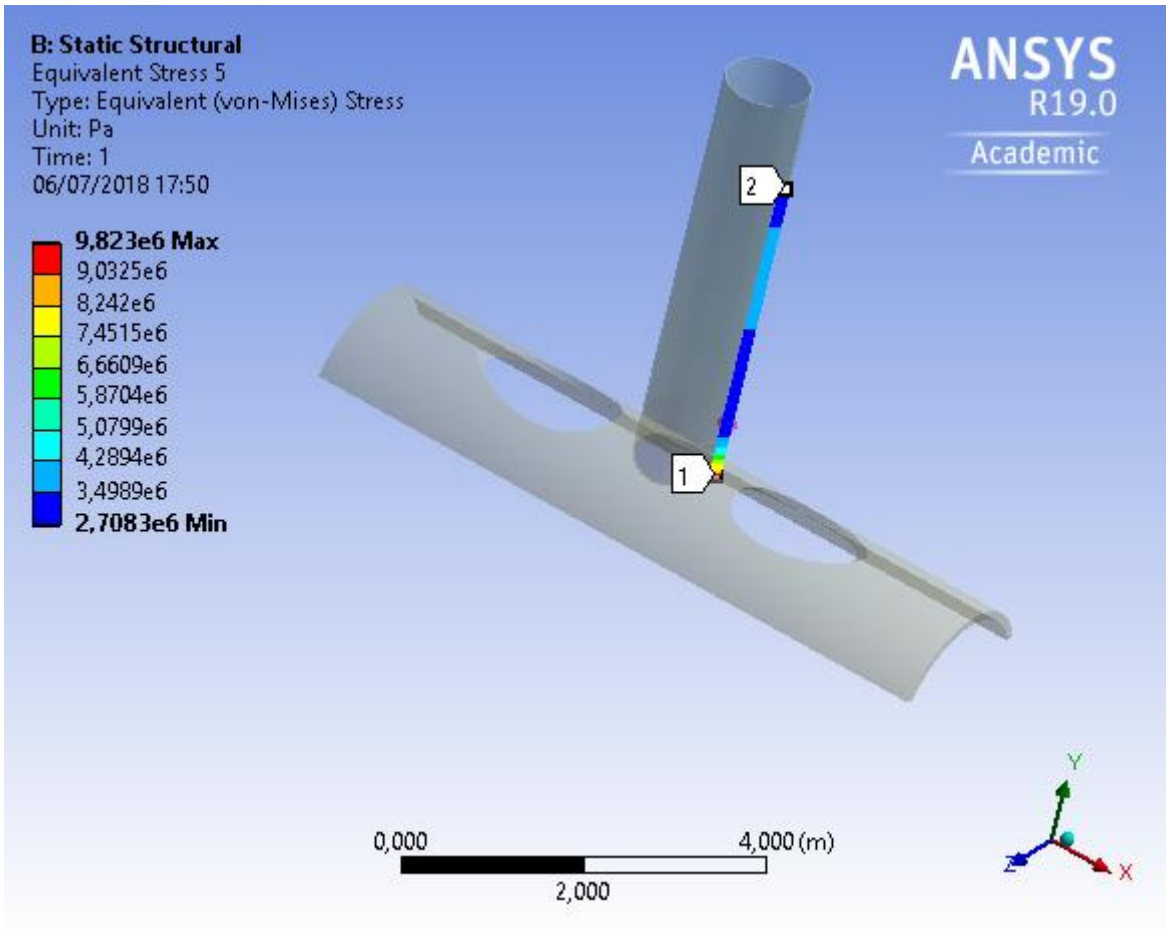

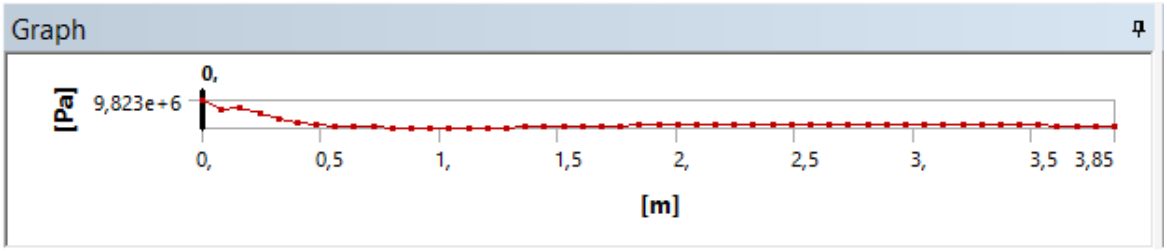

Figure 45 - Stress distribution in brace B for axial loading case: Side 2

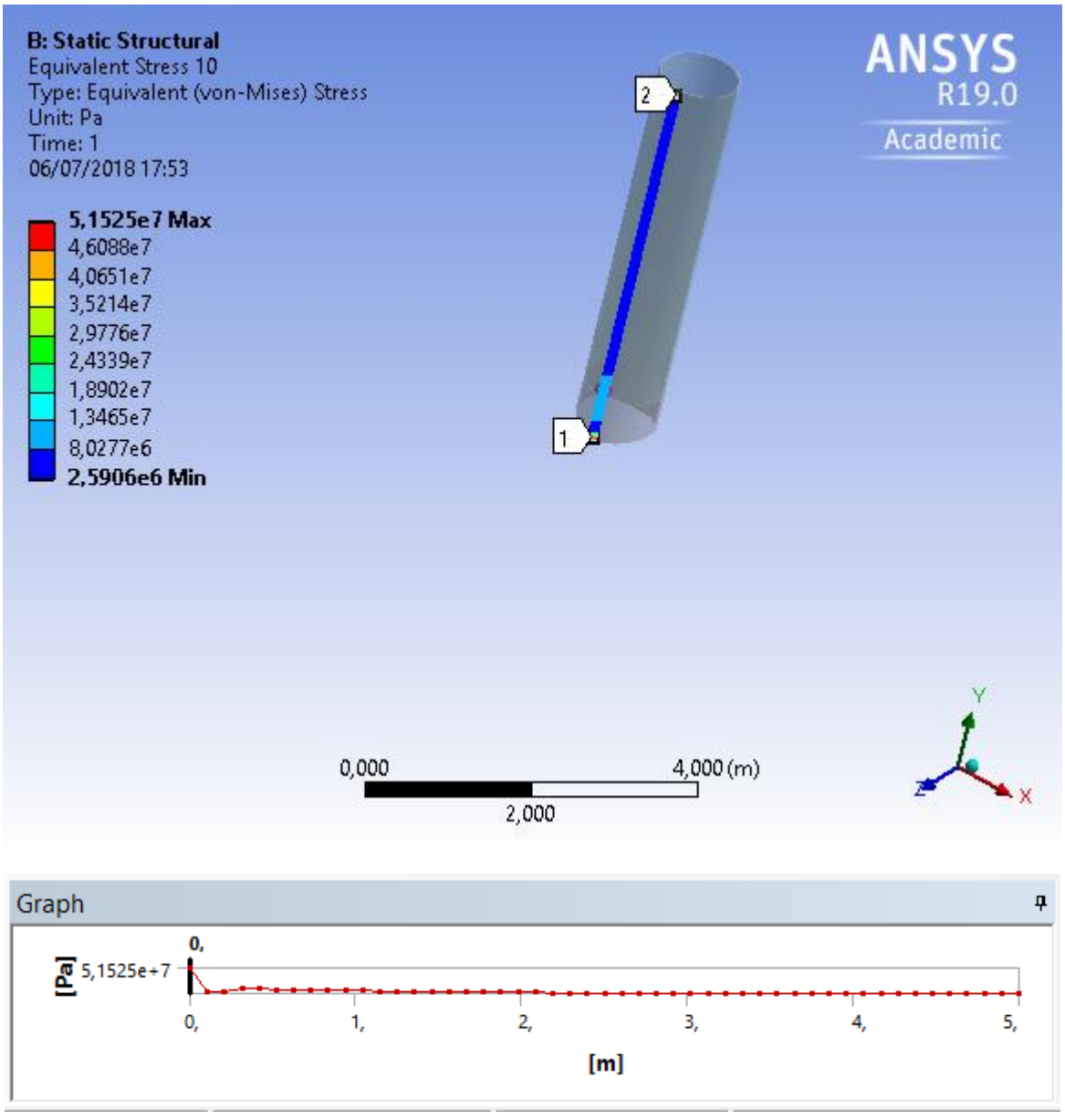

Figure 46 - Stress distribution in brace B for axial loading case: Side 3

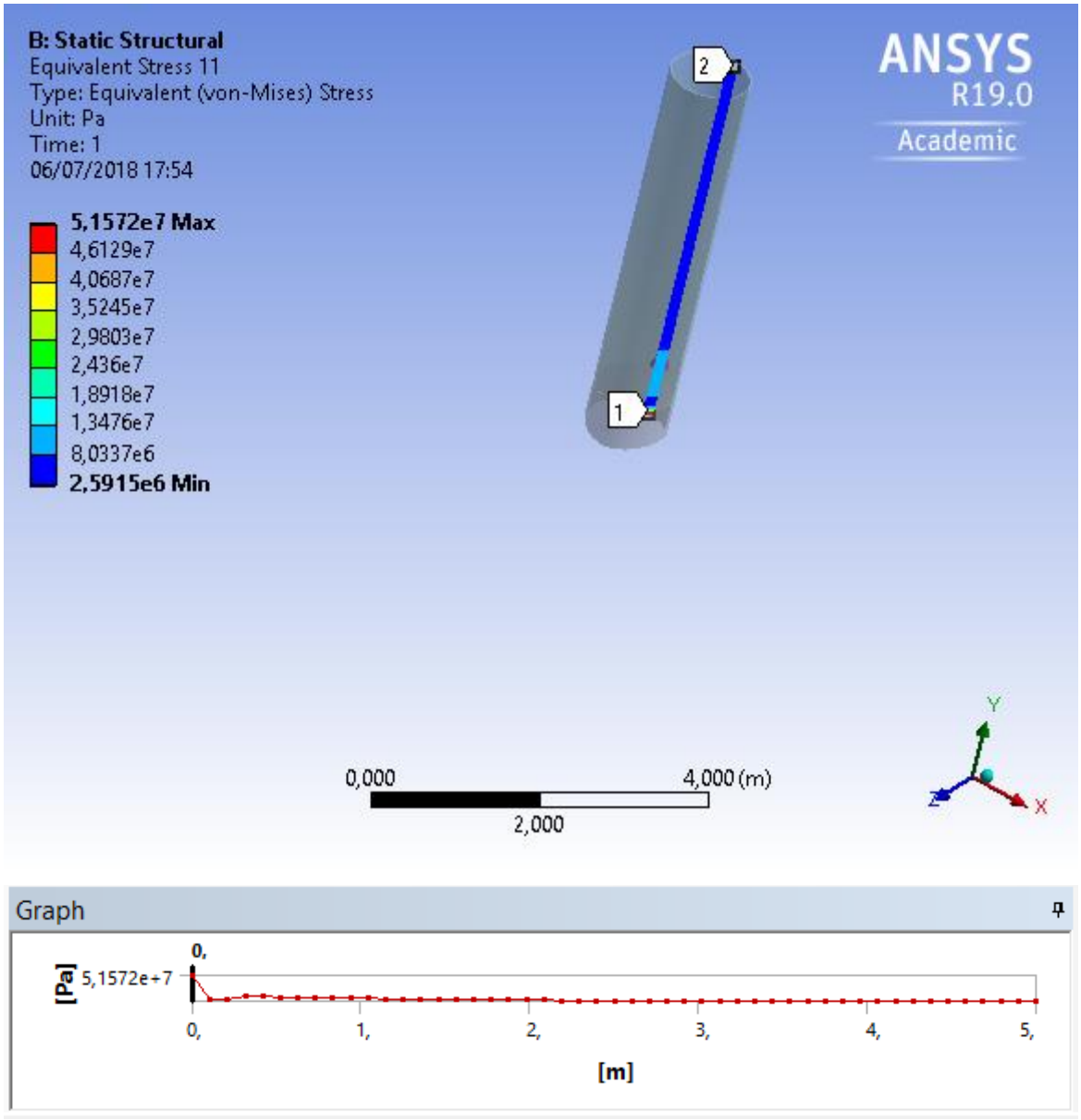

Figure 47 - Stress distribution in brace B for axial loading case: Side 4

4.3.1.3 BRACE C (5112)

In Figures 48 to 51 are displayed the stress distribution paths for the axial loading case that are used in the study of the stress concentration factor evaluation of brace C. There are 4 paths for the brace to study and are displayed with the number 1 to number 2. (see Figure 25)

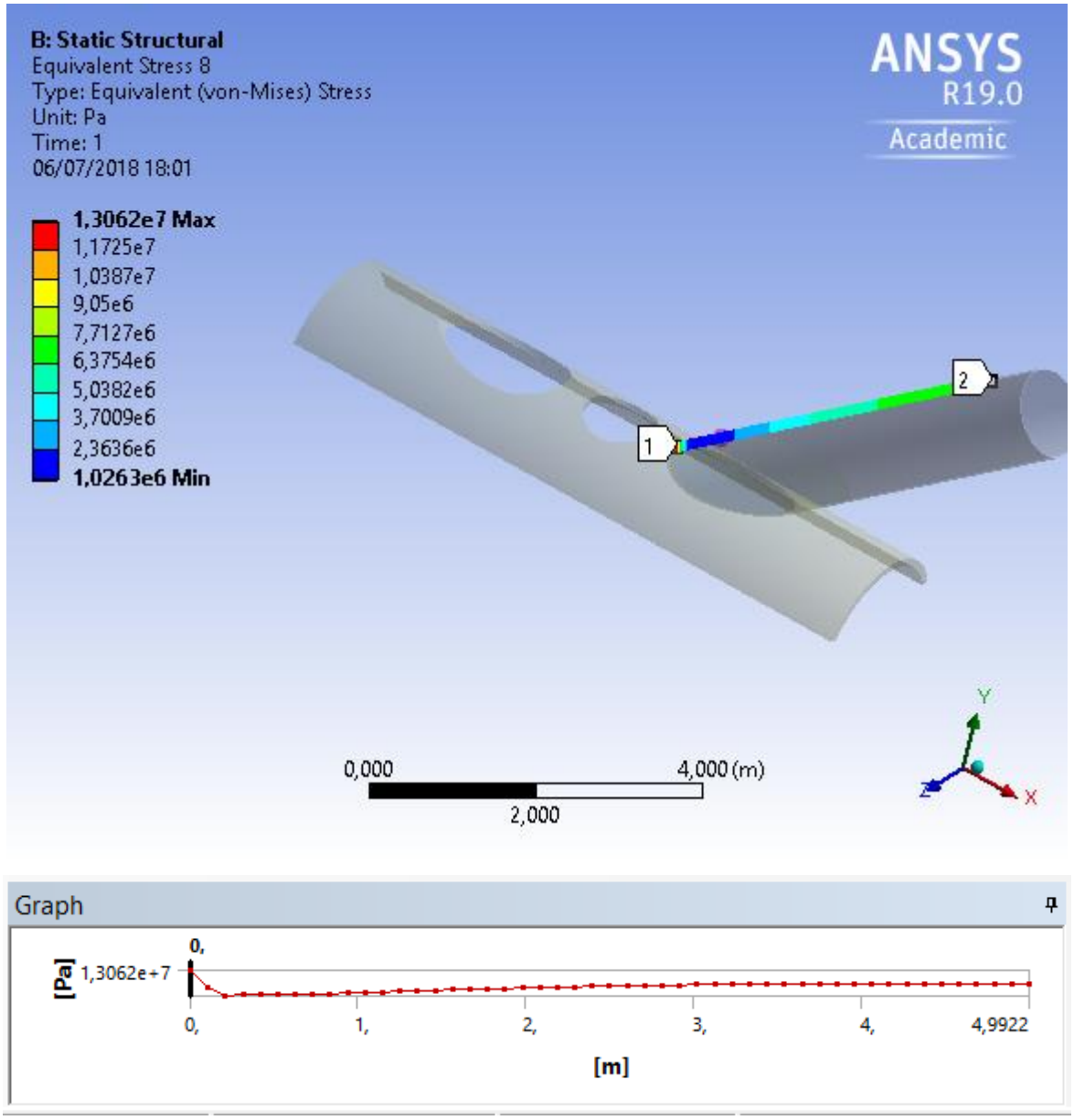

Figure 48 - Stress distribution in brace C for axial loading case: Side 1

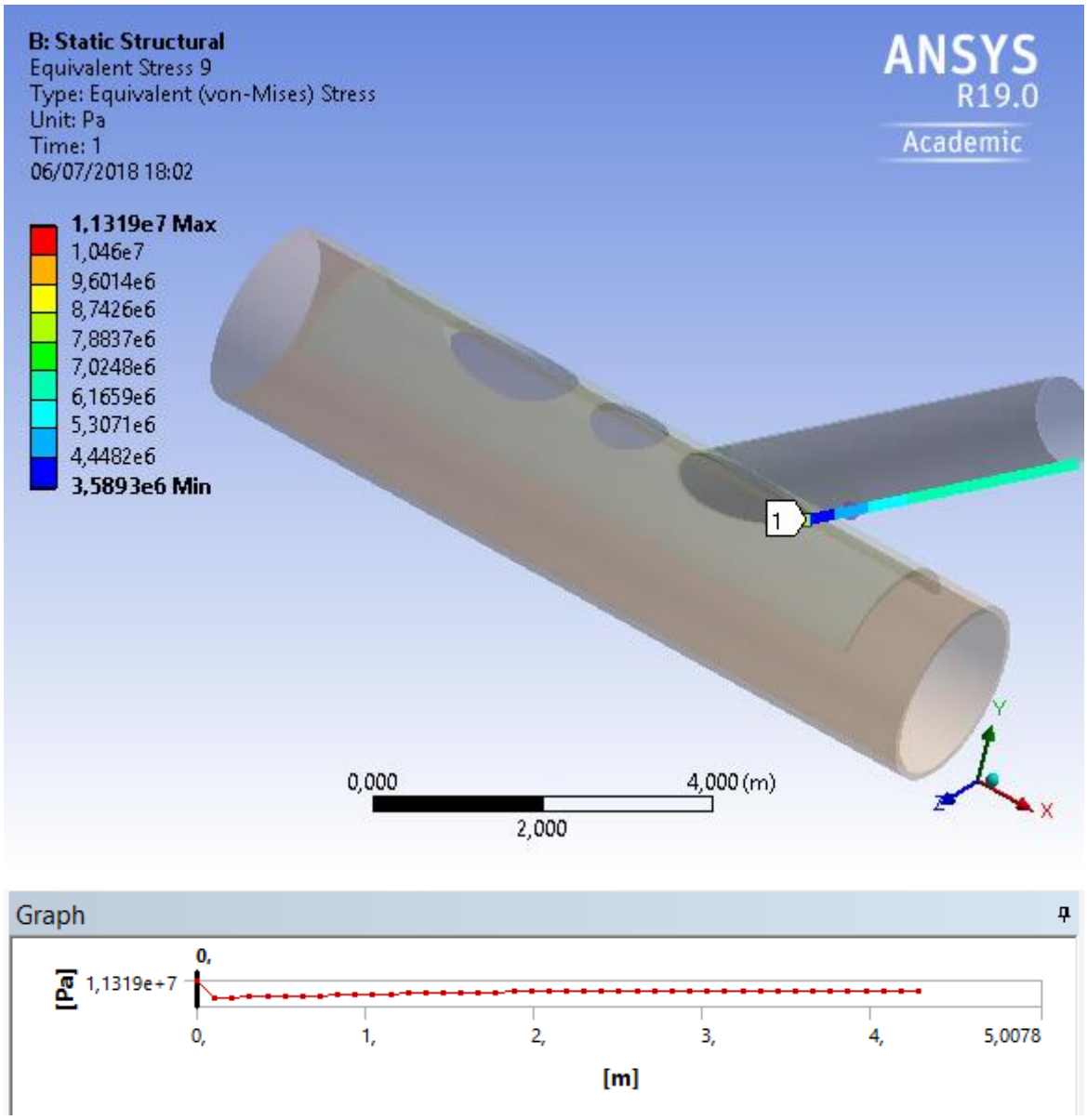

Figure 49 - Stress distribution in brace C for axial loading case: Side 2

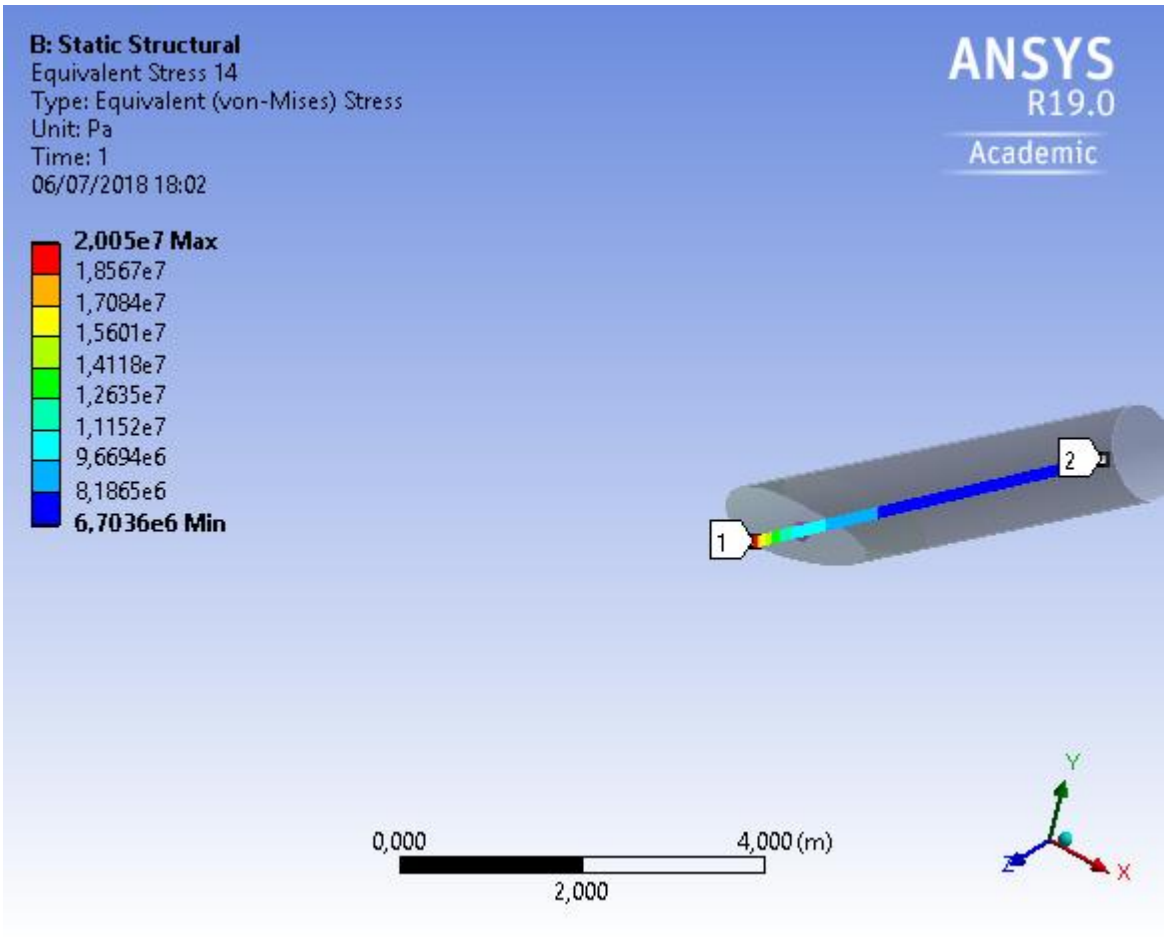

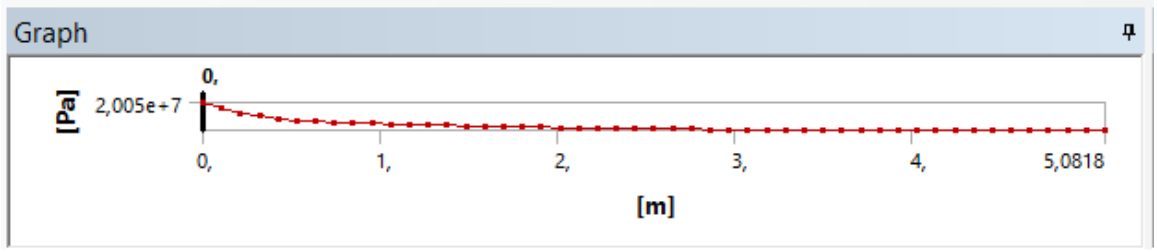

Figure 50 - Stress distribution in brace C for axial loading case: Side 3

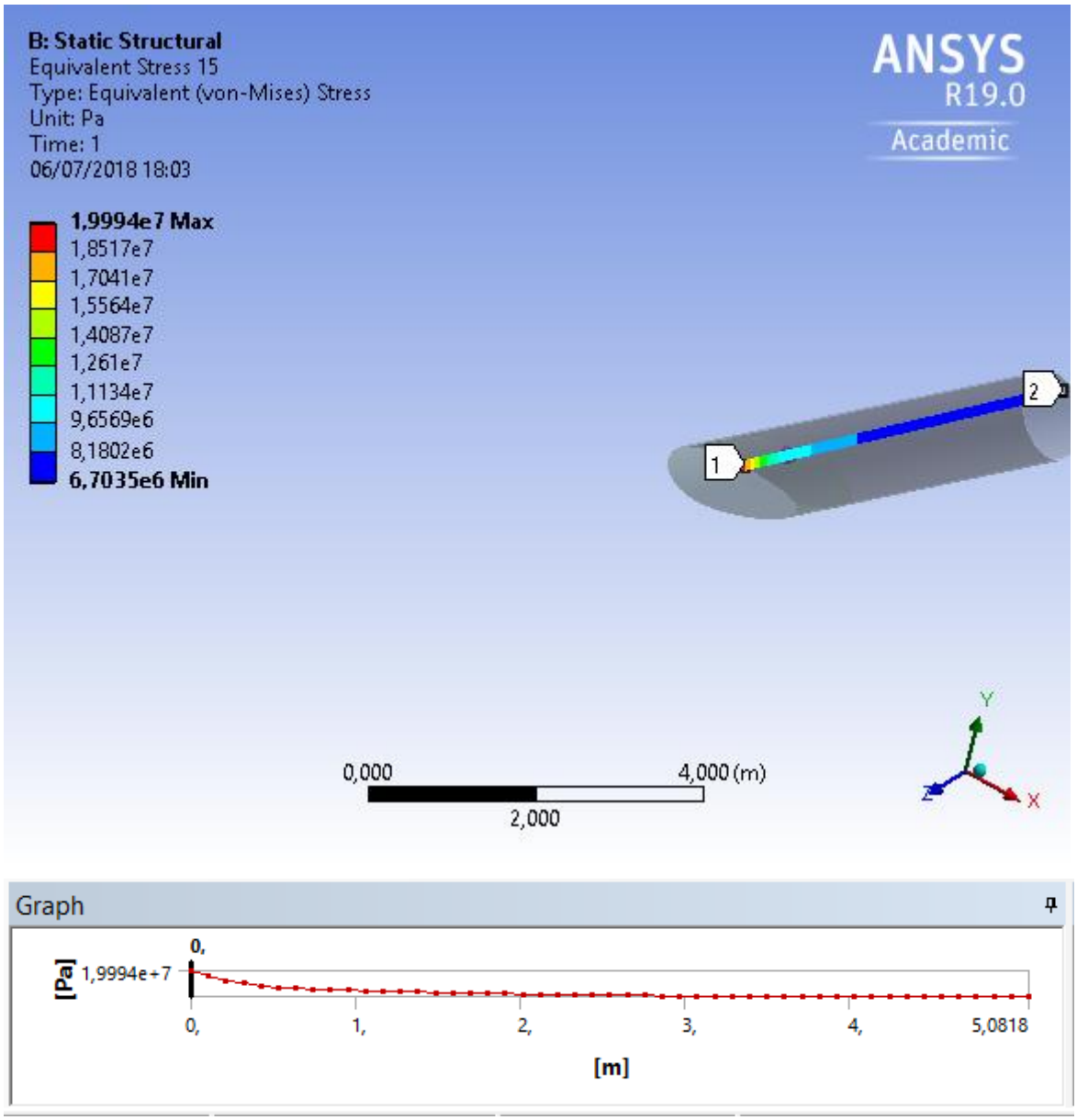

Figure 51 - Stress distribution in brace C for axial loading case: Side 4

4.3.1.4 CHORD (MEMBERS 4936-4937)

In Figure 52 is displayed the stress distribution path for the axial loading case that it's used in the study of the stress concentration factor evaluation for the chord. There is only 1 path considered to the evaluation of the stress concentration factors in the chord since the crown points have way higher stresses compared to the saddle of each brace in the chord.

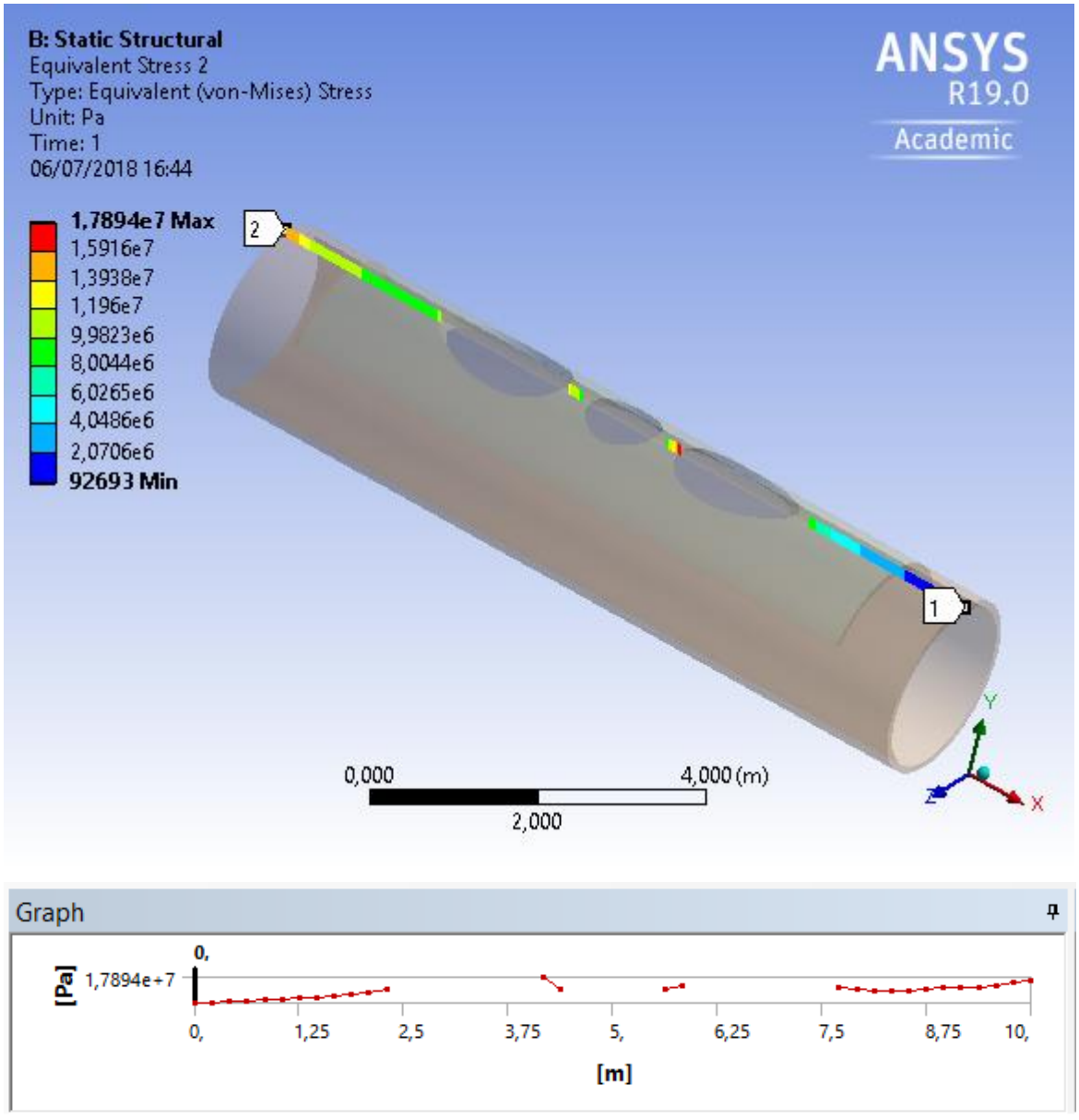

Figure 52 - Stress distribution in chord for axial loading case

4.3.2 IN-PLANE BENDING CASE

In Figures 53 and 54 are shown the stress fields considering the in-plane bending loading case. It is possible identify that the highest stresses are found at the intersection between the chord and the braces at the so-called crown and saddle places. In more detail, the linear-stress distribution paths for each element of the KT-joint are shown in the following sections.

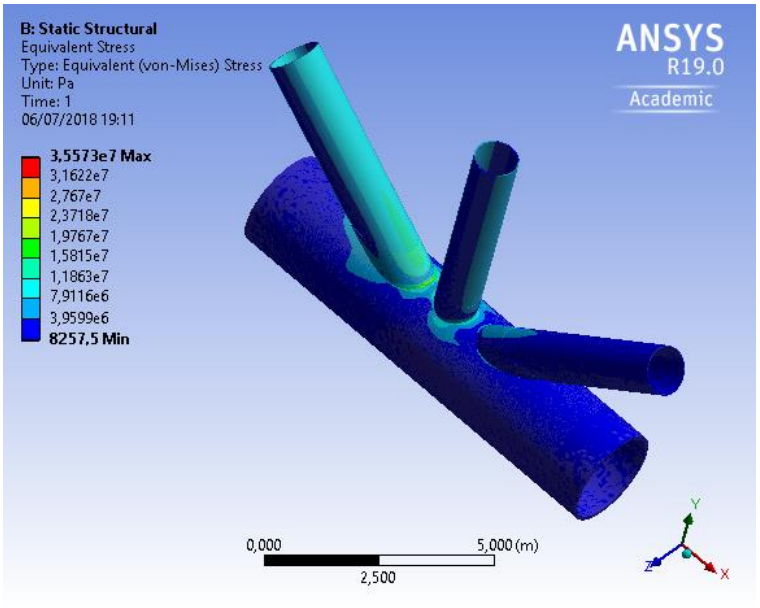

Figure 53 - Stress fields for in-plane loading case in the KT-joint under consideration

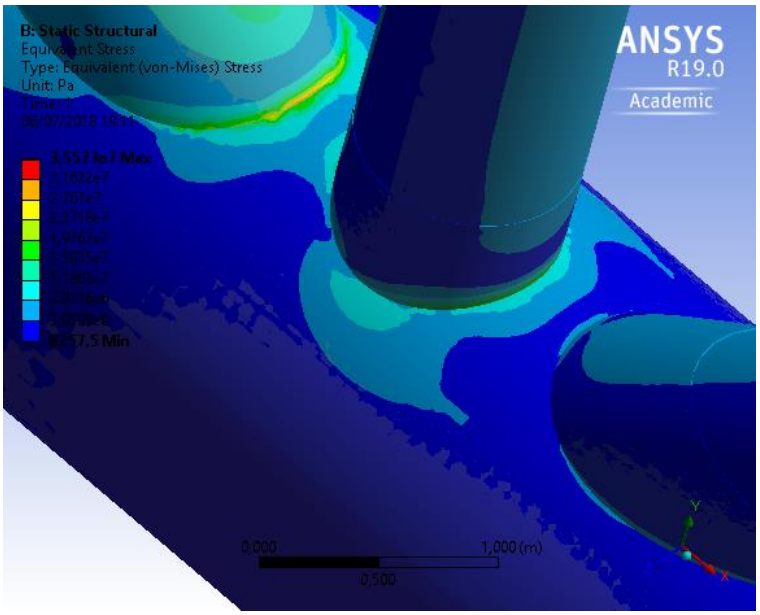

Figure 54 - Stress fields for in-plane loading case in the KT-joint under consideration (Closer look)

4.3.2.1 BRACE A (5110)

In Figures 55 to 59 are displayed the stress distribution paths for the in-plane bending loading case that are used in the study of the stress concentration factor evaluation of brace A. There are 4 paths for the brace to study and are displayed with the number 1 to number 2. (see Figure 25)

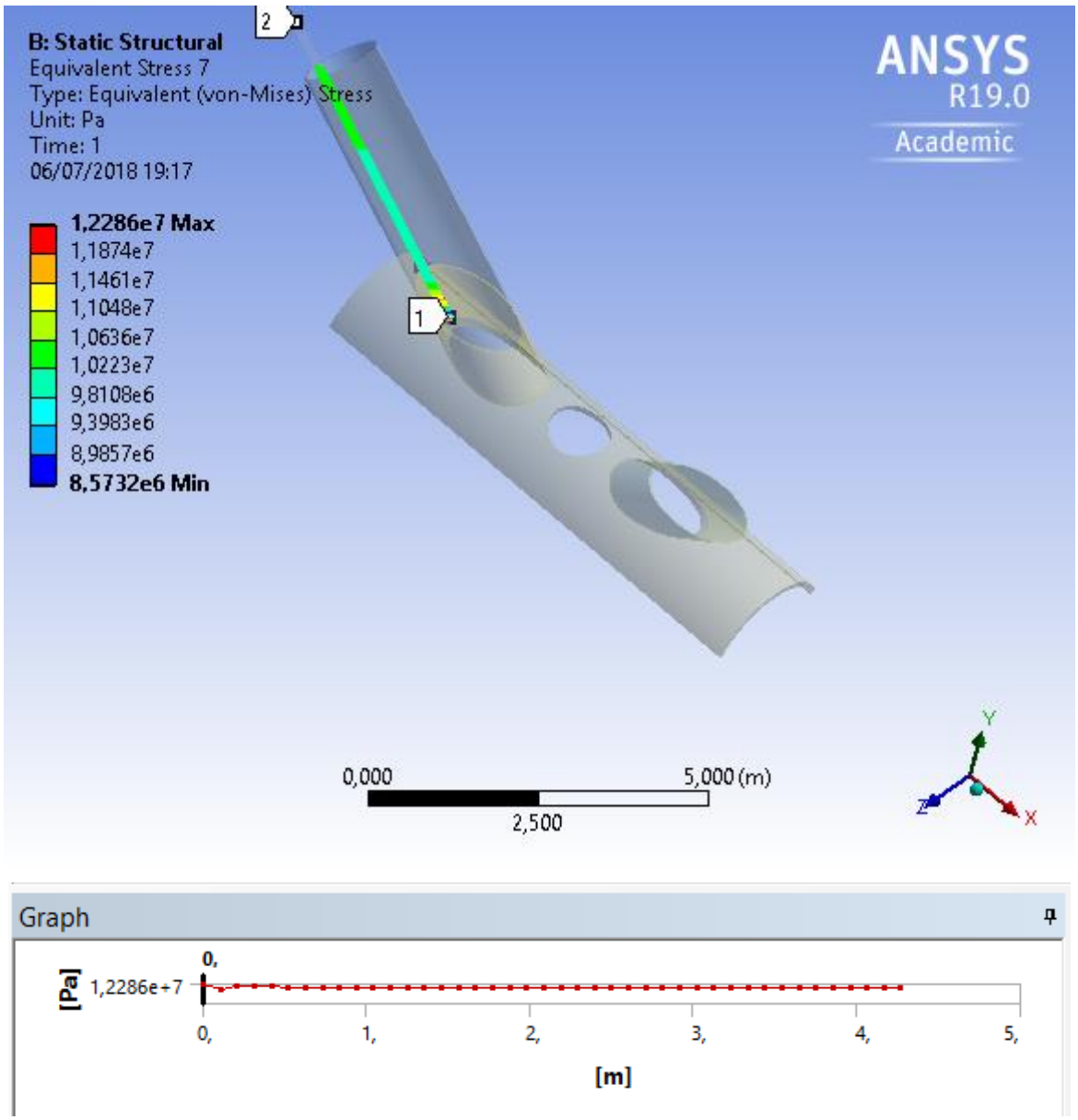

Figure 55 - Stress distribution in brace A for in-plane bending loading case: Side 1

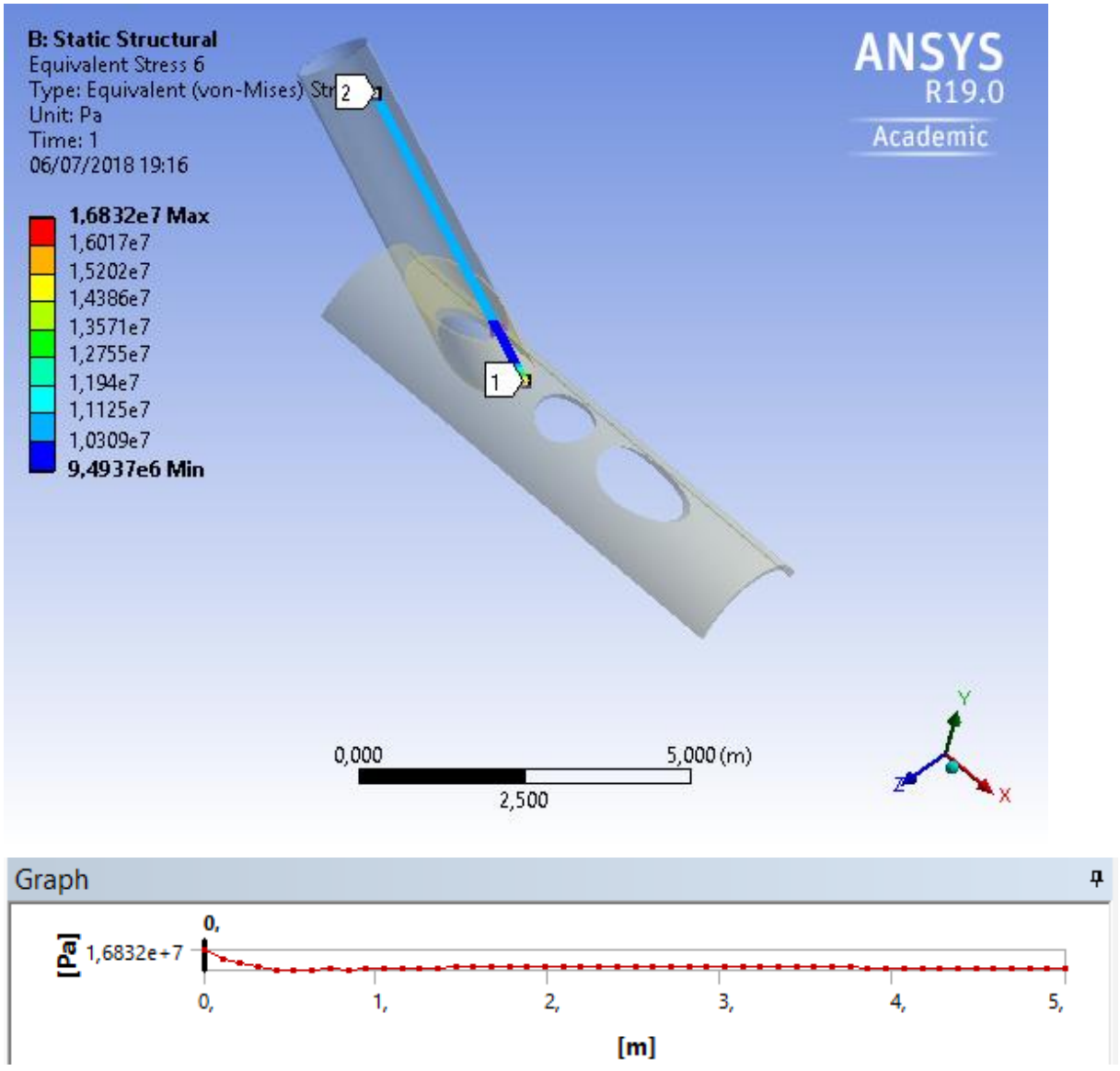

Figure 56 - Stress distribution in brace A for in-plane bending loading case: Side 2

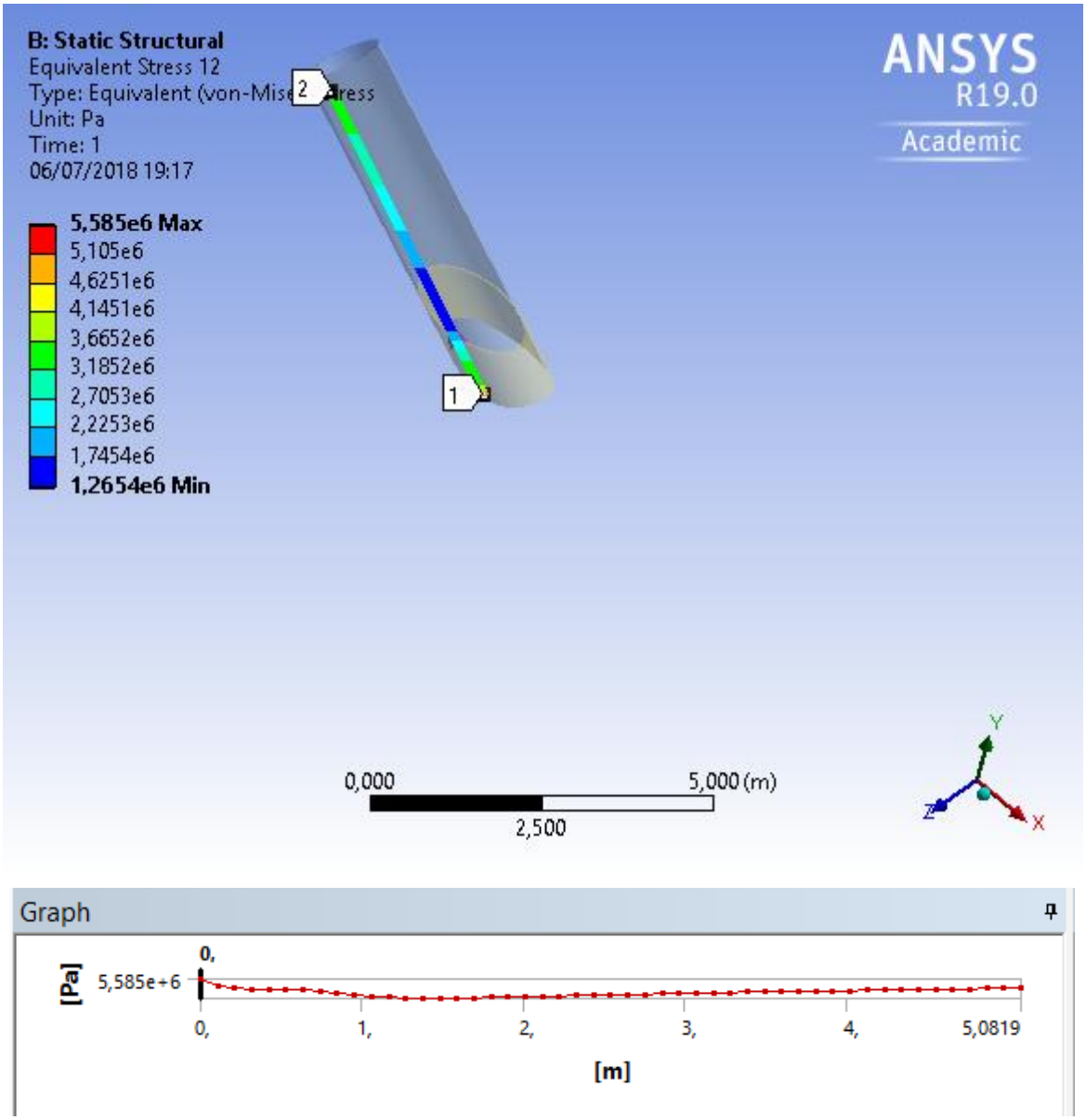

Figure 57 - Stress distribution in brace A for in-plane bending loading case: Side 3

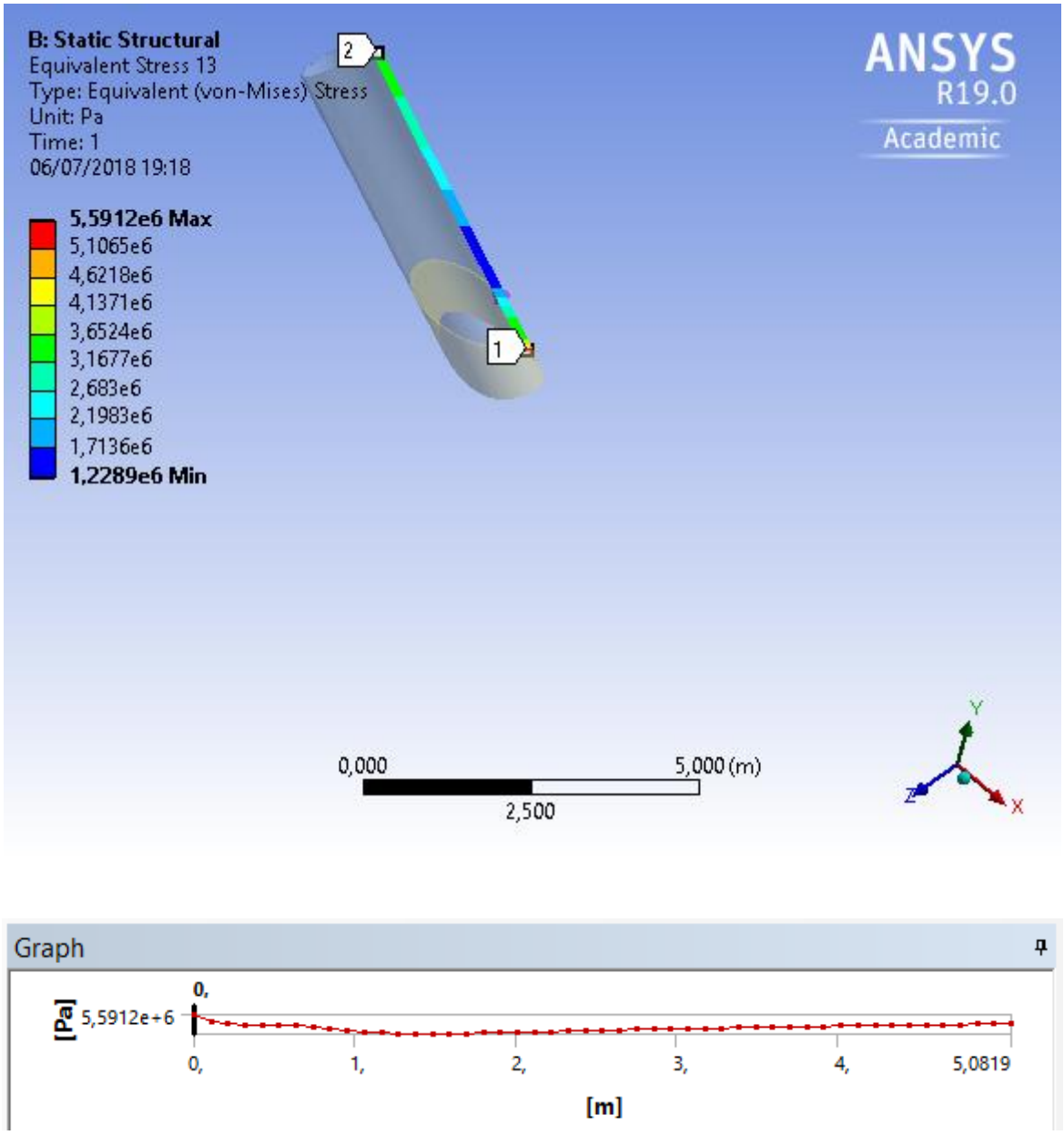

Figure 58 - Stress distribution in brace A for in-plane bending loading case: Side 4

4.3.2.2. BRACE B (MEMBER 5116)

In Figures 59 to 62 are displayed the stress distribution paths for the in-plane bending loading case that are used in the study of the stress concentration factor evaluation of brace B. There are 4 paths for the brace to study and are displayed with the number 1 to number 2. (see Figure 25)

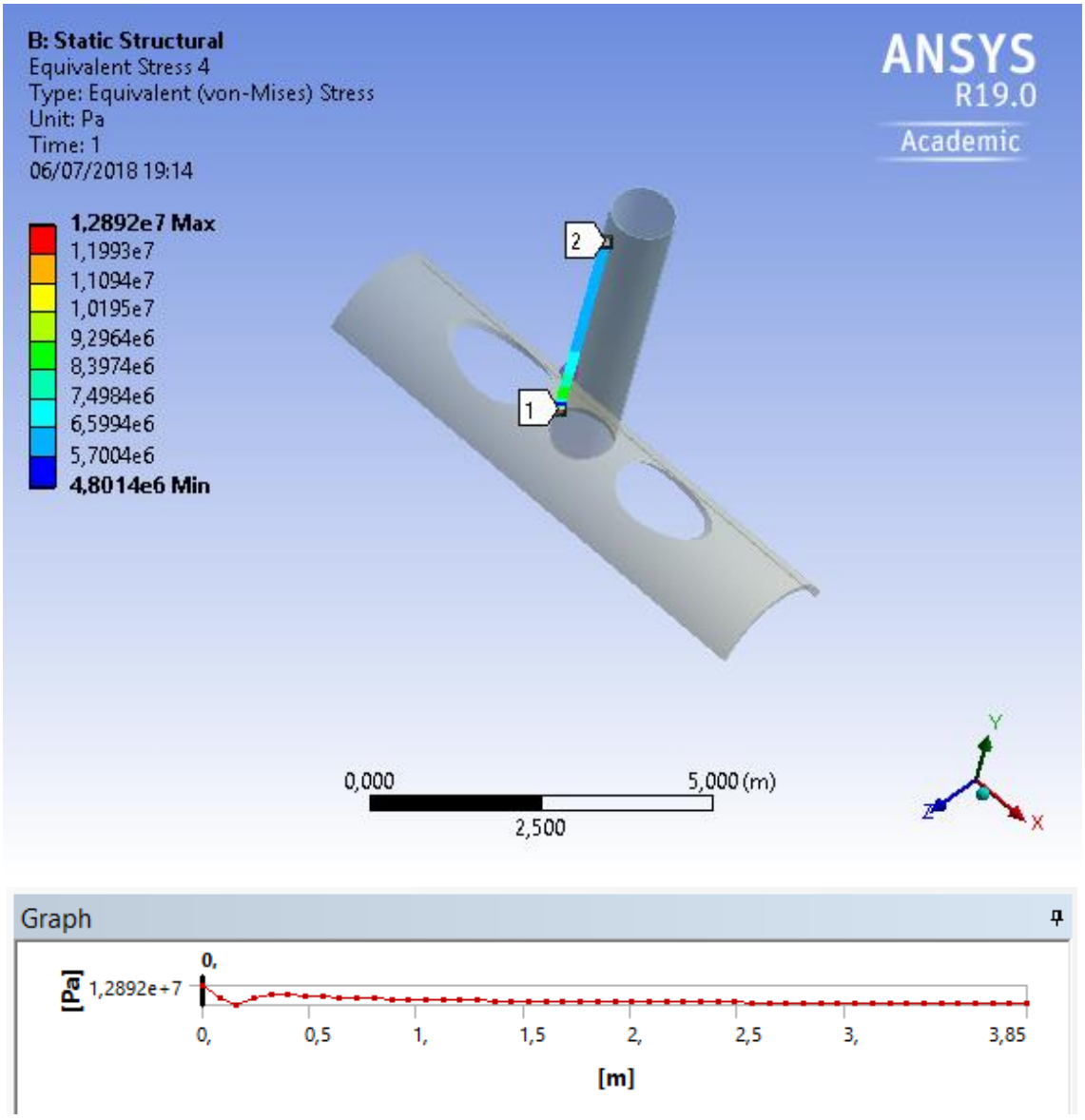

Figure 59 - Stress distribution in brace B for in-plane bending loading case: Side 1

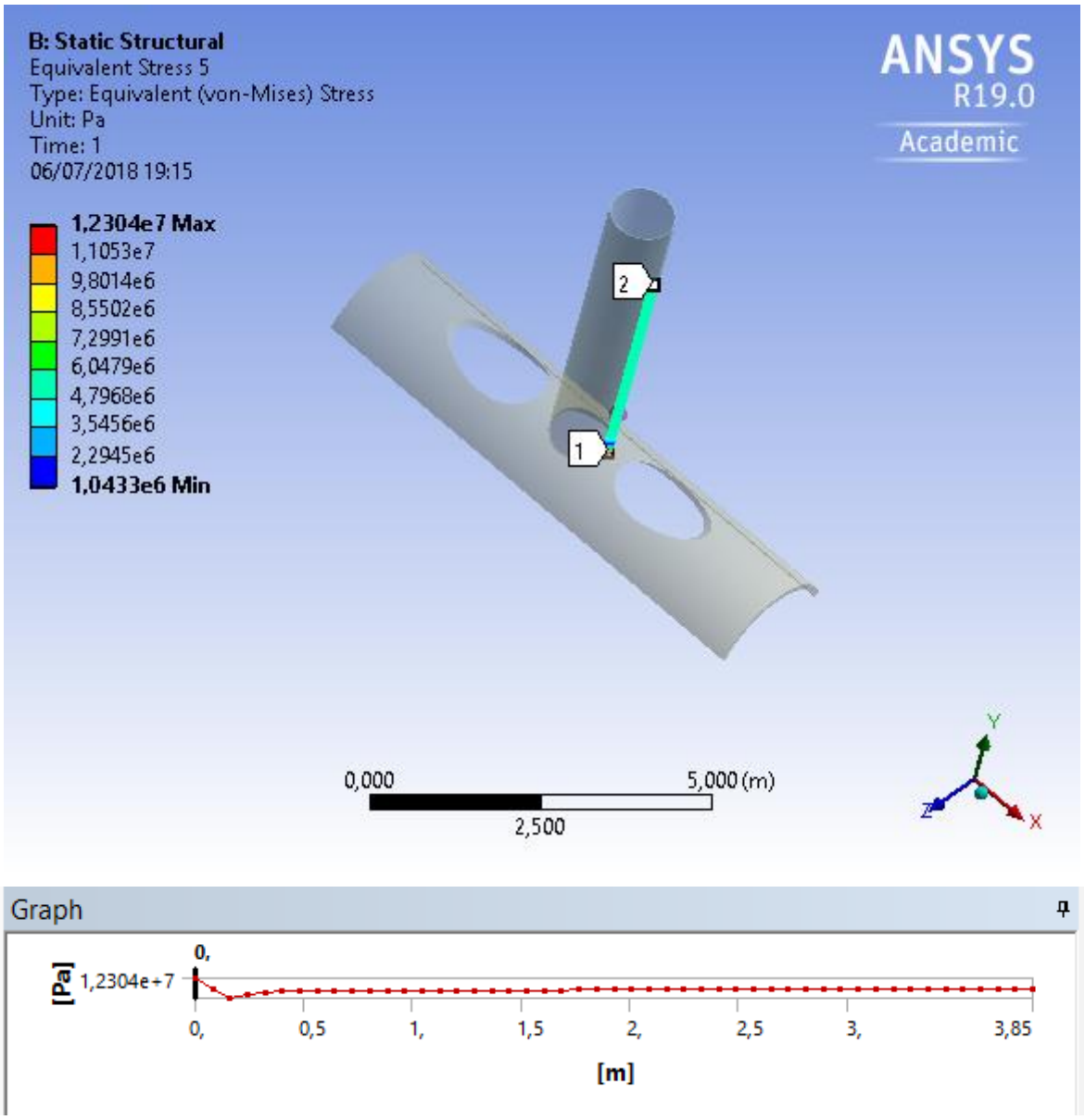

Figure 60 - Stress distribution in brace B for in-plane bending loading case: Side 2

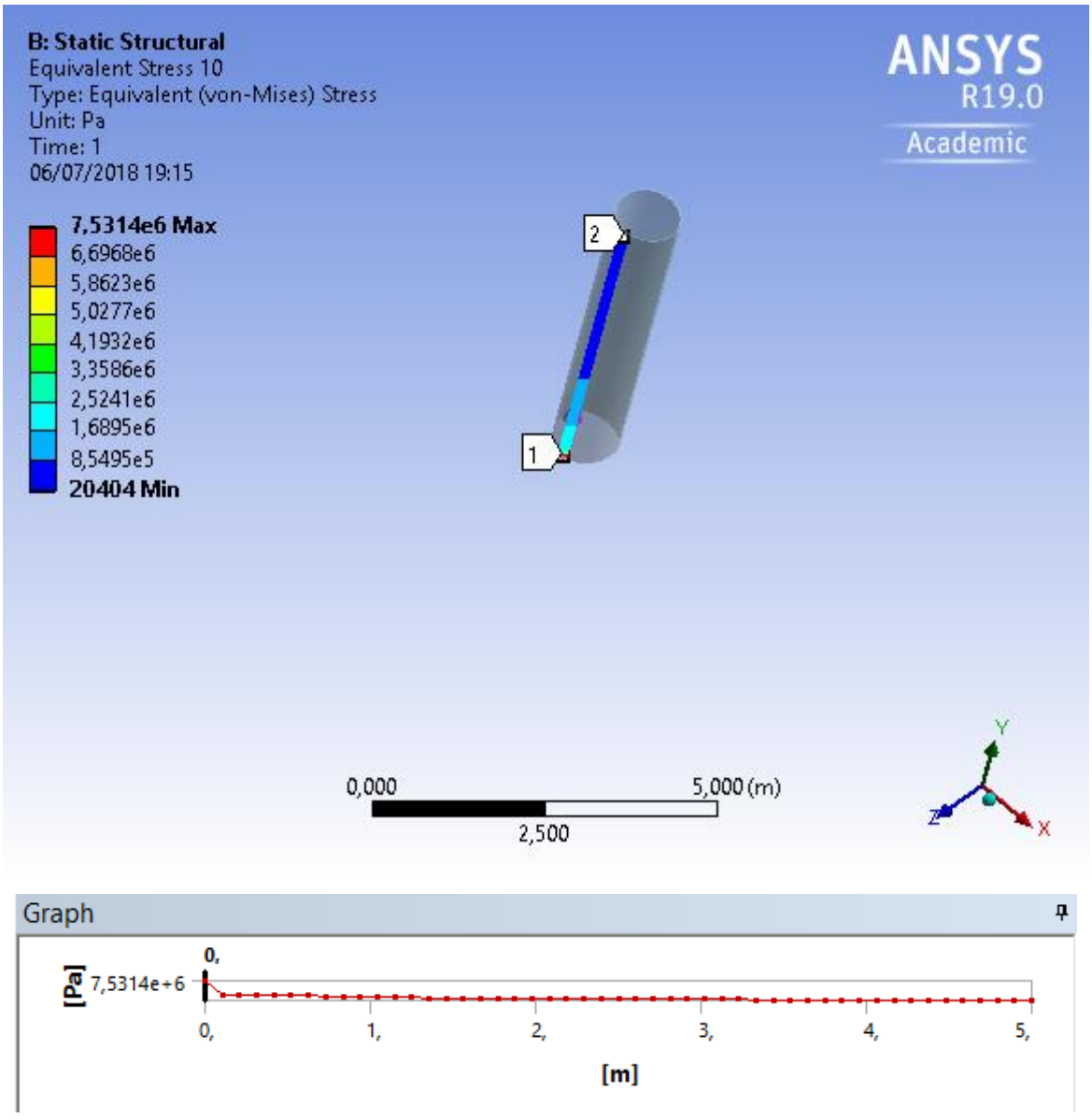

Figure 61 - Stress distribution in brace B for in-plane bending loading case: Side 3

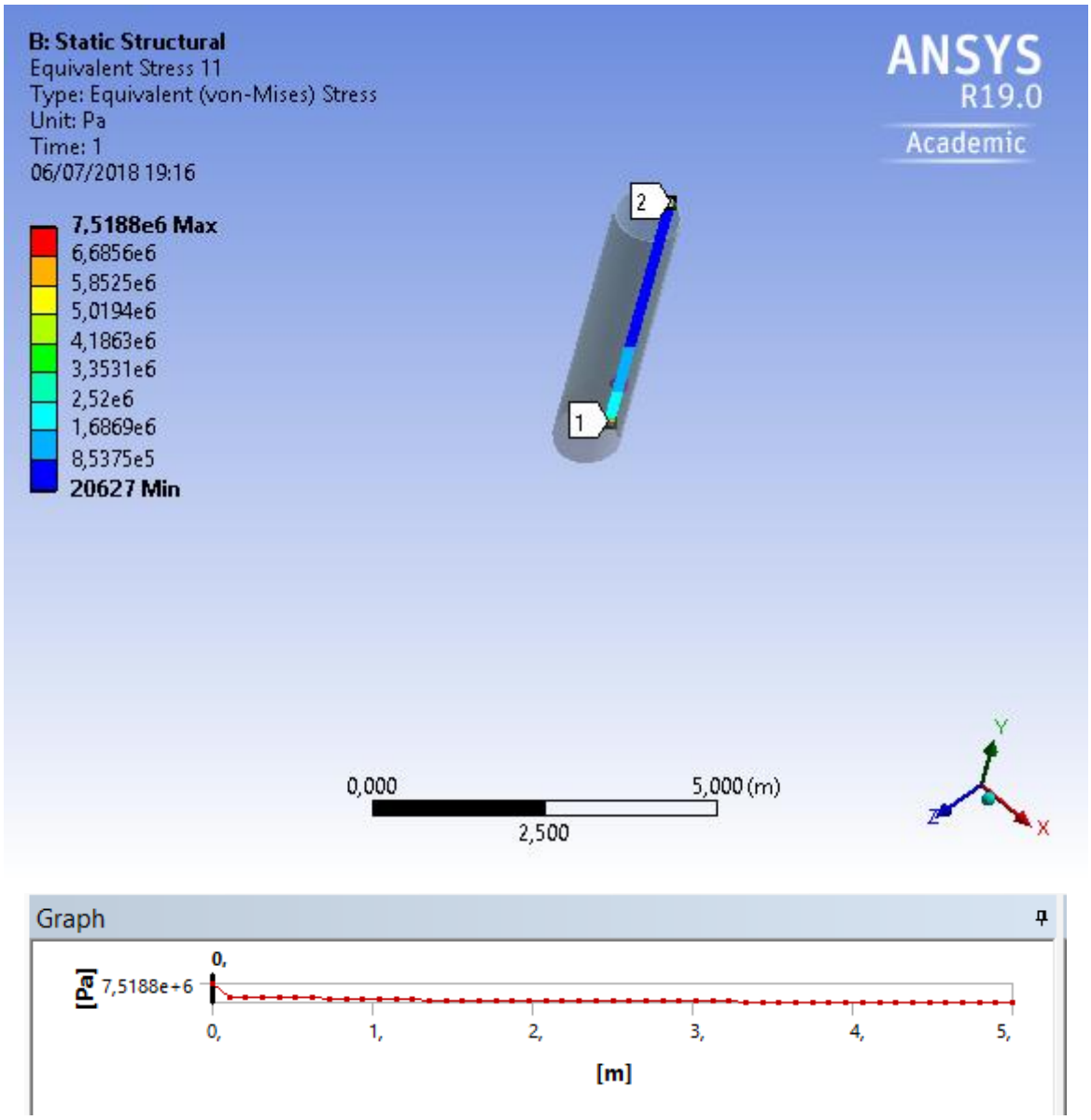

Figure 62 - Stress distribution in brace B for in-plane bending loading case: Side 4

4.3.2.3. BRACE C (MEMBER 5112)

In Figures 63 to 66 are displayed the stress distribution paths for the in-plane bending loading case that are used in the study of the stress concentration factor evaluation of brace C. There are 4 paths for the brace to study and are displayed with the number 1 to number 2. (see Figure 25)

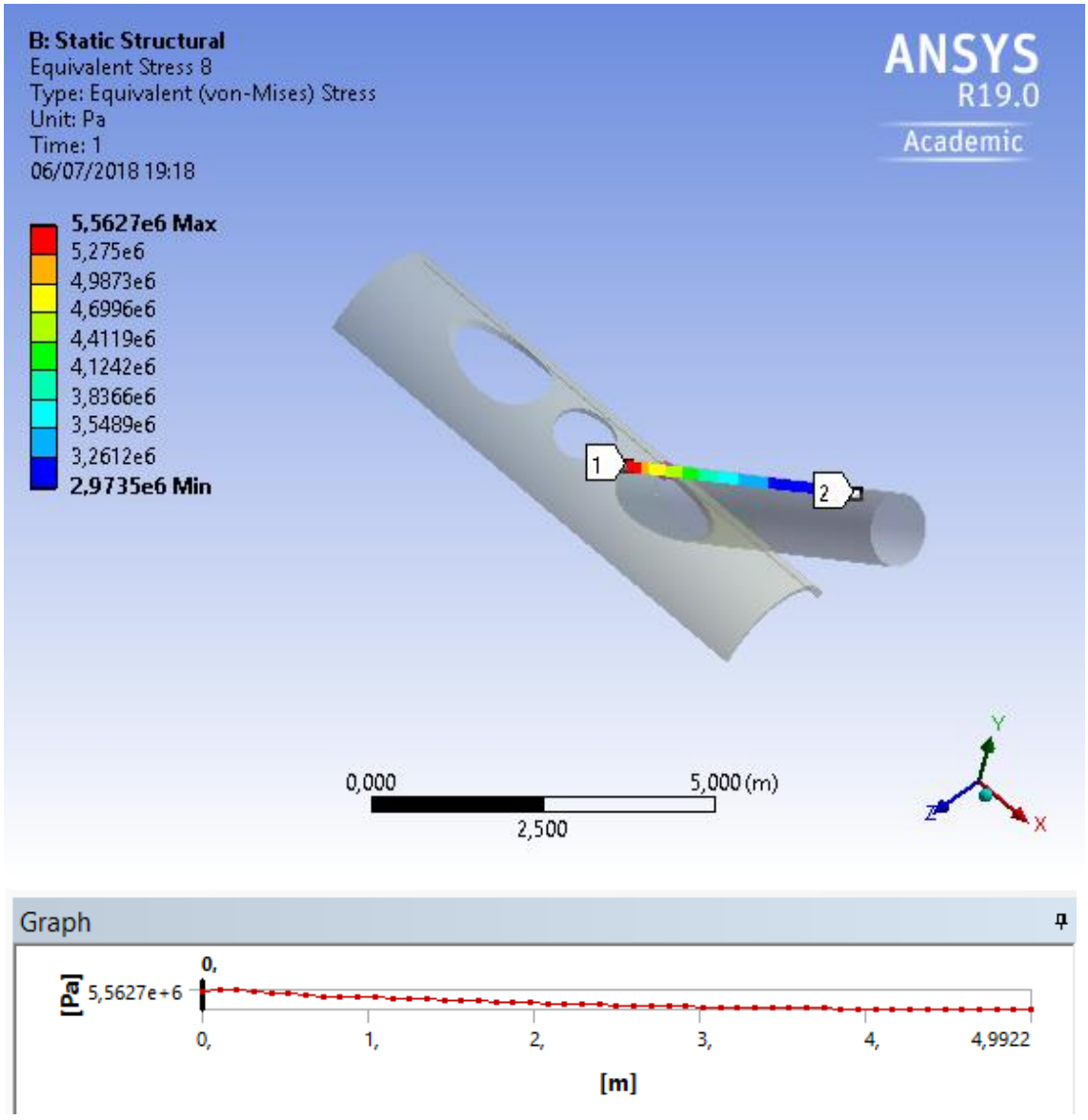

Figure 63 - Stress distribution in brace C for in-plane bending loading case: Side 1

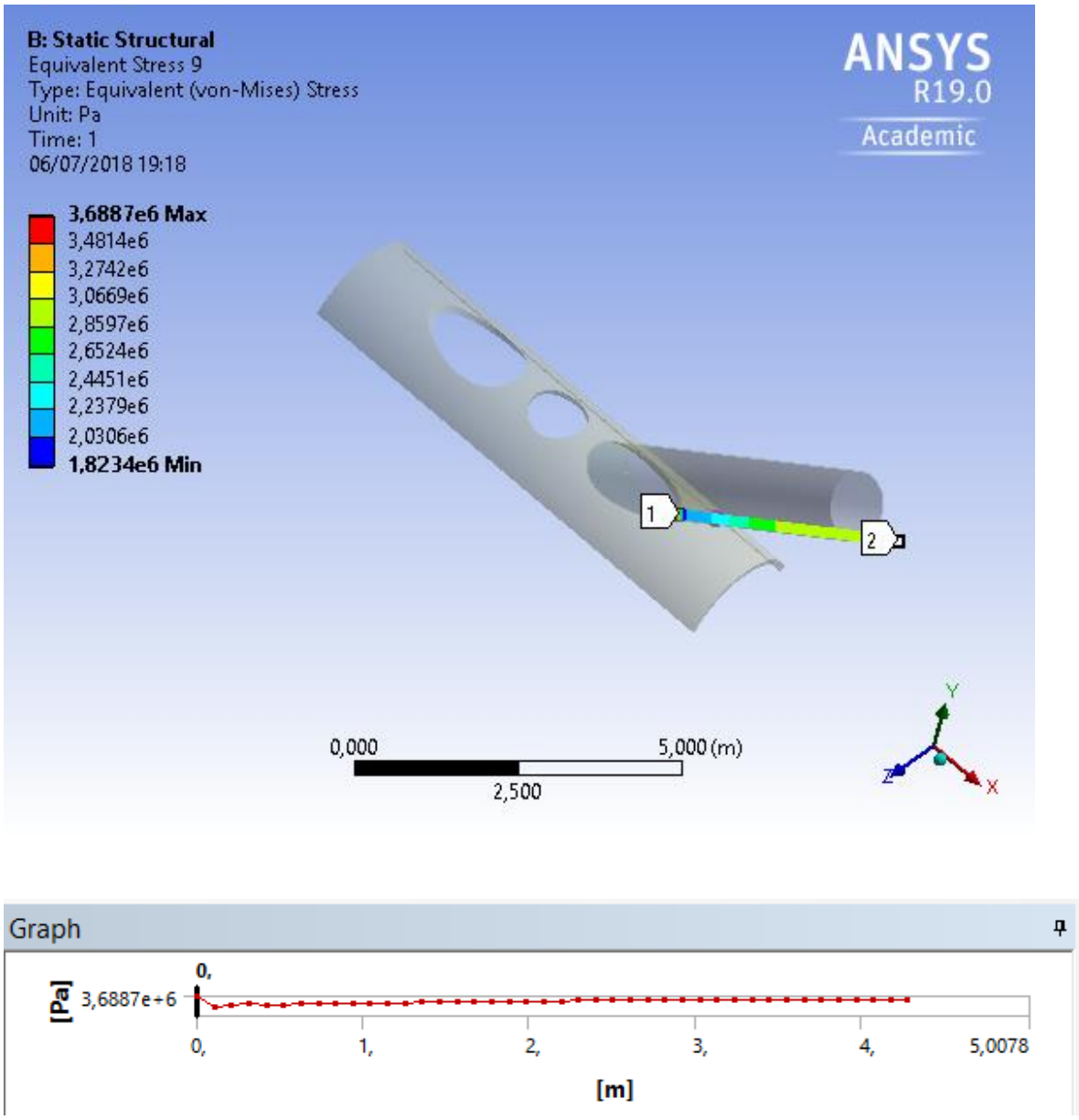

Figure 64 - Stress distribution in brace C for in-plane bending loading case: Side 2

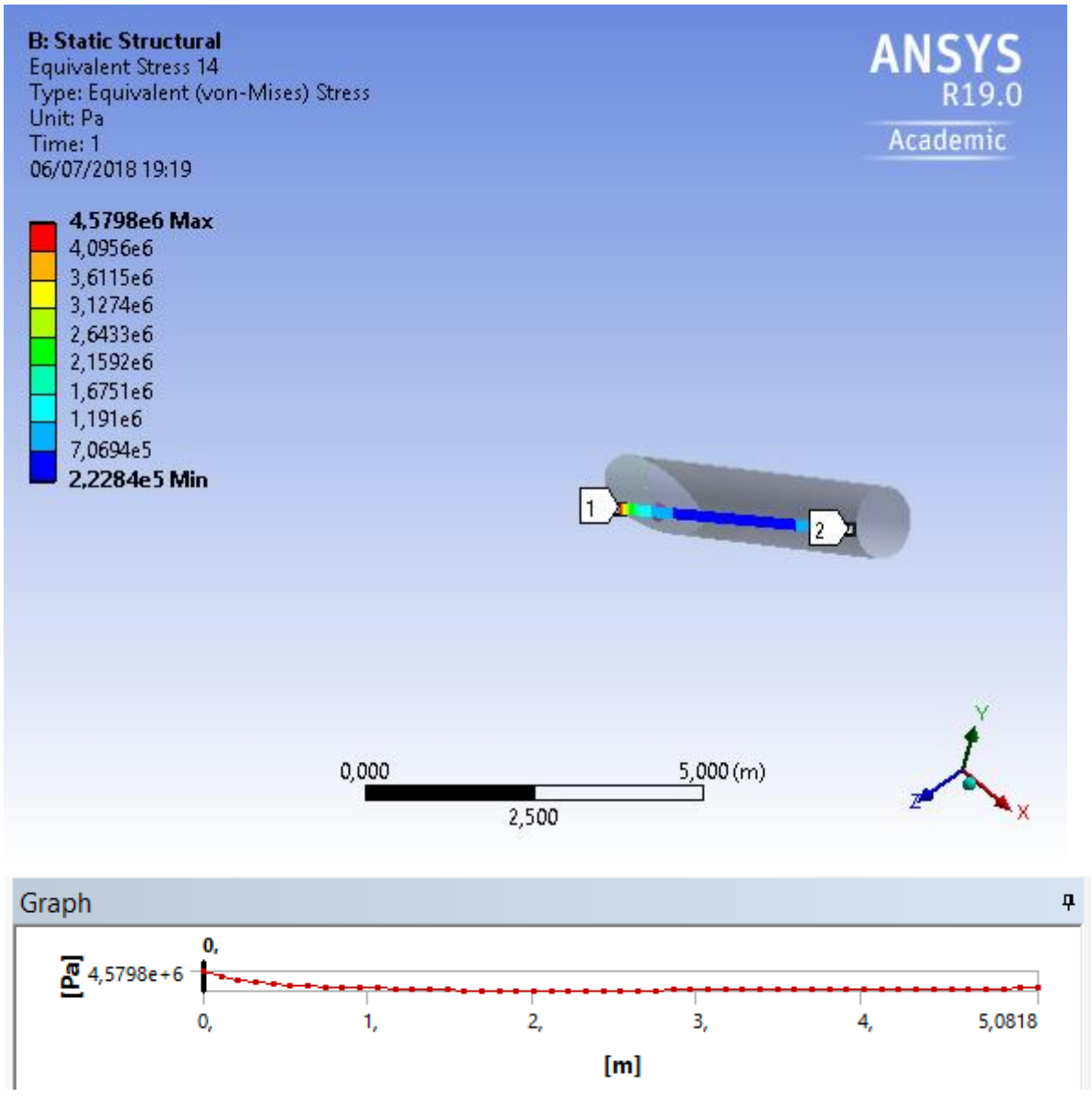

Figure 65 - Stress distribution in brace C for in-plane bending loading case: Side 3

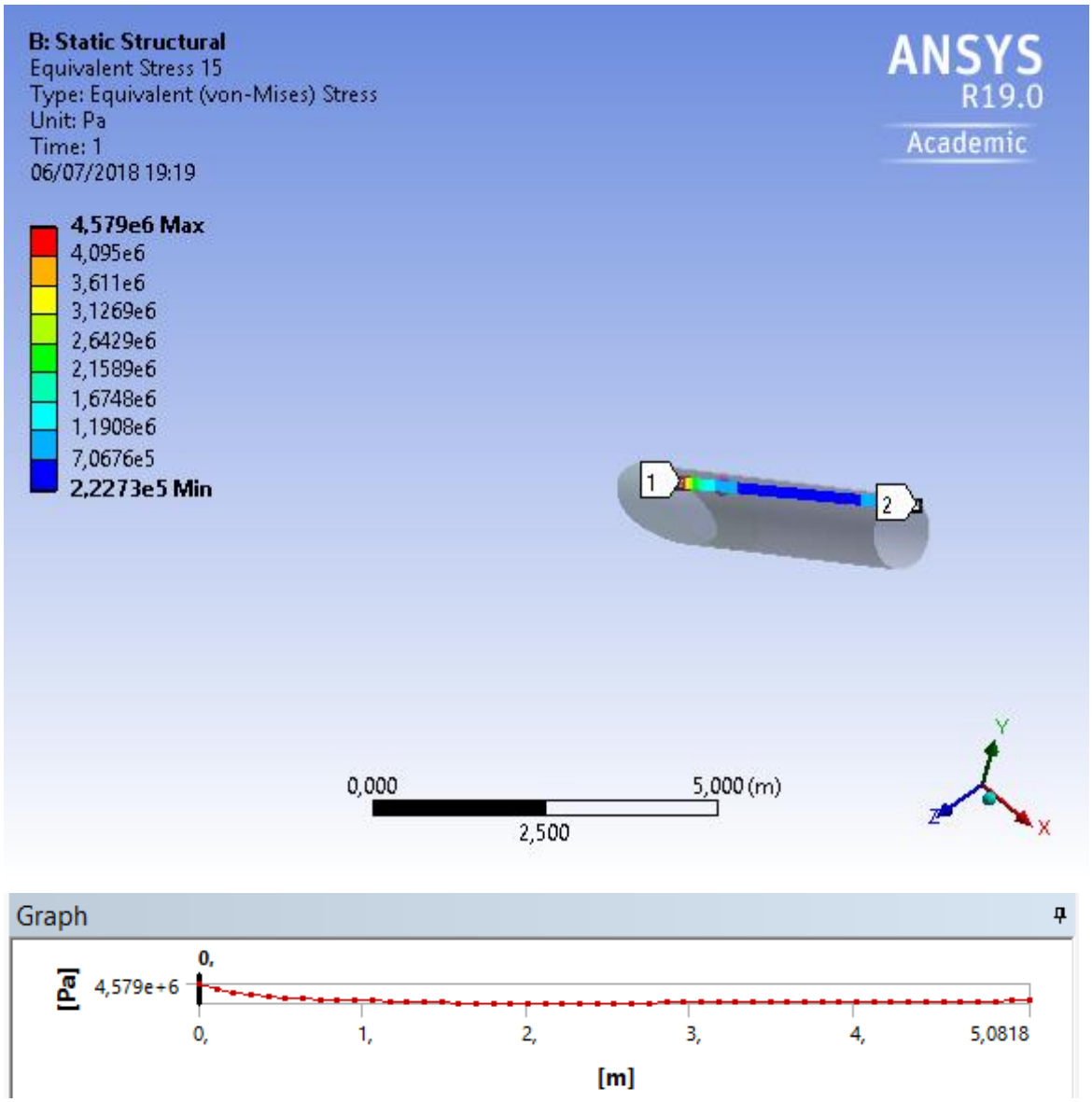

Figure 66 - Stress distribution in brace C for in-plane bending loading case: Side 4

4.3.2.4. CHORD (MEMBERS 4936-4937)

In Figure 67 is displayed the stress distribution path for the in-plane bending loading case that it's used in the study of the stress concentration factor evaluation for the chord. There is only 1 path considered to the evaluation of the stress concentration factors in the chord since the crown points have way higher stresses compared to the saddle of each brace in the chord.

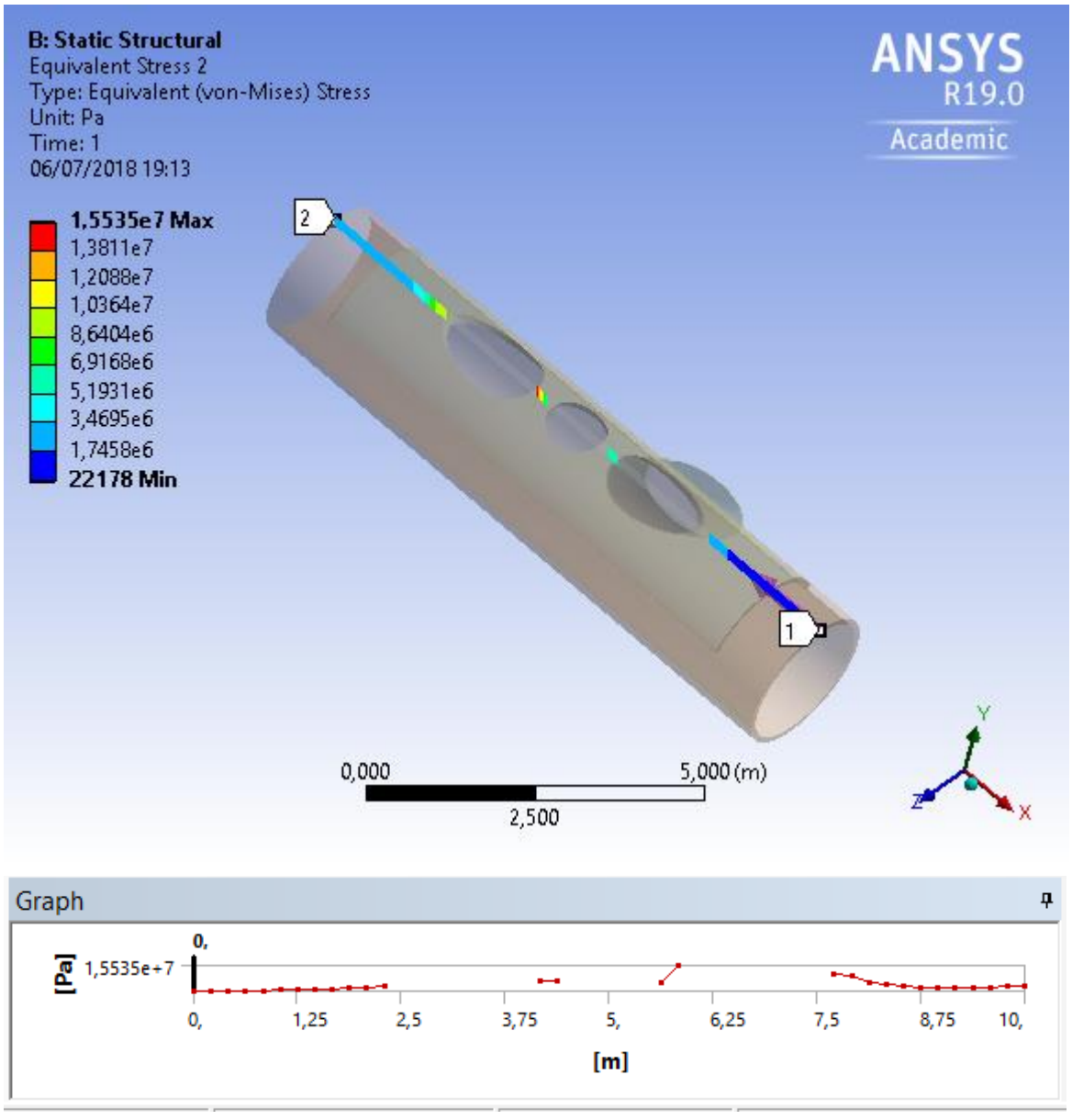

Figure 67 - Stress distribution in chord for in-plane bending loading case

4.3.3. OUT-PLANE BENDING CASE

In Figures 68 and 69 are shown the stress fields considering the out-plane bending loading case. It is possible identify that the highest stresses are found at the intersection between the chord and the braces at the so-called crown and saddle places. In more detail, the linear-stress distribution paths for each element of the KT-joint are shown in the following sections.

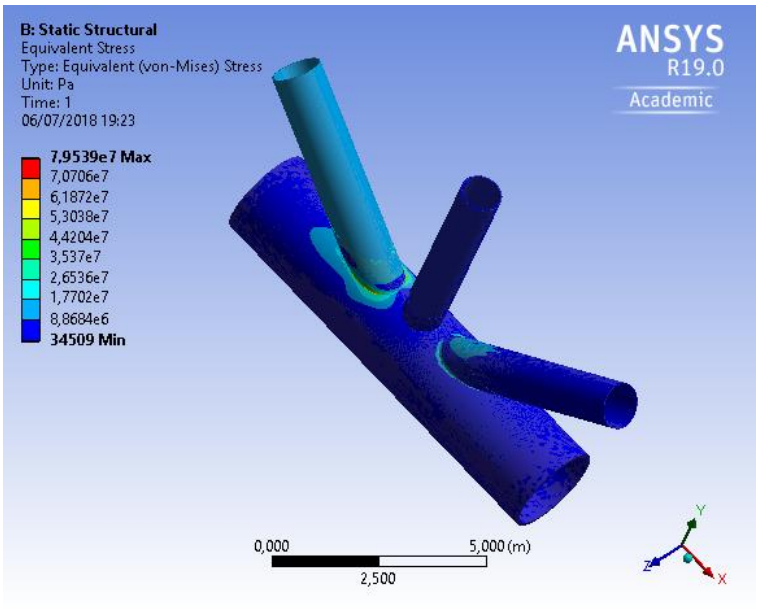

Figure 68 - Stress fields for out-plane loading case in the KT-joint under consideration

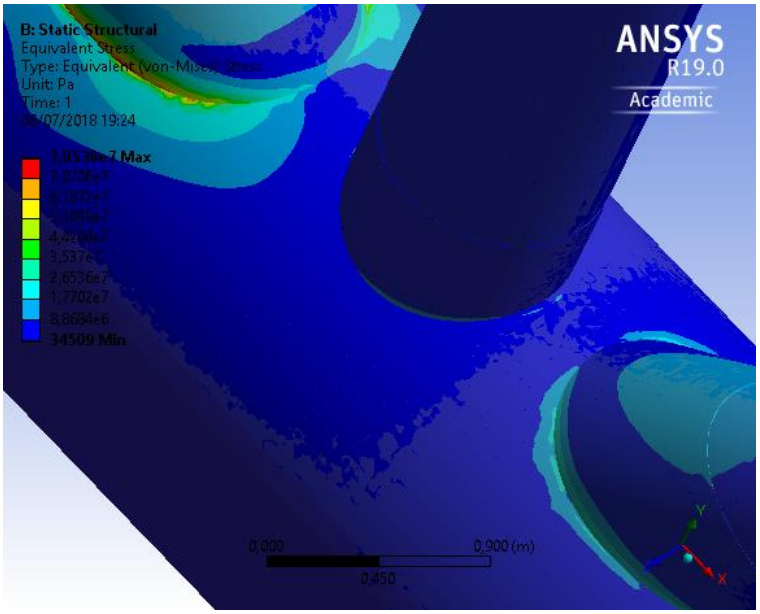

Figure 69 - Stress fields for out-plane loading case in the KT-joint under consideration (Closer look)

4.3.3.1. BRACE A (MEMBER 5110)

In Figures 70 to 73 are displayed the stress distribution paths for the out-plane bending loading case that is used in the study of the stress concentration factor evaluation of brace A. There are 4 paths for the brace to study and are displayed with the number 1 to number 2. (see Figure 25)

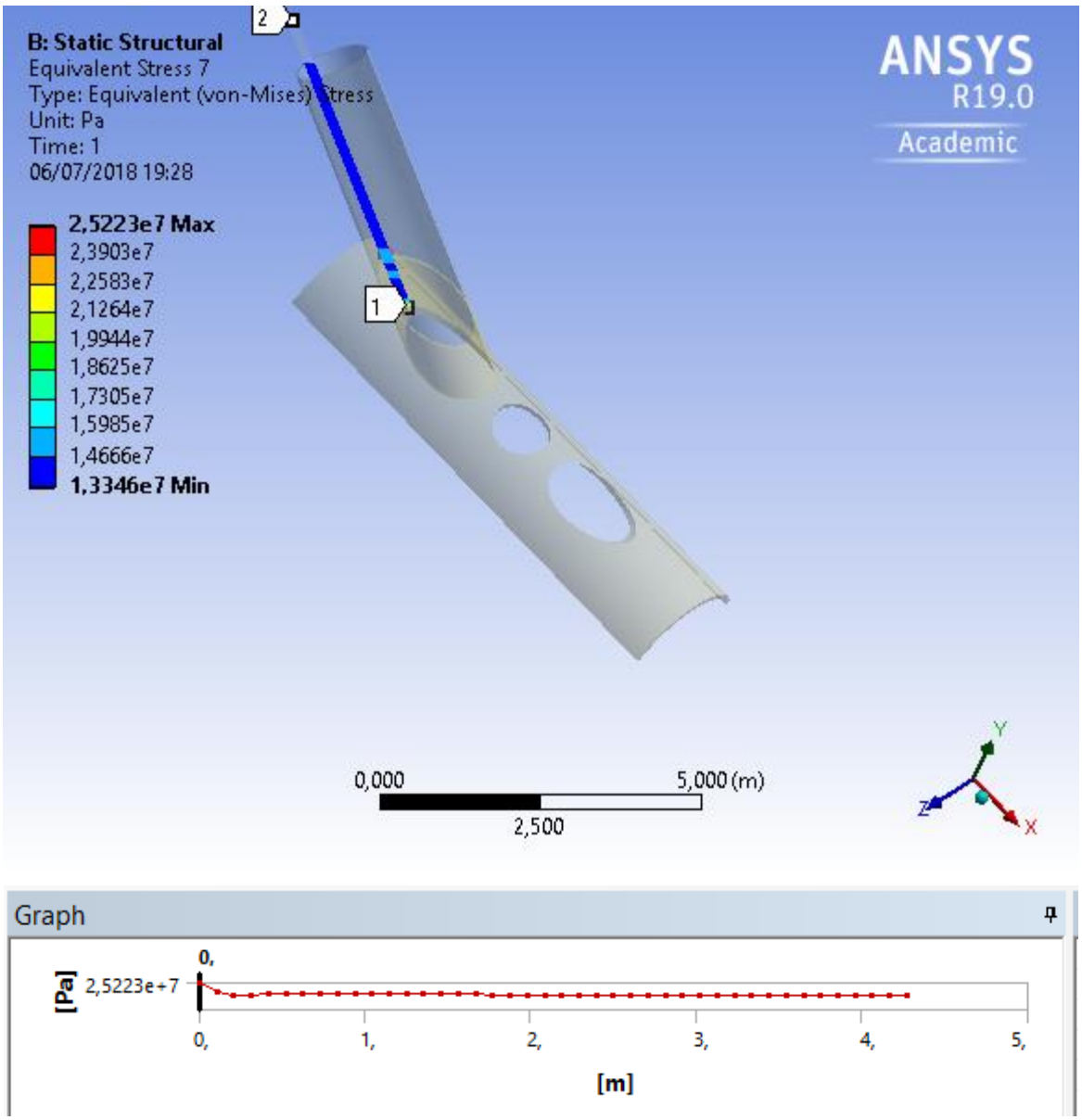

Figure 70 - Stress distribution in brace A for out-plane bending loading case: Side 1

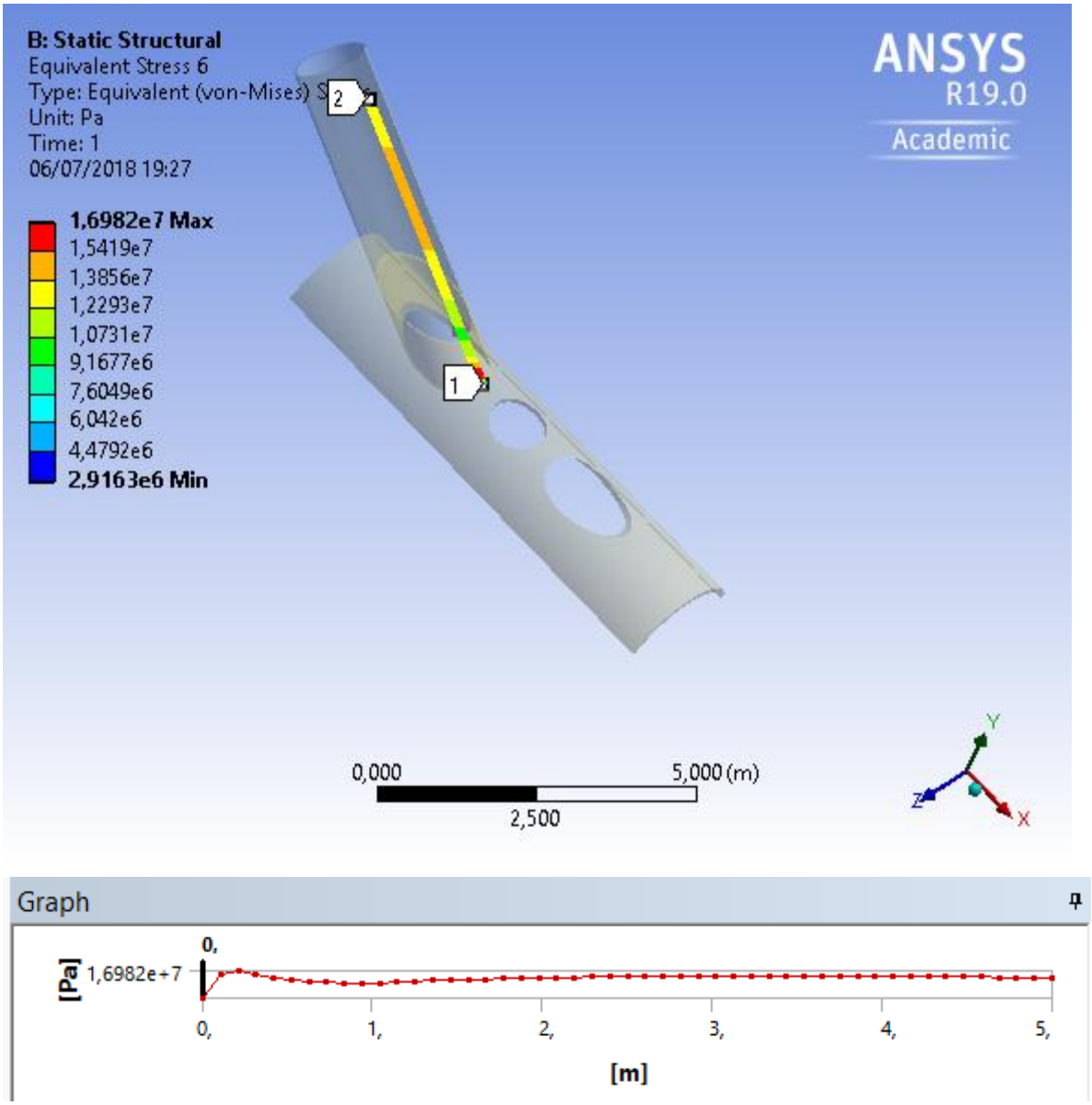

Figure 71 - Stress distribution in brace A for out-plane bending loading case: Side 2

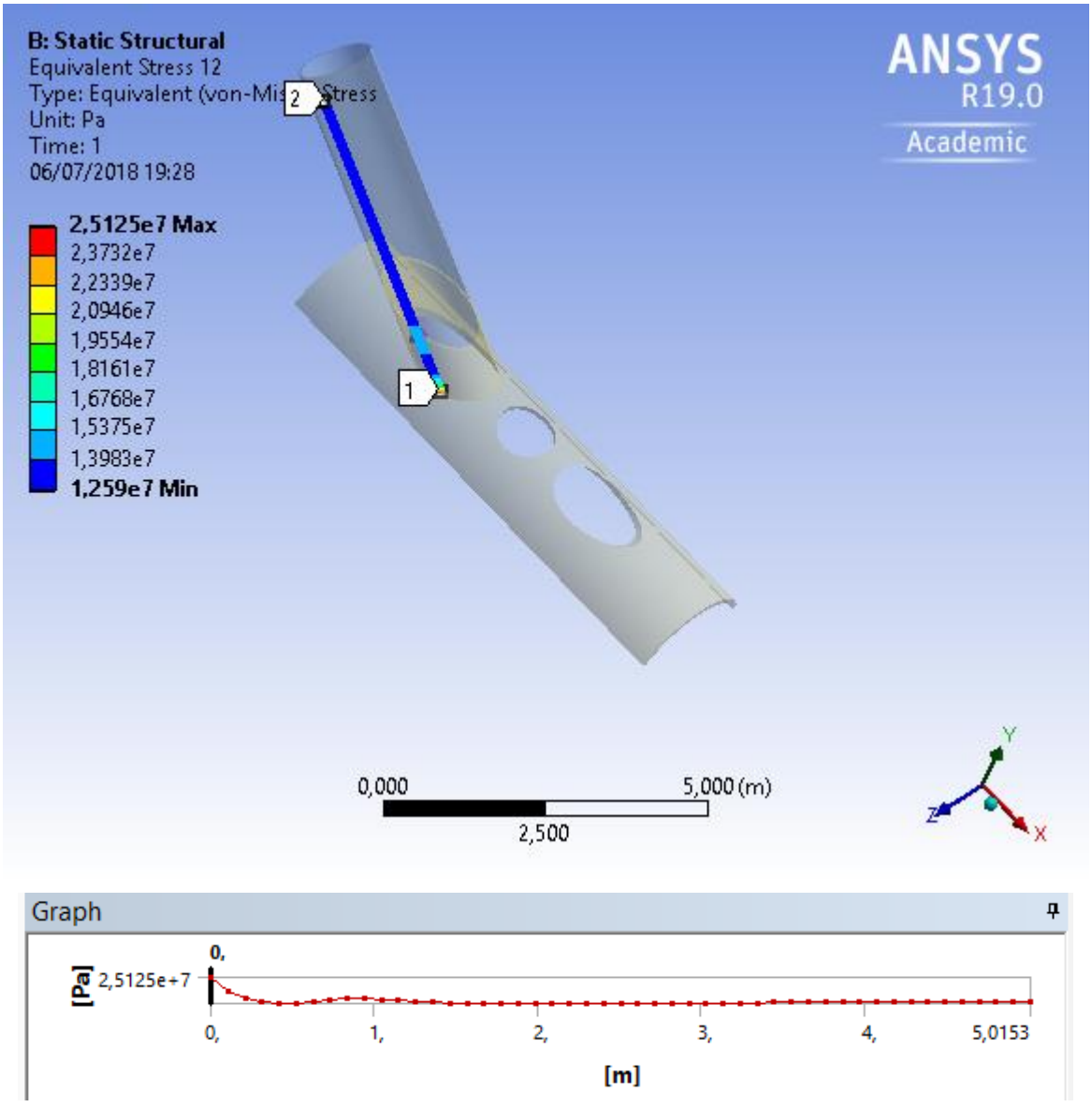

Figure 72 - Stress distribution in brace A for out-plane bending loading case: Side 3

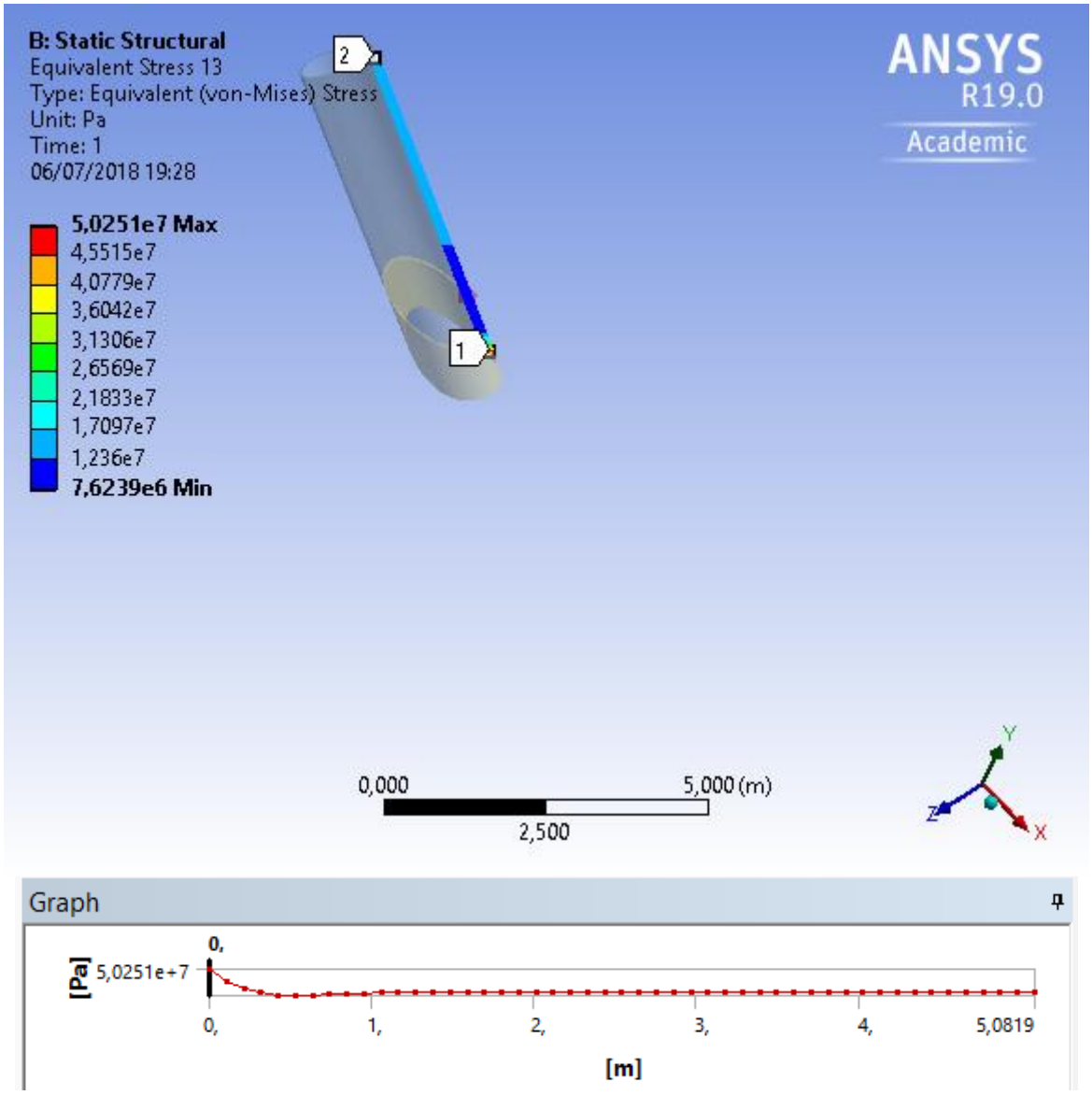

Figure 73 - Stress distribution in brace A for out-plane bending loading case: Side 4

4.3.3.2. BRACE B (MEMBER 5116)

In Figures 74 to 77 are displayed the stress distribution paths for the out-plane bending loading case that are used in the study of the stress concentration factor evaluation of brace B. There are 4 paths for the brace to study and are displayed with the number 1 to number 2. (see Figure 25)

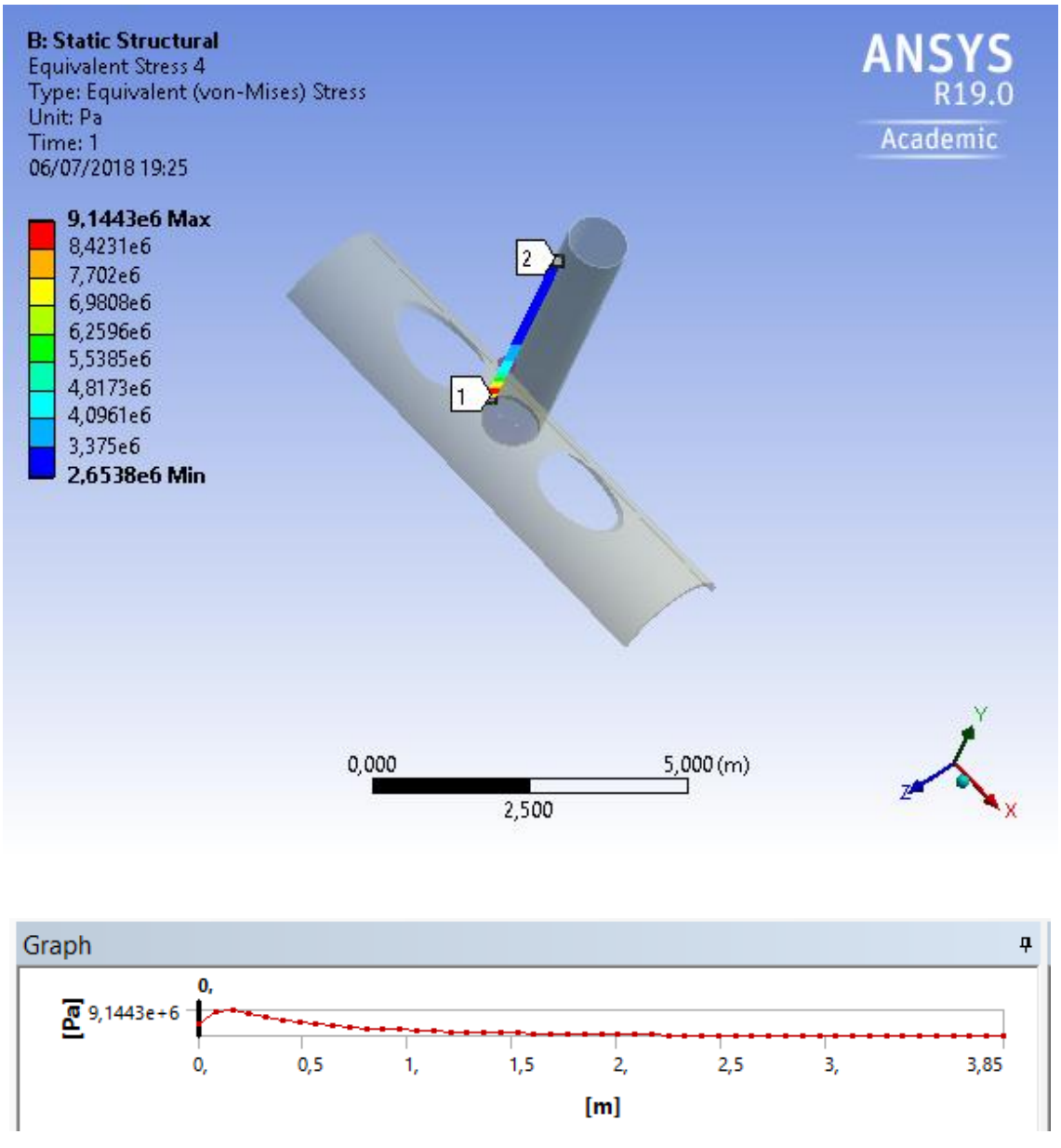

Figure 74 - Stress distribution in brace B for out-plane bending loading case: Side 1

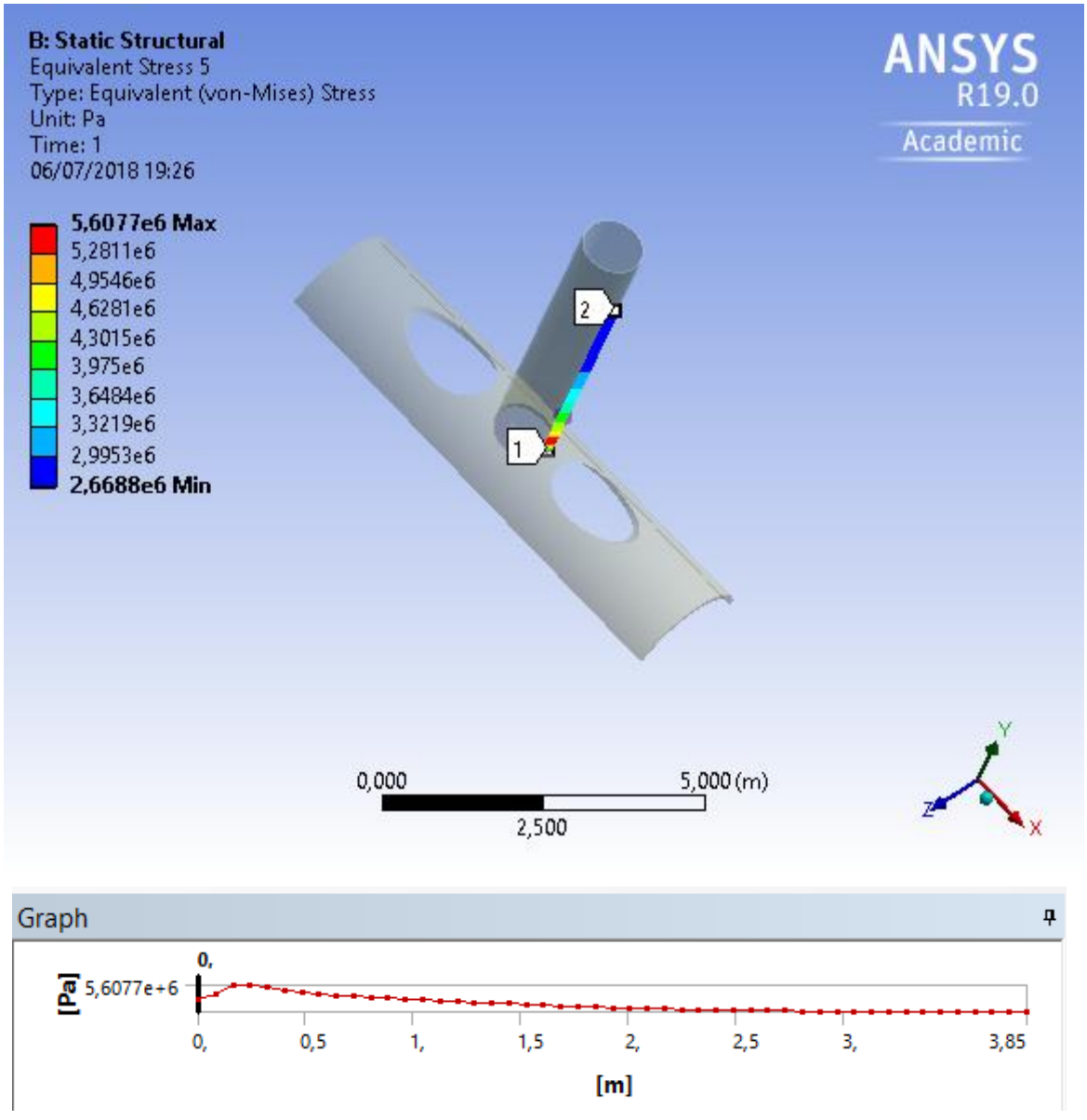

Figure 75 - Stress distribution in brace B for out-plane bending loading case: Side 2

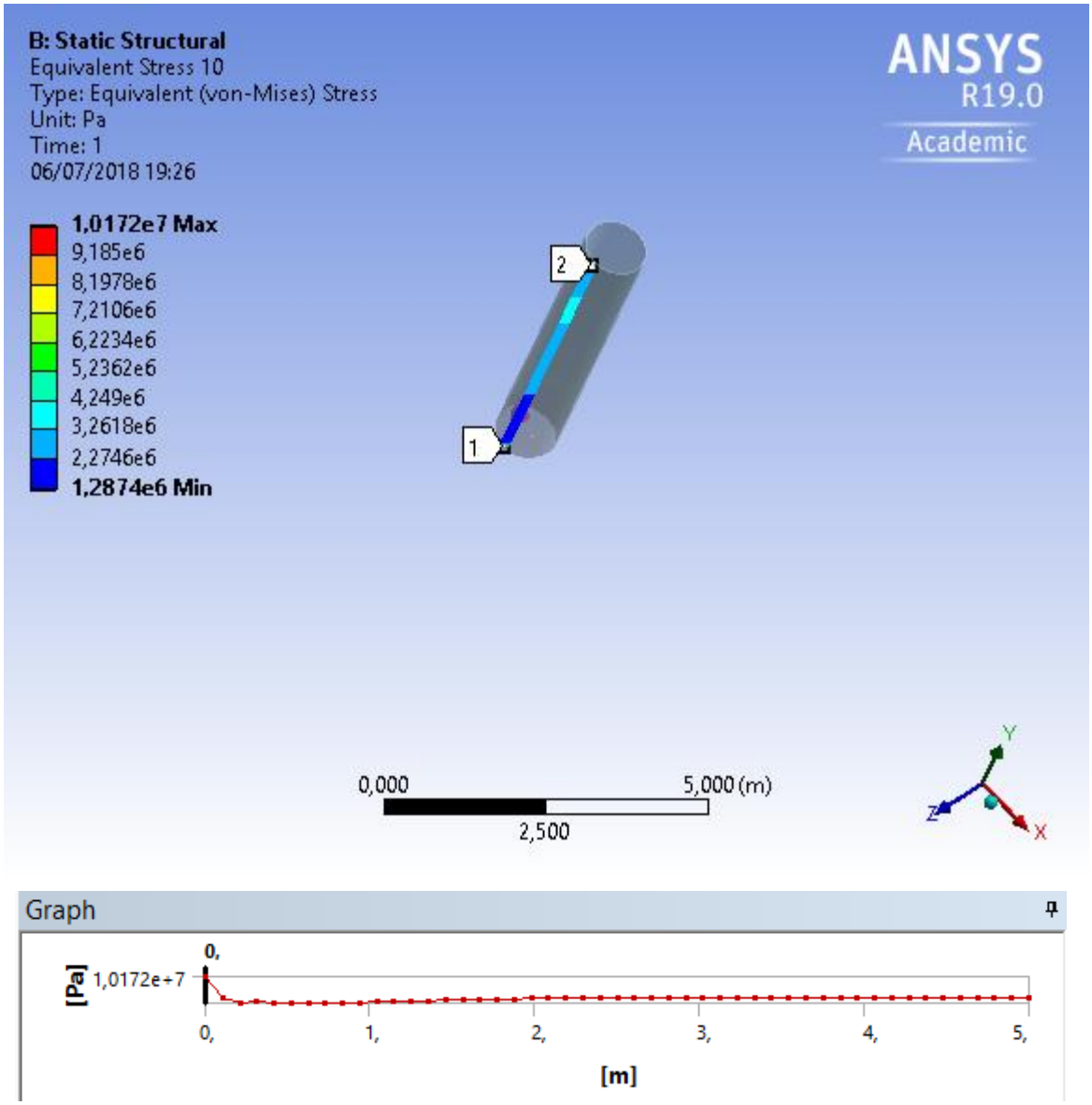

Figure 76 - Stress distribution in brace B for out-plane bending loading case: Side 3

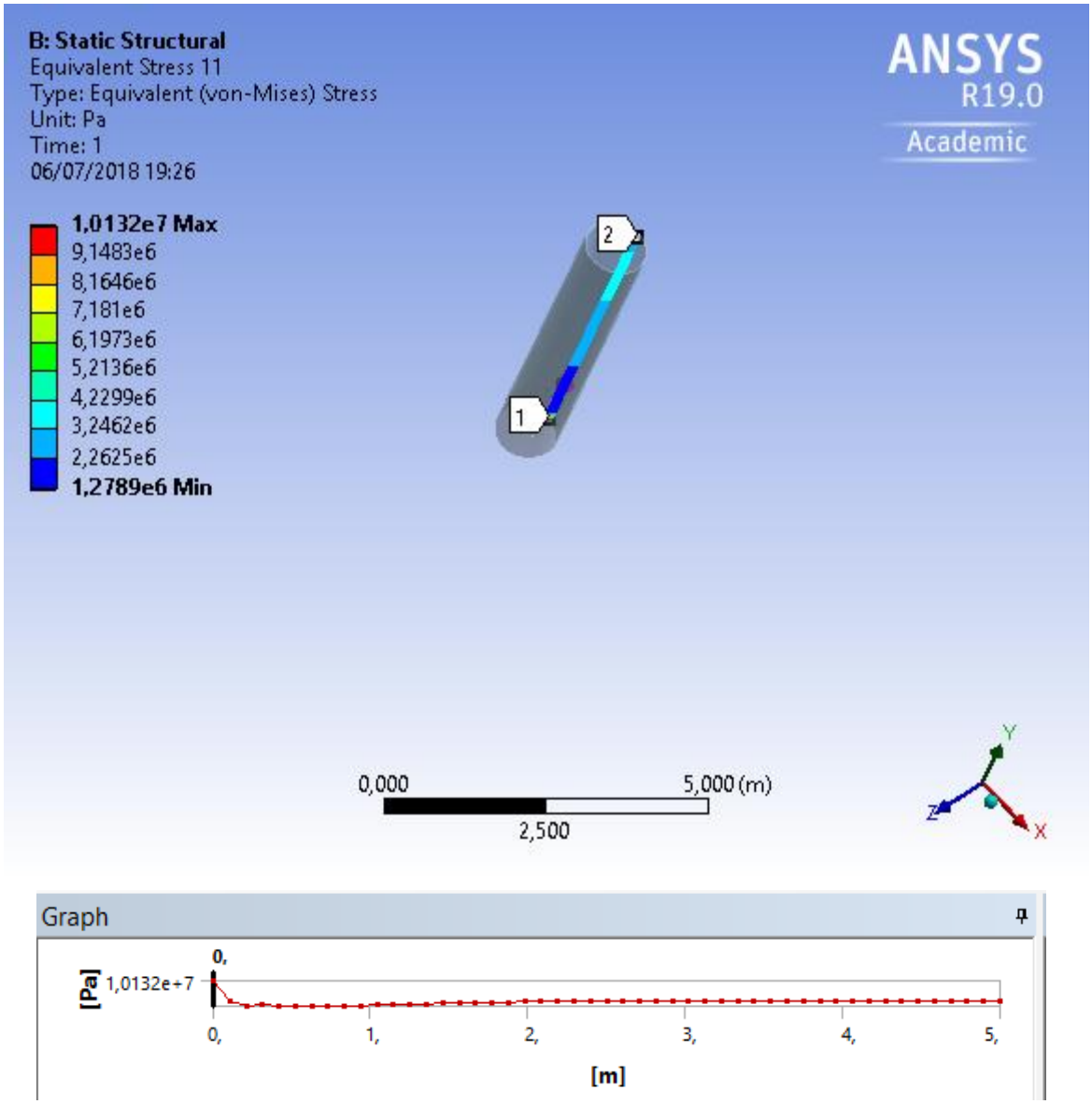

Figure 77 - Stress distribution in brace B for out-plane bending loading case: Side 4

4.3.3.4. BRACE C (MEMBER 5112)

In Figures 78 to 81 are displayed the stress distribution paths for the out-plane bending loading case that are used in the study of the stress concentration factor evaluation of brace C. There are 4 paths for the brace to study and are displayed with the number 1 to number 2. (see Figure 25)

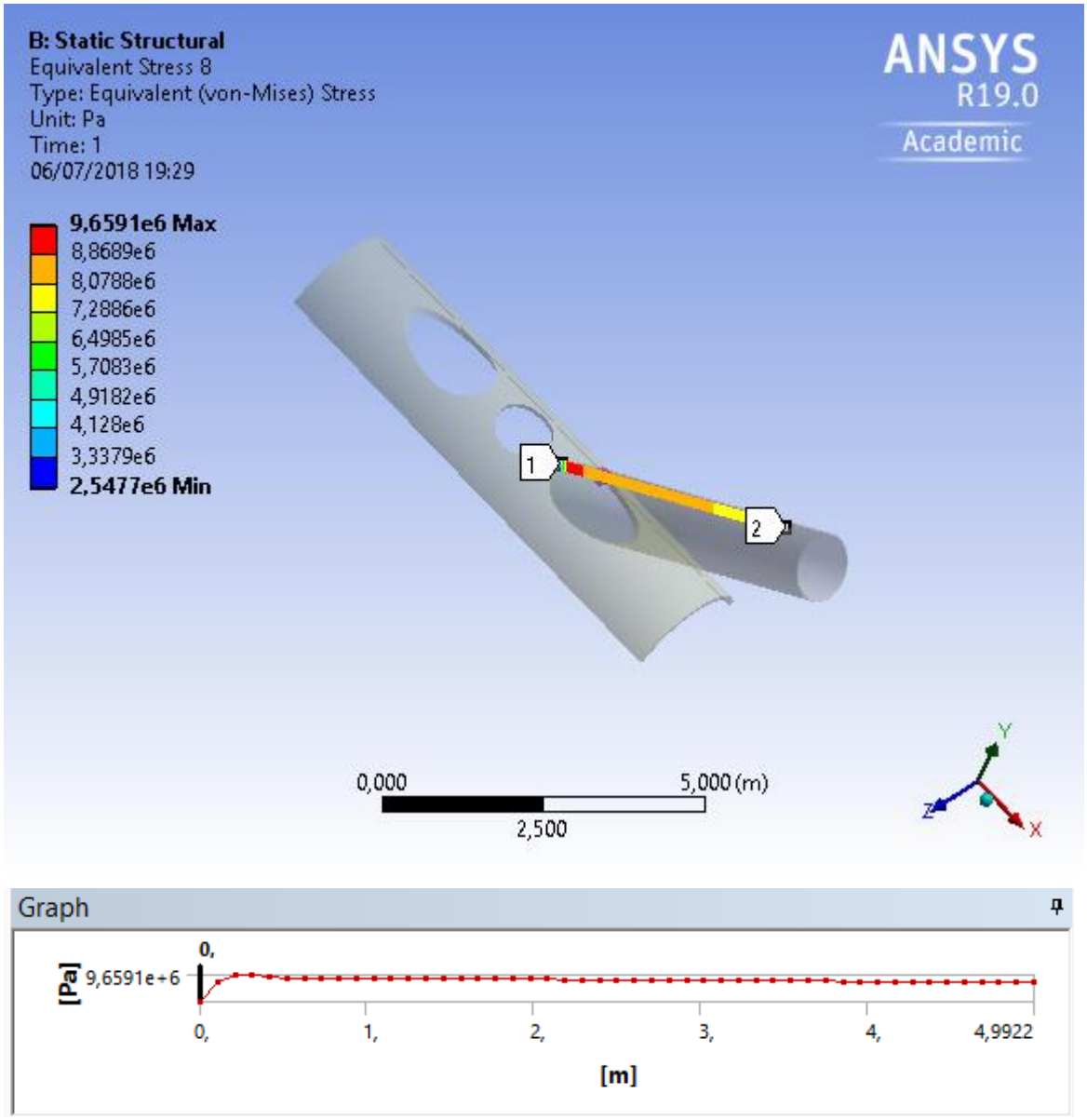

Figure 78 - Stress distribution in brace C for out-plane bending loading case: Side 1

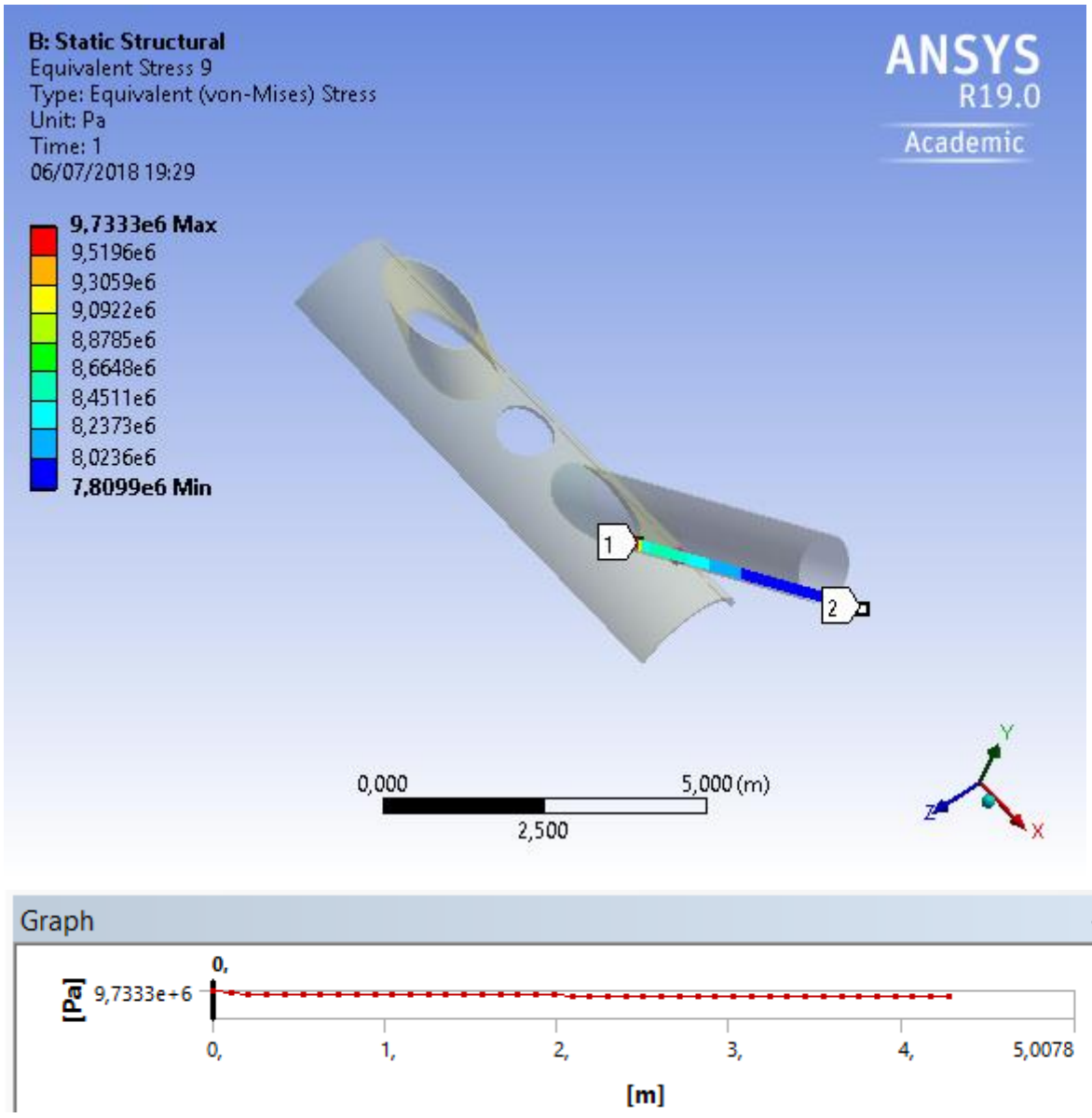

Figure 79 - Stress distribution in brace C for out-plane bending loading case: Side 2

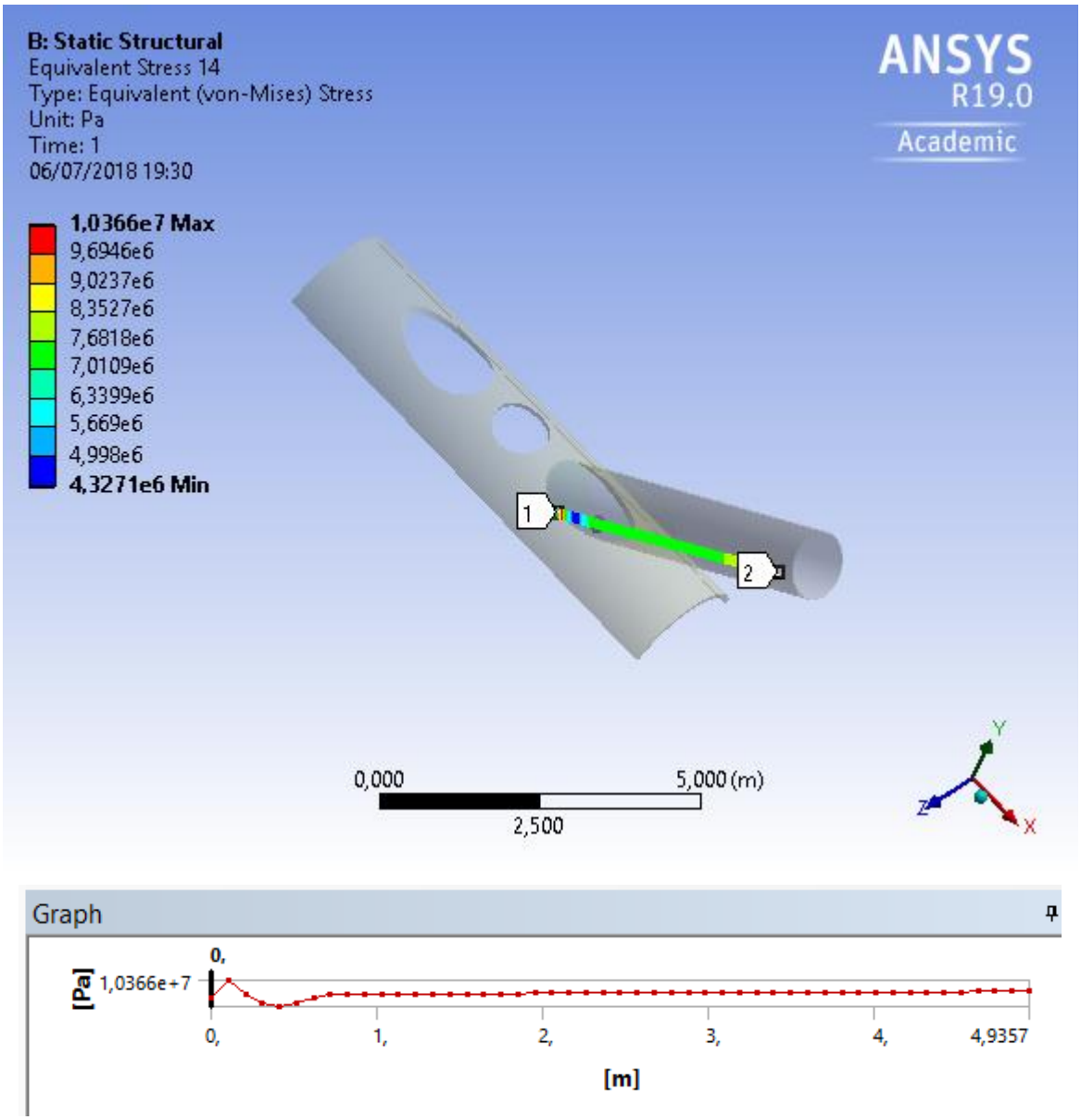

Figure 80 - Stress distribution in brace C for out-plane bending loading case: Side 3

~

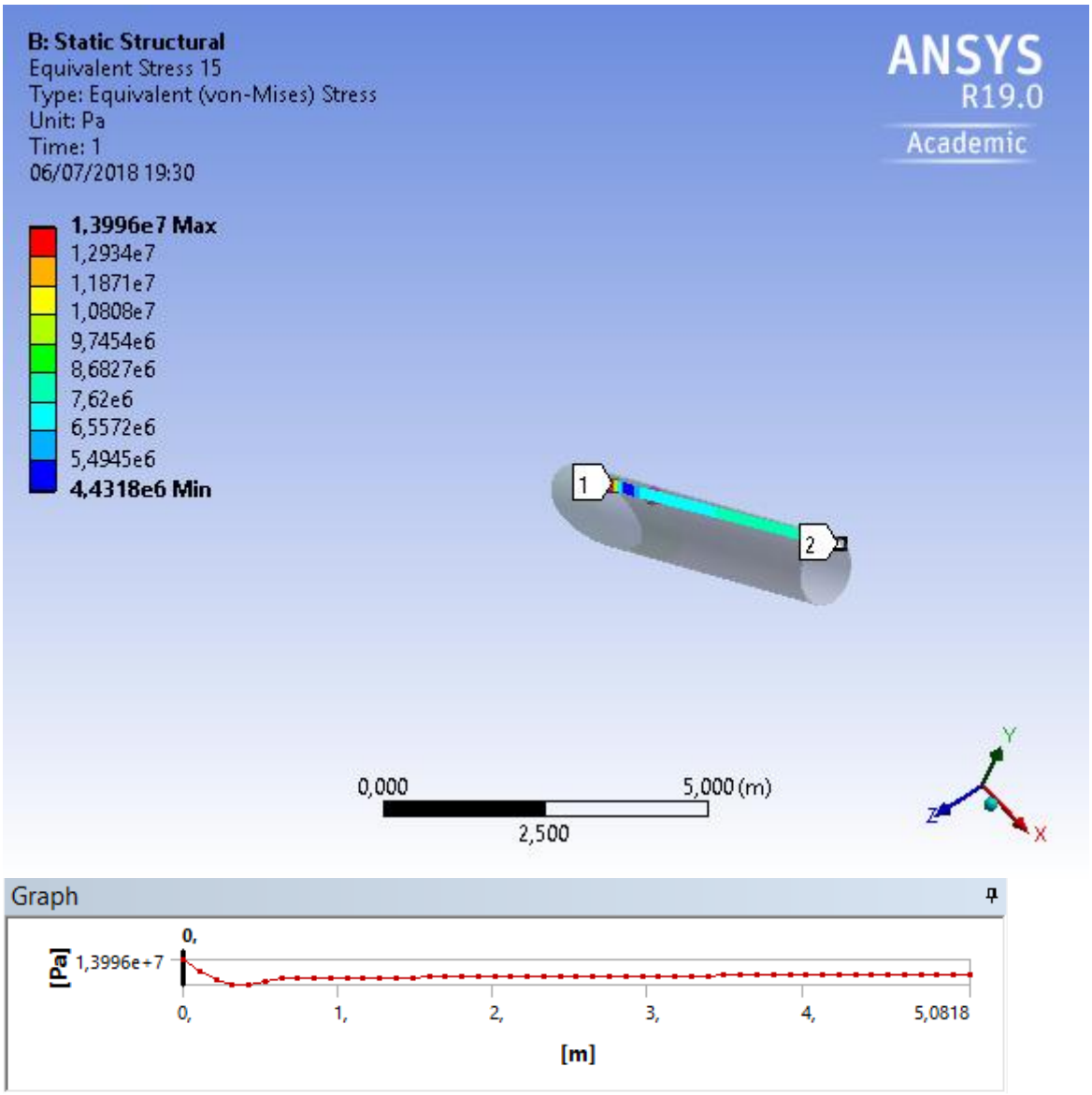

Figure 81 - Stress distribution in brace C for out-plane bending loading case: Side 4

4.3.3.4 CHORD (4936-4937)

In Figure 82 it is displayed the stress distribution path for the out-plane bending loading case that it's used in the study of the stress concentration factor evaluation for the chord. There is only 1 path considered to the evaluation of the stress concentration factors in the chord since the crown points have way higher stresses compared to the saddle of each brace in the chord.

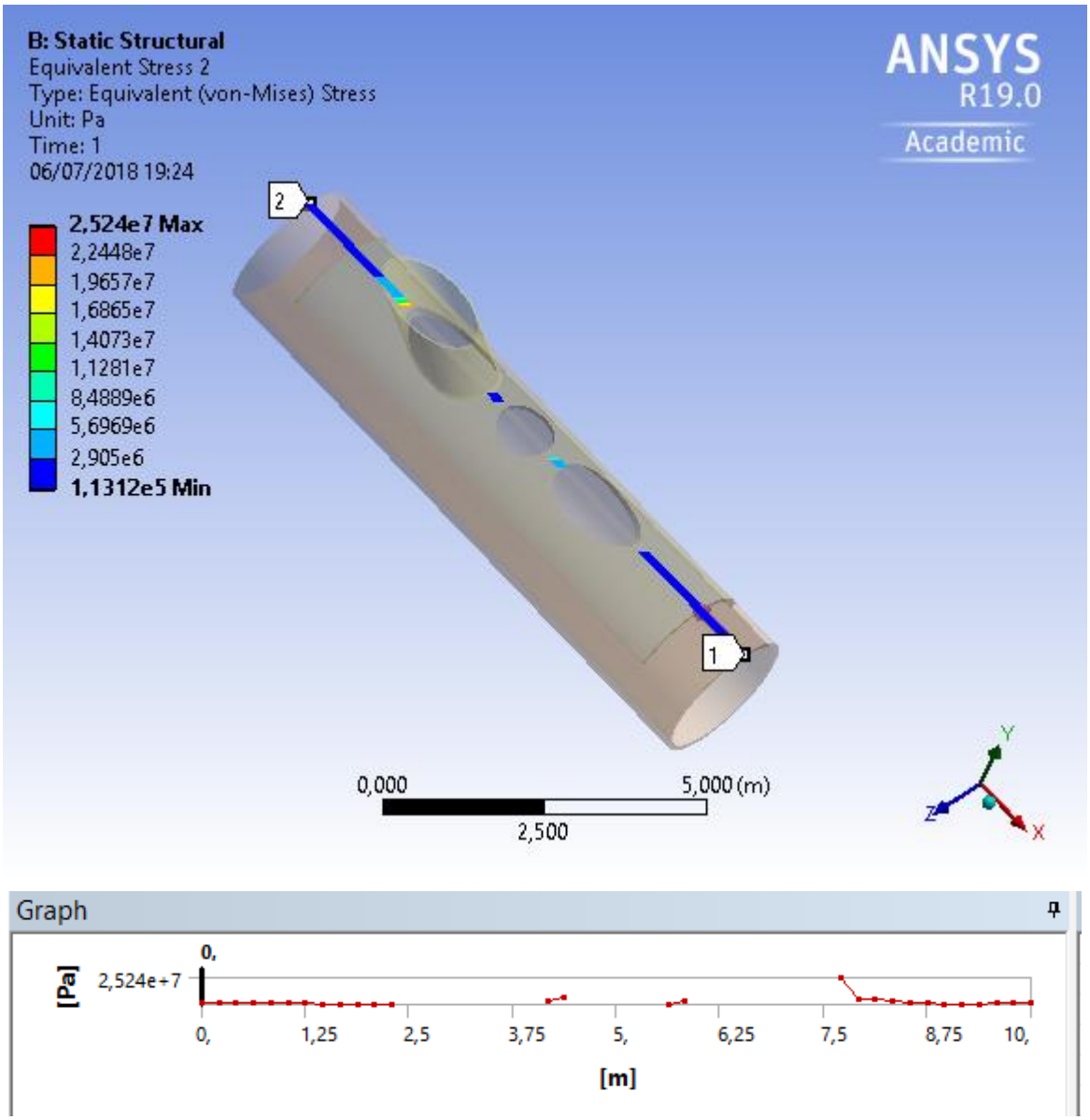

Figure 82 - Stress distribution in chord for out-plane bending loading case

4.4. ANALYSIS AND SCF CALCULATION

The accuracy of the results of tubular junction stress analysis by the finite element method depends on the types of elements used and the fineness of the mesh, especially in the vicinity of the zones of high stress concentrations. It is reasonable that the solid SCFs are slightly higher, since the shell results are measured at the mid-section, whereas the solid results are measured on the external surface. [19] The loading sustained in service lead to displacements of rotary translation of the platform surface. The numerical simulations carried out in this study consider:

- Three simple loadings: axial (Ax), In-Plane Bending (IPB) and Out-of-Plane Bending (OPB) for the validation of the calculation method and to compare with the DNVGL-RP-C203 Fatigue design code.

The hot spots coincide with the saddle and crown locations for loading Ax and OPB. Concerning to the IPB, the hot spots are placed between the saddle and crown locations. By reduced integration, the linear part of the stresses can be directly evaluated at the shell surface and extrapolated to the weld toe. Typical extrapolation paths for determining the structural hot spot stress components on the plate surface or edge are shown by arrows in Figure 83. In order to reduce computational time, the mesh of all the models is characterised by fine elements near the intersection and coarser elements in regions where the stresses are more evenly distributed, as can be observed in Figure 31. The density, Young's modulus and Poisson's ratio were taken to be 7850 kg/m^3, 207 GPa and 0.3 respectively [19]

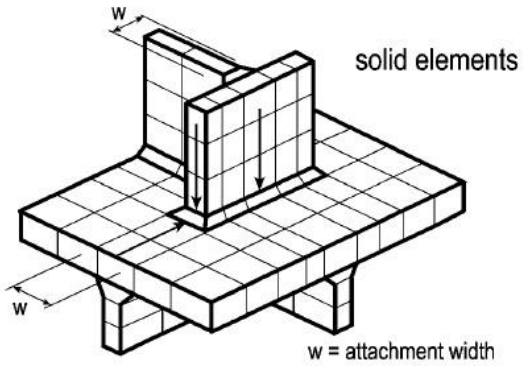

Figure 83 - Typical meshes and stress evaluation paths for a welded detail

The width of the solid element or the two shell elements in front of the attachment should not exceed the attachment width 'w'.

4.4.1 CHORD (MEMBERS 4936-4937)

It is necessary to establish the stress path to study exactly as it was done on Chapter 4 in Section 4.3. It is clearly noticeable that the gaps represented with no stress are the tubular joints and most of the highest stresses are located near the crown of tubular joints. Figures 38, 53 and 68 show the stress fields from the linear-elastic stress analysis of the KT-joint under study for the loading cases, axial, IPB and OPB. Note that the chord stresses were only extracted on the crown because it's pointless to extract from the saddle where they are minimum. Also, the chord is divided into 2 members so the highest stress for the axial loading case is in member 4936 and the highest stress for the in-plane and out-plane bending moments are in member 4937. Figures 84 to 86 show the stress paths in chord for the axial loading, in-plane bending and out-plane bending cases, respectively, and the hot spots in the crown can be identified.

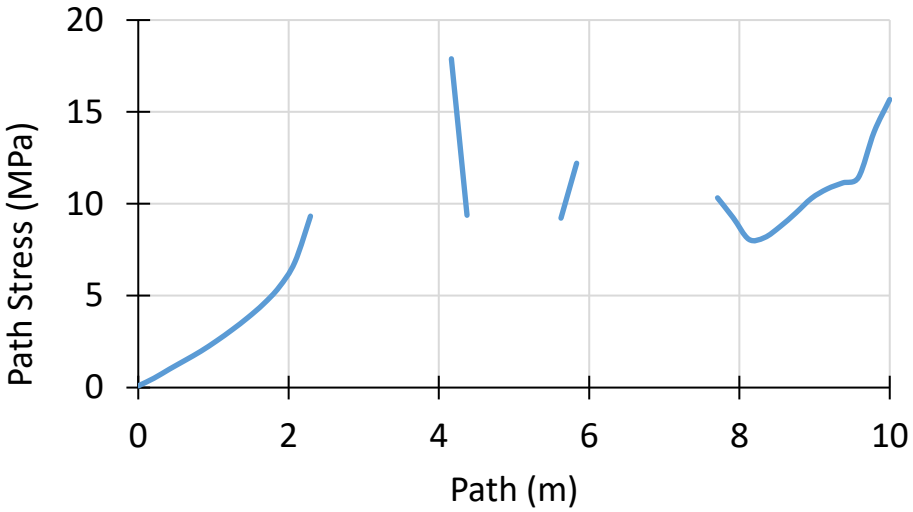

Figure 84 - Path stresses in chord crown for axial loading case

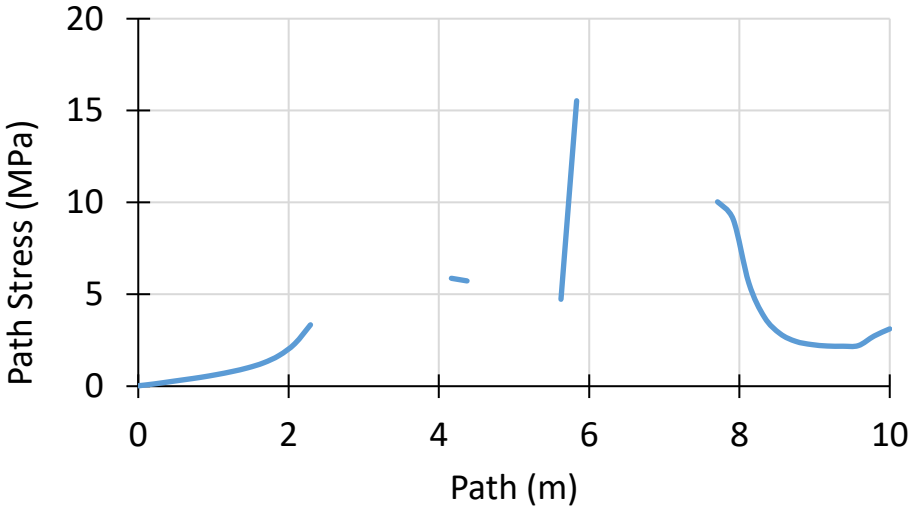

Figure 85 - Path stresses in chord crown for in-plane bending case

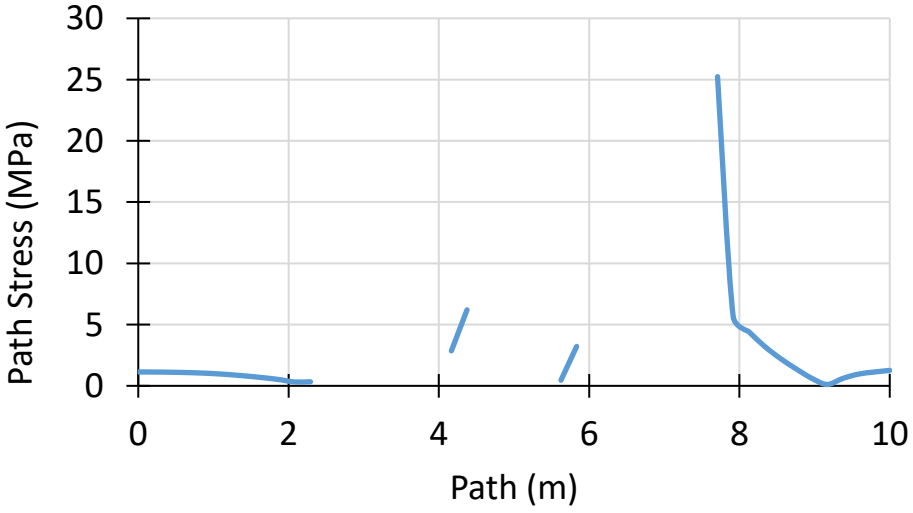

Figure 86 - Path stresses in chord crown for out-of-plane bending loading case

Having the stresses from the chord it is possible to calculate the stress concentration factor with the help of equation (14). Analyzing the Figures 85 to 87, it's possible to extract the maximum hot spot stresses associated to each type of load. The nominal stresses needed to calculate the stress concentration factors associated to the chord using Equation (14) are represented on Table 17.

Table 17 - Stress concentration factors in chord crown

	σ_{HSS} [MPa]	SCF
Axial Crown chord (4937)	17.89	3.624
IPB Crown chord (4936)	15.54	1.318
OPB Crown chord (4936)	25.24	10.064

4.4.2 BRACE A (MEMBER 5110)

For the brace A, it is necessary to establish 2 paths of stresses to obtain the hot spot stress distribution. These paths can be seen on Chapter 4 in Section 4.3 with 2 different sides for each path. Side 1 and 2 present the crown stress points and its path can be seen in Figures 41 and 42. Side 3 and 4 present the maximum saddle stress points and its path can be seen in Figures 43 and 44.

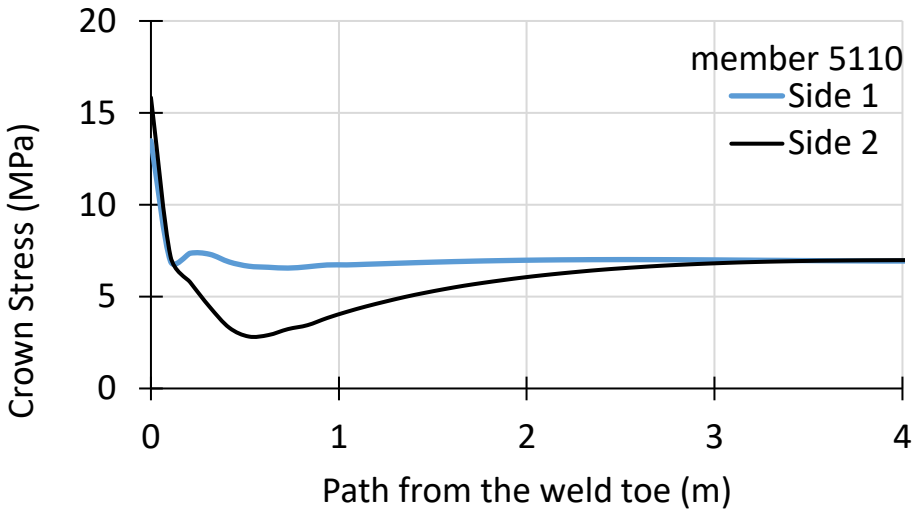

Figure 87 - Path stress in brace crown A for axial loading case (Side 1 and 2)

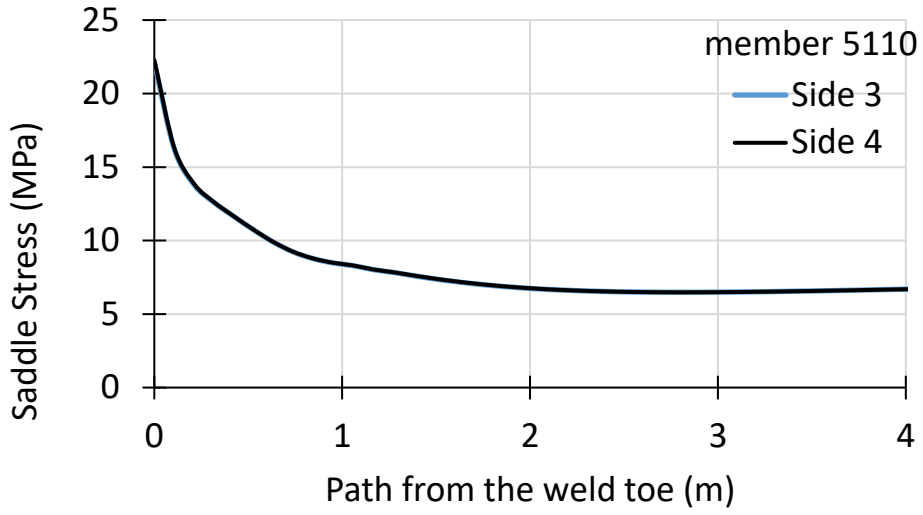

Figure 88 - Path stress in brace saddle A for axial loading case (Side 3 and 4)

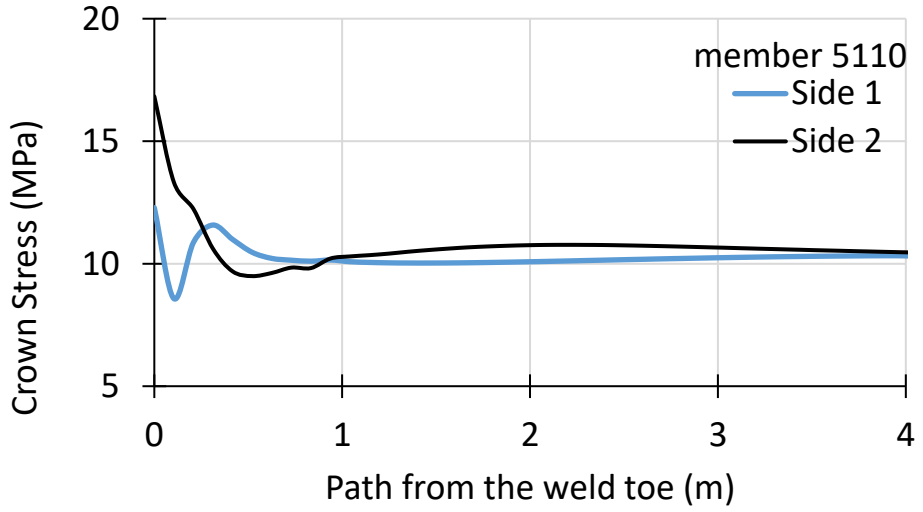

Figure 89 - Path stress in brace crown A for in-plane bending loading case (Side 1 and 2)

Figure 90 - Path stress in brace saddle A for in-plane bending loading case (Side 3 and 4)

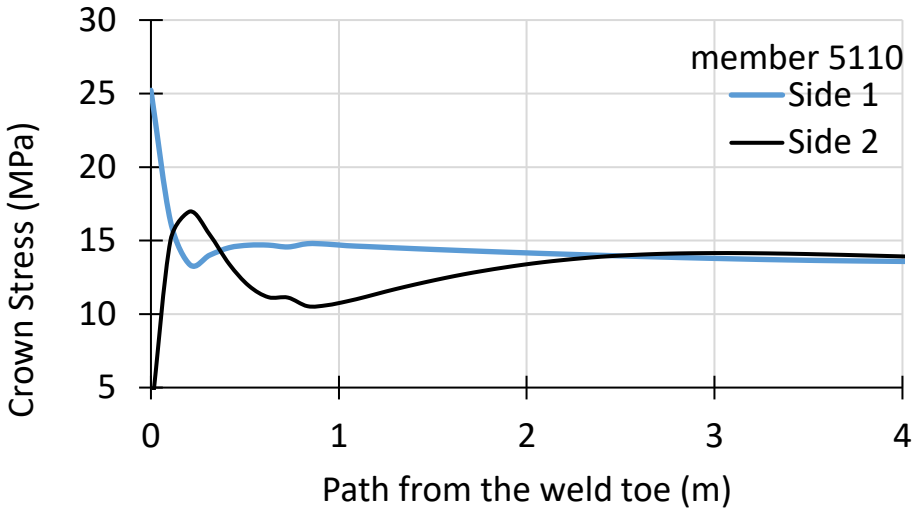

Figure 91 - Path stress in brace crown A for out-plane bending loading case (Side 1 and 2)

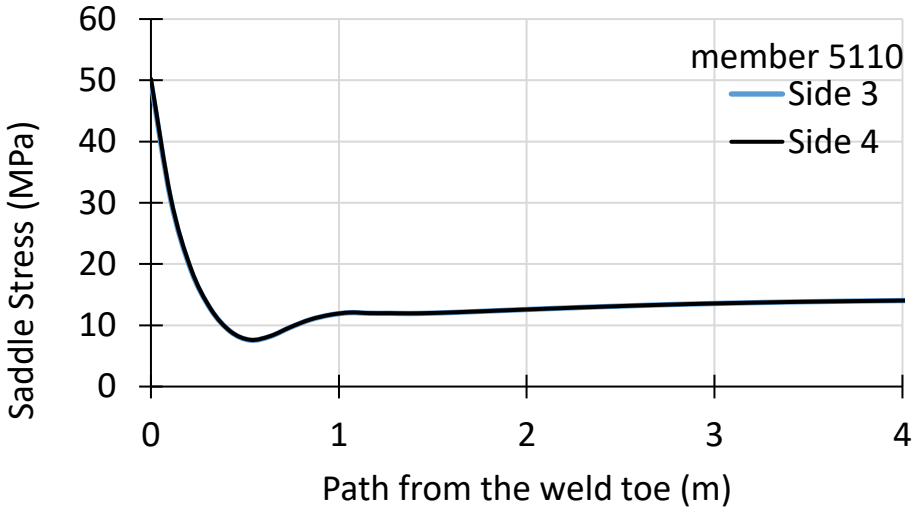

Figure 92 - Path stress in brace saddle A for out-plane bending loading case (Side 3 and 4)

Evaluating and extracting the hot spot stresses, it is possible to calculate the stress concentration factors associated to the brace A using Equation (14).

Table 18 - Results of the hot-spot stress distribution and stress concentration factor for Brace A

		σ_{HSS} [MPa]	SCF
Axial crown Brace A (5110)	Side 1	13.48	0.998
	Side 2	15.83	1.171
Axial saddle Brace A (5110)	Side 3	51.53	1.638
	Side 4	51.57	1.649
In-plane bending Brace A crown (5110)	Side 1	12.29	0.626
	Side 2	16.83	0.857
In-plane bending Brace A saddle (5110)	Side 3	5.59	0.284
	Side 4	5.49	0.285
Out-of- plane bending Brace A crown (5110)	Side 1	25.22	0.819
	Side 2	16.98	0.551
Out-of- plane bending Brace A saddle (5110)	Side 3	49.75	1.615
	Side 4	50.25	1.631

4.4.3 BRACE B (MEMBER 5116)

For the brace B, it is necessary to establish 2 paths of stresses to obtain the hot spot stress distribution. These paths can be seen on Chapter 4 in Section 4.3 with 2 different sides for each path. Side 1 and 2 present the crown stress points and its path can be seen in Figures 44 and 45. Side 3 and 4 represent the maximum saddle stress points and its path can be seen in Figures 46 and 47.

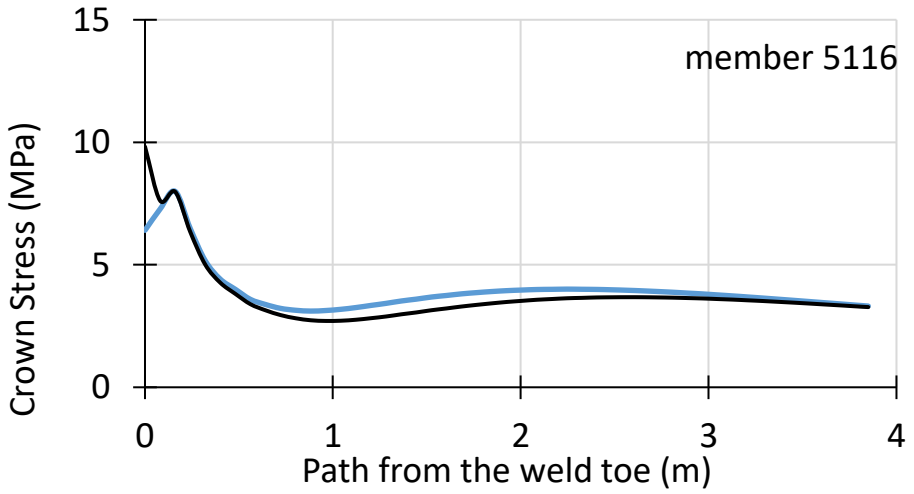

Figure 93 - Path stress in brace crown B for axial loading case (Side 1 and 2)

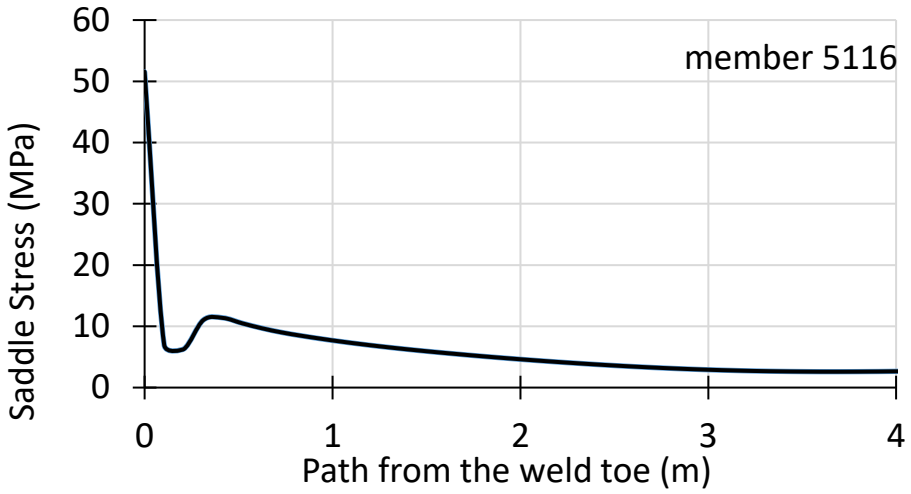

Figure 94 - Path stress in brace saddle B for axial loading case (Side 3 and 4)

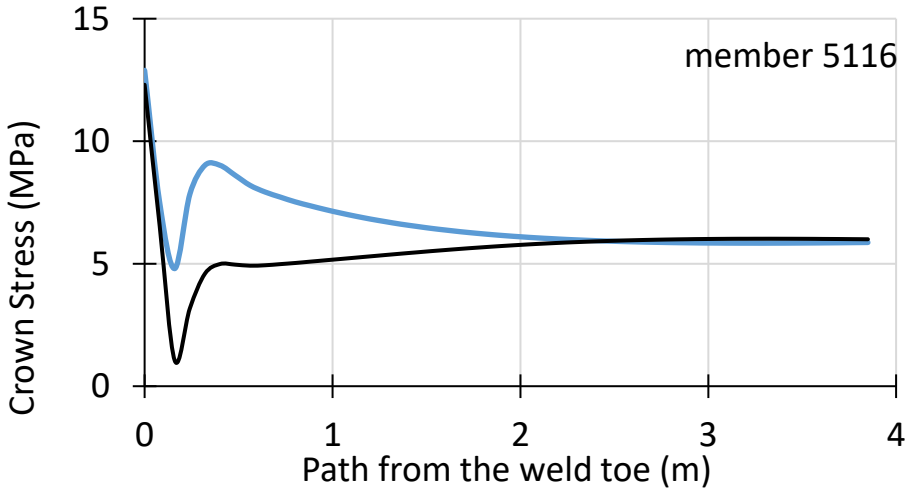

Figure 95 - Path stress in brace crown B for in-plane bending loading case (Side 1 and 2)

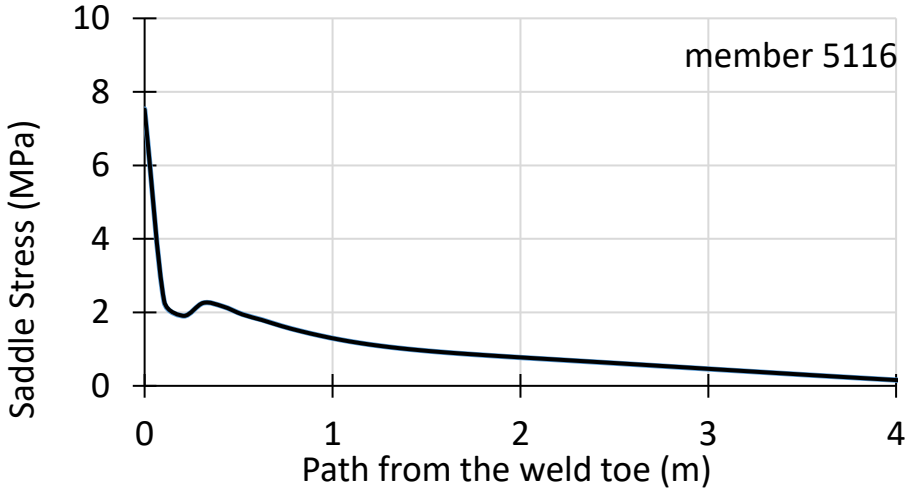

Figure 96 - Path stress in brace saddle B for in-plane bending loading case (Side 3 and 4)

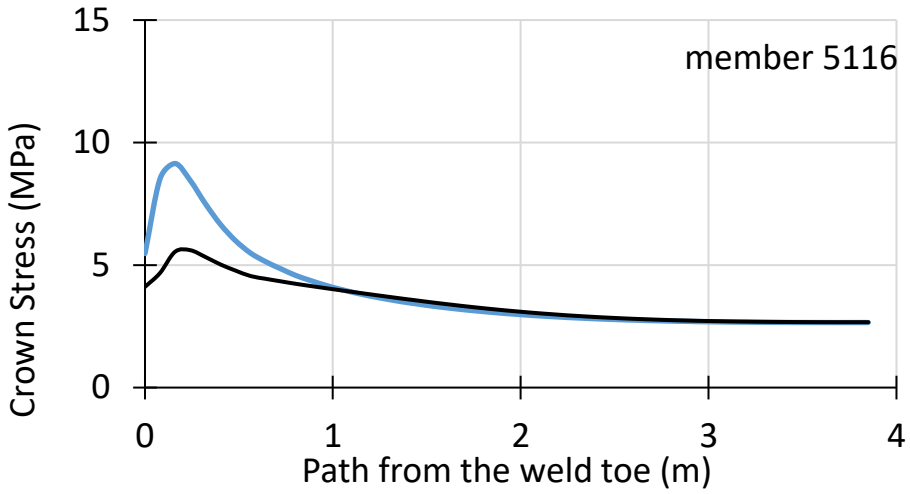

Figure 97 - Path stress in brace crown B for out-of-plane bending loading case (Side 1 and 2)

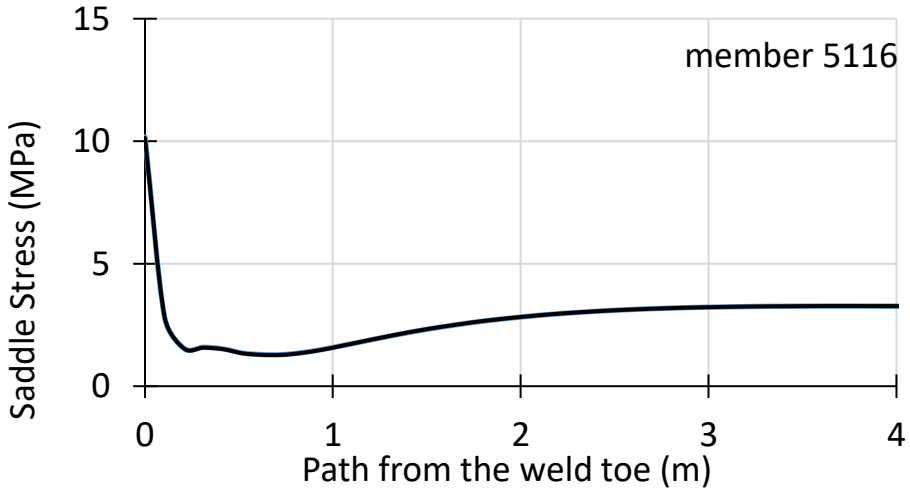

Figure 98 - Path stress in brace saddle B for out-of-plane bending loading case (Side 3 and 4)

Evaluating and extracting the hot spot stresses it is possible to calculate the stress concentration factors associated to the brace B using Equation (14).

Table 19 - Results of the hot-spot stress distribution and stress concentration factor for Brace B

		σ_{HSS} [MPa]	SCF (Eq. 14)
Axial crown Brace B (5116)	Side 1	8	1.375
	Side 2	9.82	1.688
Axial saddle Brace B (5116)	Side 3	51.53	8.855
	Side 4	51.57	8.863
In-plane bending Brace B crown (5116)	Side 1	12.89	1.130
	Side 2	12.30	1.079
In-plane bending Brace B saddle (5116)	Side 3	7.53	0.660
	Side 4	7.52	0.659
Out-of-plane bending Brace B crown (5116)	Side 1	9.14	1.408
	Side 2	5.61	0.863
Out-of- plane bending Brace B saddle (5116)	Side 3	49.75	1.566
	Side 4	50.25	1.560

4.4.4 BRACE C (MEMBER 5112)

For the brace B, it is necessary to establish 2 paths of stresses to obtain the hot spot stress distribution. These paths can be seen on Chapter 4 in Section 4.3 with 2 different sides for each path. Side 1 and 2 represent the crown stress points and its path can be seen in Figures 48 and 49. Side 3 and 4 represent the maximum saddle stress points and its path can be seen in Figures 50 and 51.

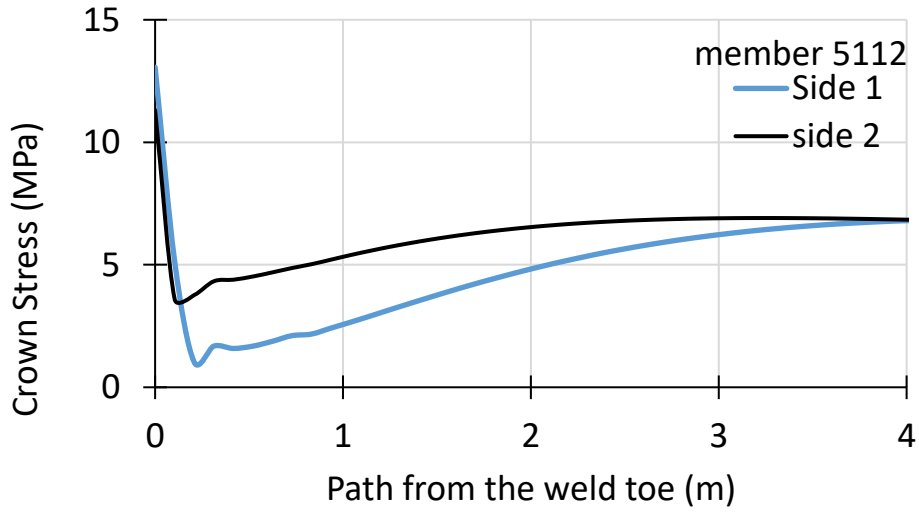

Figure 99 - Path stress in brace crown C for axial loading case (Side 1 and 2)

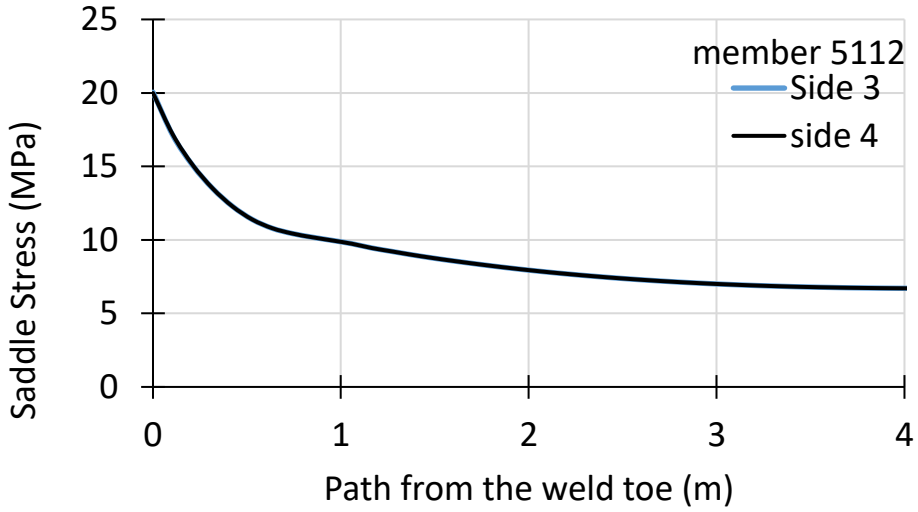

Figure 100 - Path stress in brace saddle C for axial loading case (Side 3 and 4)

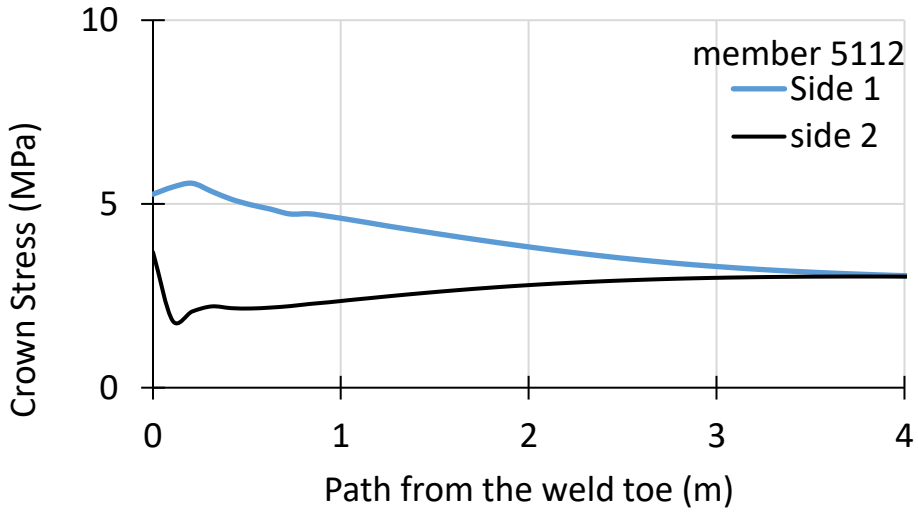

Figure 101 - Path stress in brace crown C for in-plane bending loading case (Side 1 and 2)

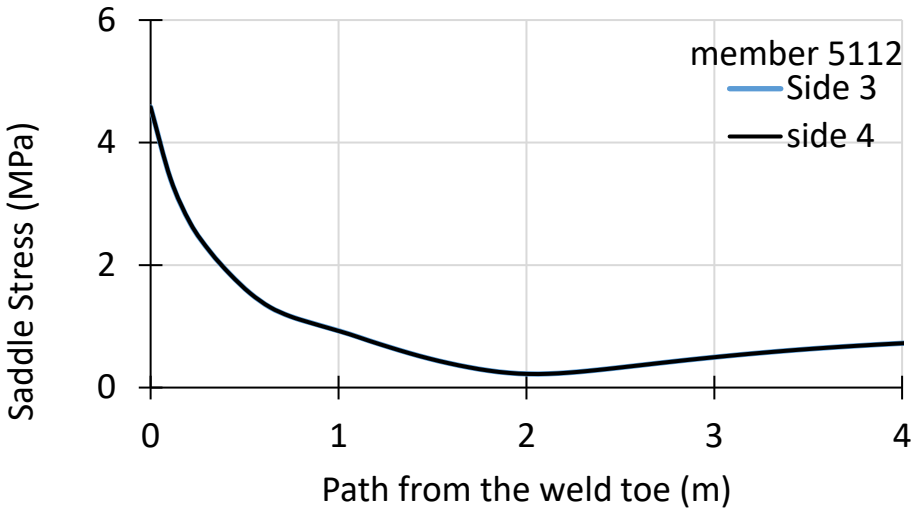

Figure 102 - Path stress in brace saddle C for in-plane bending loading case (Side 3 and 4)

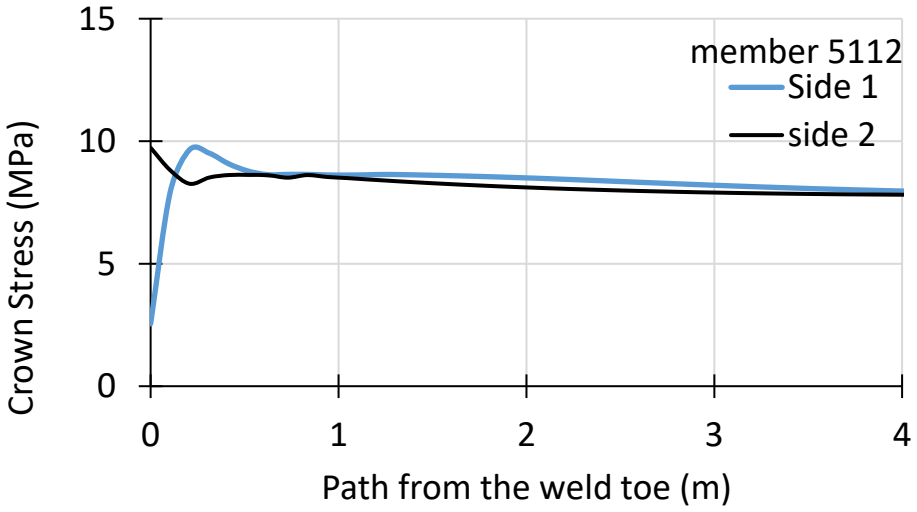

Figure 103 - Path stress in brace crown C for out-of-plane bending loading case (Side 1 and 2)

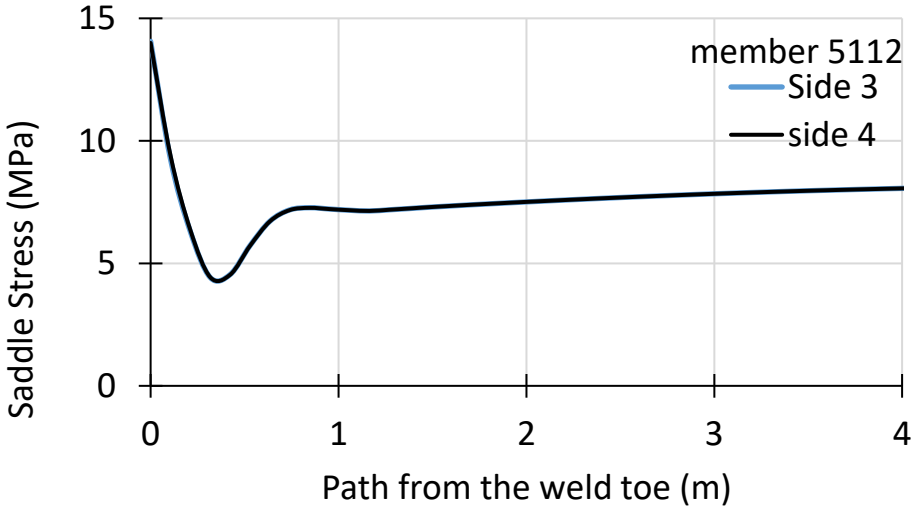

Figure 104 - Path stress in brace saddle C for out-of-plane bending loading case (Side 3 and 4)

Evaluating and extracting the hot spot stresses it is possible to calculate the stress concentration factors associated to the brace C with the auxiliary help of the Equation (14).

Table 20 - Results of the hot-spot stress distribution and stress concentration factor for Brace C

		σ_{HSS} [MPa]	SCF (Eq. 14)
Axial crown Brace C (5112)	Side 1	13.06	0.970
	Side 2	11.32	0.840
Axial saddle Brace C (5112)	Side 3	20.05	1.488
	Side 4	19.99	1.484
In-plane bending Brace C crown (5112)	Side 1	5.56	0.954
	Side 2	3.69	0.633
In-plane bending Brace C saddle (5112)	Side 3	4.58	0.786
	Side 4	4.58	0.786
Out-of- plane bending Brace C crown (5112)	Side 1	9.66	0.540
	Side 2	9.73	0.545
Out-of- plane bending Brace C saddle (5112)	Side 3	14.06	0.787
	Side 4	14.00	0.783

4.5. COMPARISON AND DISCUSSION

In this section, a comparison and discussion of the stress concentration factors results between the Lloyd's register KT joint equations, DNVGL parametric equations and FE analysis are presented. In Tables 21 to 23 are shown the maximum values of the stress concentration factors obtained using the Lloyd and DNVGL parametric equations and finite element analysis. The deviation obtained from the DNVGL equations for the Lloyd's register equations and finite element analysis are presented in Tables 24 to 26. The deviation is calculated in percentage, where positive magnitude denotes increase in SCF and negative magnitude denotes decrease in SCF compared to SCFs obtained in DNV-RP-C203.

Table 21 - Stress concentration factors for axial loading case from the Lloyd and DNVGL parametric equations and finite element analysis

Comparision	SCF AS/AC				
	DNV	Lloyd		FEA	
Chord		Crown	Saddle		
A (5110)	1.601	1.773	1.733	3.624	
B (5116)	2.949	1.598	0.935	0.341	
C (5112)	1.369	1.117	1.047	0.444	
Brace	DNV	Crown	Saddle	Crown	Saddle
A (5110)	1.823	1.861	1.596	1.171	1.649
B (5116)	3.409	1.480	0.217	1.688	8.863
C (5112)	1.786	1.861	1.250	0.970	1.488

Table 22 - Stress concentration factors for in-plane bending case from the Lloyd and DNVGL parametric equations and finite element analysis

Comparision	SCF MIP			
Chord	DNV	Lloyd	FEA	
		Crown/Saddle		
A (5110)	1.299	1.487	1.255	
B (5116)	1.371	1.861	1.225	
C (5112)	0.860	1.346	1.318	
Brace	DNV	Crown/Saddle	Crown	Saddle
A (5110)	1.624	1.391	0.857	0.285
B (5116)	2.172	1.790	1.130	0.660
C (5112)	1.515	1.347	0.954	0.786

Table 23 - Stress concentration factors for out-of-plane bending case from the Lloyd and DNVGL parametric equations and finite element analysis

Comparision	SCF MOP				
Chord	DNV	Lloyd		FEA	
		Crown	Saddle		
A (5110)	1.299	-	-	2.086	
B (5116)	1.371	-	-	2.037	
C (5112)	0.860	-	-	10.064	
Brace	DNV	Crown	Saddle	Crown	Saddle
A (5110)	1.624	-	-	0.819	1.631
B (5116)	2.172	-	-	1.408	1.566
C (5112)	1.515	-	-	0.545	0.787

For the axial loading case between the FE model-DNV and between the FE model-Lloyd, the SCF chord in brace A is way more conservative for the finite element model but for the other brace locations where the SCF is located, the SCF is conservative for the analytical solutions. For braces A and C, the decreasing percentage varies from 11% to 58% where the parametric equations are way more conservative compared to the FE model. SCF saddle for brace B calculated using FE analysis is way too conservative and is unrealistic. DNV parametric equations only have relevant differences when comparing chord locations or brace B with the FE analysis but for Lloyd's the values are way more divergent.

According to report OTH354, the values of stress concentration factor of less than 1.5 should not be considered in fatigue analysis. Therefore, a limit for SCF should be imposed according to this report of 1.5.

The DNVGL standard does not specify a lower limit for the SCF. However, values lower than 1 should not be considered, since they are not conservative. However, the DNVGL standard states that due to the axial stress in the chord should be increased by a SCF = 1.20 for calculation of additional hot spot stress at the crown toe and the crown heel for dynamic loading in the axial direction of the chord. In this way, the SCF values obtained according DNVGL standard for chord in crown location should be increased from 1.2.

Table 24 - Deviation of stress concentration factors between DNV-FEA and between Lloyd-FEA for axial loading case

Deviation	SCF AS/AC		
Chord	DNV vs. FEA	Lloyd vs. FEA	
		Crown	Saddle
A (5110)	55,8%	104.4%	109.1%
B (5116)	-764,7%	-78.7%	-63.5%
C (5112)	-208,2%	-60.2%	-57.6%
Brace	DNV vs. FEA	Lloyd vs. FEA	
A (5110)	-11,4%	-37.1%	3.3%
B (5116)	160,0%	14.0%	3984.3%
C (5112)	-16.7%	-47.9%	19.0%

For the in-plane bending case between the FE model-DNV and between the FE model-Lloyd, the SCF values don't differentiate from each other that much. In chord, only the SCF factor in brace C calculated with DNV is less conservative for the finite element. SCF on brace side at location A, B and C for tmentioned load assignment, the decreasing percentage varies from 37% to 80% as for DNV code and for Lloyd's register equations. For chord side the only relevant SCF difference is in location C where the FE analysis is more conservative compared to DNV code. It's important to note that don't exist Lloyd equations to estimate the SCF on chord side saddle.

Table 25 - Deviation of stress concentration factors between DNV-FEA and between Lloyd-FEA for in-plane bending case

Deviation	SCF MIP		
Chord	DNV vs. FEA	Lloyd vs. FEA	
		Crown	Saddle
A (5110)	1.5%	-15.6%	-
B (5116)	-10,6%	-34.2%	-
C (5112)	53.3%	-2.1%	-
Brace	DNV vs. FEA	Lloyd vs. FEA	
A (5110)	-47.2%	-38.4%	-79.5%
B (5116)	-48,0%	-36.9%	-63.1%
C (5112)	-37,0%	-29.2%	-41.6%

For the out-plane bending case between the FE model-DNV on chord side there is an absurd increase of the SCF factor especially in brace C so it's conclusive that DNV equations are preferred when estimating SCF near the braces. On brace side, the FE analysis is less conservative and the decreasing percentage varies between 27% to 48% for brace B and C but for brace A the difference is minimal. It's not possible to compare the FE model values with Lloyd's out-of-plane bending case because the parametric equations for it do not exist or were created.

Table 26 - Deviation of stress concentration factors between DNV-FEA and between Lloyd-FEA for out-plane bending case

Deviation	SCF MOP		
Chord	DNV vs. FEA	Lloyd vs. FEA	
		Crown	Saddle
A (5110)	60.6%	-	-
B (5116)	48.6%	-	-
C (5112)	1070.7%	-	-
Brace	DNV vs. FEA	Lloyd vs. FEA	
A (5110)	0.5%	-	-
B (5116)	-27.9%	-	-
C (5112)	-48.0%	-	-

5

Conclusions and Future Works

5.1. CONCLUSIONS

In this section, conclusions between the analytical parametric equations and FEM analysis is made. It can be verified that the values of SCF in general from the analytical parametric equations are more conservative when compared with finite element analysis. However, the finite element analysis leads to better results for the values of stress concentration factor for chord-brace A, chord-brace C, and for Chord in axial force, in-plane bending and out-of-plane loading cases, respectively. As a rule, the out-plane bending case is of little relevance in fatigue analysis, however, it should be noted that the finite element analysis is more conservative than the parametric analytical equations, especially for the chord. The parameters that have caused influence in evaluation of SCF beside the non-dimensional geometric parameters in finite element study are; boundary condition at brace and chord ends with their respective length, type of mesh element and the mesh refinement around the intersection of the braces and the chord. In finite element study, a sufficiently long chord length was assumed according to Efthymiou [26] criteria of short chord length, $\alpha < 12$, to ensure that the stresses between brace-to-chord intersection are not affected by the end condition, but the examination between end condition of fixed and pinned support is observed to contribute influence in SCF with assumed length. That way it is noticeable that the finite element analysis for the stress concentration factor calculation in the braces and chord is more appropriate to estimate the fatigue life of offshore tubular joints.

5.2 FUTURE WORKS

As future works, a numerical study with the influence of welding fillet need to be considered. After having valuable information regarding the weld it's possible to extract more accurate results on the finite element model and that way estimate even better the stress concentration factor associated to each brace and chord. A mesh refinement study need to be made with aims to observe the influence of the finite element size in the evaluating the values of SCF. Also, the application of quadratic extrapolation approach helps refining the hot-spot stresses and estimate accurate results. A spacial KT-joint considering different loading cases could be used to estimate the values of the stress concentration factors rather than an analysis of two distinct plans.

BIBLIOGRAPHIC REFERENCES

[1] Adepipe, Oyewole, Brennan, Feargal, Kolios, Athanasios, *Review of corrosion fatigue in offshore structures: Present status and challenges in the offshore wind sector*, ScienceDirect, 30th March 2016, 14 pages, United Kingdom

[2] Ray-Chaudrhuri, Samit, Saini, Dikshant Singh, Karmakar, Debasis, *A review of stress concentration factors in tubular and non-tubular joints for design of offshore installations*, ScienceDirect, 4th August 2016, 17 pages, India

[3] Kajolli, Redion, *A new approach for estimating fatigue life in offshore steel structures*, Master Thesis, University of Stavanger, 2013

[4] Charkrabarti, Subrata K., *Handbook of Offshore Engineering Volume I*, Elsevier, USA, 2005

[5] Moan, T., Offshore Structures (chapter 7), *Modeling Complex Engineering Structures*, Editor Robert Melchers and Richard Hough, 378 pages, 2007, USA

[6/] Jovašević, S., Correia, J.A.F.O., Pavlović, M., Rebelo, C., De Jesus, A.M.P, Veljković, M., Simões da Silva, L., *Global fatigue life modelling of steel half-pipes bolted connections*, ScienceDirect, 17th September 2016, 7 pages, Coimbra, Portugal.

[7] Patil, Torna, Pratbha, Alandkar, *Dynamic Response of Offshore Structures – an overview*, International Journal of Latest Technology in Engineering, Management & Applied Science, August 2017, 5 pages, India

[8] Gudmestad, O.T., *Marine Technology and Design*, University of Stavanger, Norway, 2012

[9] Det Norske Veritas, *DNV-RP-C205: Environmental Conditions and Environmental Loads*, Norway, 2014

[10] Det Norske Veritas, *DNV-RP-C203: Fatigue Design of Offshore Structures*, Norway, 2016

[11] Gudmestad, O.T., *Marine Operations*, University of Stavanger, Norway, 2012

[12] Standards Norway, *NORSOK Standard: Actions and Actions Effects*, Norway, 2007

[13] Wilson, J.F., *Dynamics of Offshore Structures*, John Wiley & Sons, New Jersey, 2003

[14] Institute of Building Technology and Structural Engineering, *Structural Reliability Theory*, University of Aalborg, Denmark, 1998

[15] ESDEP lectures - *WG15-A: Structural Systems: Offshore* (http://fggweb.fgg.unilj.si/~/pmoze/esdep/master/toc.htm), ICL, 2007.

[16] Barbarin, Jérémy de, *Session 4: Jacket Sizing*, 2016

[17] Kuang, J.G.; Potvin, A.B. and Leick, R.D., *Stress concentration in tubular joints*, Offshore Technology Conference, OTC 2205, 1975

[18] Pilkey, W.D. and Pilkey, D.F., *Peterson's stress concentration factors*, 3rd Ed., 2008

[19] Minguez, Estivaliz Lozano, *Fatigue & Fracture Mechanics of Offshore wind turbine support structures*, 2015

[20] American Petroleum Institute (API), *API RP 2A-WSD Recommended Practice for Planning, Designing and Constructing Fixed Offshore Platforms: Working Stress Design*, 2005

[21] Hobbacher, A., *Recommendations for Fatigue Design of Welded Joints and Components*, 2008

[22] Sørensen, J.D. and Toft, H.S, *Probabilistic Design of Wind Turbines*, 2010

[23] American Bureau of Shipping, *Guide for The Fatigue Assessment of Offshore Structures*, 2010

[24] Djavit, Djan Eirik, Strande, Erik, *Master's Thesis: Fatigue failure analysis of fillet welded joints used in offshore structures*, 2013

[25] Radaj, Dieter, *Design and Analysis of Fatigue Resistant Welded Structures*, 1990

[26] Zhao X.L., Herion, S., Packer, J.A, R. Puthli, *Design Guide for Circular and Rectangular Hollow Section Joints Under Fatigue Loading*, 2000

[27] Health and Safety Executive – Offshore Technology Report, *STRESS CONCENTRATION FACTORS FOR SIMPLE TUBULAR JOINTS: Assessment of Existing and Development of New Parametric Formulae*, 1997

[28] Ahmadi, Hamid, Nejad, Ali Ziyei, *Stress Concentration factors in uniplanar tubular KT-joint of jacket structures subjected to in-plane bending loads*, 2016

[29] Efthymiou, M., *Development of SCF formulae and generalised influence functions for use in fatigue analysis*, Surrey, 1988

[30] https://www.steelconstruction.info/Material_selection_and_product_specification, Junho 2018

[31] Belhour, Samira, Kahoul Hafida, Bellaouar Ahmed, Murer Sébastien, *Effect of Geometric parameters and combined loading on stress distribution of Tubular T-Joints*, 2000